

Multimonopoles

Conor J. Houghton
Trinity College
Cambridge

*Dissertation submitted for the degree of Doctor of Philosophy
at the University of Cambridge*

December 1997

*Born laughing, I've believed in the Absurd,
Which brought me this far; henceforth, if I can,
I must impersonate a serious man.*¹

¹John Updike, *Midpoint*.

Acknowledgements

It has been my good fortune to work under the supervision of Dr N.S. Manton and I am very grateful to him for all his help and encouragement throughout the course of this research. I am indebted to Dr P.M. Sutcliffe with whom I have collaborated and from whom I have learned much. I also benefited greatly from discussions with Professor N.J. Hitchin.

I thank the Foreign and Commonwealth Office, the Engineering and Physical Sciences Research Council, Trinity College and Fitzwilliam College for financial support.

I thank Adrian, Art, Danielle, Jim, Pat, Pete, Sazzad, Simon, Trevor and other members of DAMTP for their friendship and tolerance. I am grateful for the support of Liz, Paula, Bodil, Richard and Steve. I acknowledge the help and encouragement of my sweetheart Jenny, my sister Catherine, my brother Kieran and my parents. It is to my family that I dedicate this thesis.

Declaration

Except where reference is made to the work of others, the research described in this thesis is original. Some of this research was carried out in collaboration. This thesis is not substantially the same as any that I have submitted for a degree or diploma or other qualification at any other University. I further state that no part of my thesis has already been or is being concurrently submitted for any such degree, diploma or other qualification. Some of the research in this thesis has been, or is to be, published. The results of Sect. 1.7 are in [Ho]. Some of Sect. 2.1 and 2.2 and most of 3.2 are in [HS1]; the aside in Sect. 2.1 is mostly to be found in [HS5]. Sections 2.3 and 2.4 and some of 2.5 are in [HS2], Sections 2.6, 3.5 and 3.6 are in [HS3]. Results from Sect. 2.7 and 2.8 are in [HMS]. Section 3.4 is in [HS4]. The solutions of the D_2 3×3 Nahm equations have not been published, special cases have appear in [HS3] and [HS5].

- [Ho] C.J. Houghton, Phys. Rev. D **56** (1997) 1120.
- [HMS] C.J. Houghton, N.S. Manton and P.M. Sutcliffe, hep-th/9705151, Nucl. Phys. **B**.
- [HS1] C.J. Houghton and P.M. Sutcliffe, Commun. Math. Phys. **180** (1996) 342.
- [HS2] C.J. Houghton and P.M. Sutcliffe, Nonlinearity **9** (1996) 385.
- [HS3] C.J. Houghton and P.M. Sutcliffe, Nucl. Phys. **B464** (1996) 59.
- [HS4] C.J. Houghton and P.M. Sutcliffe, Nonlinearity **9** (1996) 1609.
- [HS5] C.J. Houghton and P.M. Sutcliffe, J. Maths. Phys. **38** (1997) 5576.

Contents

1	Monopoles and the Nahm equations	1
1.1	Bogomolny-Prasad-Sommerfield monopoles	4
1.2	The Nahm equations	7
1.3	Solving the Nahm equations	8
1.4	The eigenvector bundle	14
1.5	Spectral curves, monopoles and Nahm data	16
1.6	Other gauge groups	18
1.7	New hyperKähler manifolds	22
1.7.1	Dancer’s family of hyperKähler manifolds	23
1.7.2	A new family of hyperKähler manifolds	27
1.7.3	Nonsingularity of the new hyperKähler manifolds	28
1.7.4	Other fixed monopole spaces	31
1.7.5	Applications	32
1.7.6	A note on $([1], 2, [1])$ -monopoles	36
2	Symmetric Monopoles	39
2.1	Tetrahedral and cubic monopoles	41
2.1.1	Platonic symmetries	42
2.1.2	Tetrahedral 3-monopole and cubic 4-monopole	43
2.1.3	Tetrahedral $(3, [2], [1])$ -monopoles	45
2.2	Symmetric Nahm data	49
2.3	Dodecahedral 7-monopole	52

2.4	Octahedral 5-monopole	59
2.5	Monopoles and rational maps	63
2.5.1	The Donaldson rational map and symmetry	64
2.5.2	C_{4h} 5-monopoles, an example	67
2.6	Twisted line scattering	69
2.7	Symmetry and the Jarvis rational map	72
2.7.1	The tangent space to a symmetric monopole	80
3	Elliptic solutions to the Nahm equations	83
3.1	The genus one cases	84
3.2	Tetrahedral 4-monopoles	87
3.3	D_2 3-monopoles	95
3.4	Inversion symmetric 3-monopoles	102
3.5	Twisted line scattering of 3-monopoles	106
3.6	The zeros of the Higgs field	111
4	Conclusions	119
4.1	Symmetric multimonopoles	119
4.2	Nahm data and new hyperKähler manifolds	121
4.3	Multimonopoles and Skyrmons	122

List of Figures

1.1	Axially symmetric 2-monopole	6
1.2	Period rectangles for the Jacobi elliptic functions	11
1.3	The Jacobi elliptic functions	12
1.4	Two unfixed monopoles and a fixed one	26
1.5	Two unfixed monopoles and two fixed ones	28
1.6	Table of dimensions for the threebrane and fivebrane configuration	33
1.7	A typical configuration of branes	33
1.8	The fivebrane and threebrane configuration equivalent to $N(\boldsymbol{\lambda}, \boldsymbol{\mu})$	35
1.9	The fivebrane and threebrane configuration equivalent to $M(\boldsymbol{\lambda})$	35
1.10	The space \mathfrak{K}	38
2.1	Invariant polynomials	44
2.2	Tetrahedral 3-monopole	46
2.3	Cubic 4-monopole	47
2.4	Tetrahedral scattering of a $(3, [2], [1])$ -monopole	48
2.5	Dodecahedral 7-monopole	58
2.6	Octahedral 5-monopole	63
2.7	Schematic representation of twisted line scattering	71
3.1	Schematic representation of 4-monopole scattering	93
3.2	Tetrahedral 4-monopole scattering	94
3.3	Head-on scattering geodesics	96
3.4	The α -sphere of D_2 symmetric rational maps	97

3.5	The northern hemisphere of the α -sphere	98
3.6	The (x, y) region corresponding to the shaded wedge	102
3.7	Scattering of inversion symmetric 3-monopoles	107
3.8	Rotating 3-monopole	108
3.9	Twisted line scattering of 3-monopoles	109
3.9	continued.	110
3.10	Components of the Higgs field of the tetrahedral 3-monopole	113
3.11	Energy density of the tetrahedral 3-monopole	114
3.12	Motion of zeros of the Higgs field during twisted line scattering	115
3.13	Components of the Higgs field for a 3-monopole with seven zeros 1	117
3.14	Components of the Higgs field for a 3-monopole with seven zeros 2	118
4.1	Two Skyrmions attracting	122
4.2	Three Skyrmions	123

Chapter 1

Monopoles and the Nahm equations

The Euler-Poinsot equations for the motion of a spinning top in the absence of an external field are both solvable and nonlinear. Although this thesis concerns monopoles, the techniques that are used often originate with the Euler-Poinsot equations. This is because Bogomolny-Prasad-Sommerfield (BPS) monopoles are solutions to the Bogomolny equation, this equation is equivalent to the Nahm equations and the Nahm equations are, in turn, spinning top equations.

In SU_2 Yang-Mills-Higgs theory, with a suitable symmetry breaking potential, the classical Euler-Lagrange equations have solutions which are topological solitons. Far from these solitons, the Higgs field is approximately constant and breaks the SU_2 theory to a U_1 theory. Here, a conventional magnetic field can be defined and from a great distance the solitons resemble Dirac monopoles. This is why the solitons are called magnetic monopoles. Unlike a Dirac monopole, however, a solitonic monopole is smooth and has an extended core. It is outside of this core that it resembles a point source of scalar and magnetic fields.

The topological enumeration of solitonic magnetic monopoles relies on the asymptotic symmetry breaking due to the Higgs potential. However, if the symmetry breaking is adopted as a boundary condition, this enumeration can occur without Higgs self-coupling. In the past, it was common to imagine this boundary condition as the residuum of a now-removed symmetry breaking potential. This zero self-coupling case is called the Prasad-Sommerfield limit [PS].

In the Prasad-Sommerfield limit, there is a first order equation for static minimum energy solutions [Bo]. This is the Bogomolny equation. Solutions of the Bogomolny equation necessarily solve the Euler-Lagrange equations. Unlike the Euler-Lagrange equations, the Bogomolny equation is integrable. Its solutions are classified by the topological charge; a topological charge k solution is called a k -monopole. Remarkably, there is a $(4k - 1)$ -dimensional space of gauge inequivalent k -monopoles. Although the moduli space is the space of static monopoles, a monopole in motion can be approximated by a static monopole, if the motion is sufficiently slow. Furthermore, the motion itself is approximated by geodesic flow in the moduli space [Ma2, St].

The monopole moduli space is isometrically diffeomorphic to the moduli space of solutions to the Nahm equations. These are a set of ordinary nonlinear differential equations for three matrix valued functions known as Nahm data. The Nahm equations are described in Sect. 1.2 and the equivalence of Nahm data and BPS monopoles is discussed in Sect. 1.5.

The Nahm data are known for 2-monopoles. In this case the Nahm equations reduce to the Euler-Poincaré equations and are solved by elliptic functions. This is described in Sect. 1.3. The Euler-Poincaré equations are the subject of considerable historic investigation. In Sect. 1.4, it is explained why, from general arguments, it is unsurprising that their solutions are elliptic.

The final introductory section is Sect. 1.6. It explains the Nahm equations for SU_n BPS monopoles. If the unbroken gauge group is SU_n and the boundary conditions break this to the maximal torus, then monopoles corresponding to different U_1 's in the maximal torus are distinct. Each distinct monopole type has its own Nahm data.

SU_n monopoles are used in Sect. 1.7 to construct new hyperKähler manifolds. Monopole moduli spaces are essentially hyperKähler manifolds. HyperKähler manifolds are manifolds with anticommuting complex structures and are of contemporary interest. Those hyperKähler manifolds which are monopole moduli spaces have a natural isometric SO_3 action: rotation of the monopole in space. In Sect. 1.7, it is noted that this SO_3 isometry can be broken. Because monopoles corresponding to different U_1 factors are distinct, it

is possible to independantly change the mass of one type of monopole. The infinite mass limit breaks the SO_3 isometry and yields a new hyperKähler manifold. This construction may lead to a great number of new hyperKähler manifolds. However, because the Nahm equations are not solved in general, only two cases are studied. These are the cases where two monopoles of one type have finite mass and either one or two monopoles of distinct type are fixed by infinite mass. It is found that the resulting hyperKähler manifolds are nonsingular for most, but not all, fixed monopole positions.

A multimonopole is a monopole of charge higher than two. Until recently, few multimonopoles were known. In Chapter 2, there are new multimonopoles. These multimonopoles are discovered as Nahm data. They have large symmetries; the symmetries of Platonic solids. The symmetry is imposed to simplify the Nahm equations to the point of tractability. In fact, the Nahm data are elliptic. By using symmetry, it is also possible to discuss some low energy scattering processes during which these monopoles are formed.

In Chapter 3, it is explained why the Nahm data of Chapter 2 are elliptic. This follows from the same general argument as that used to explain why the 2-monopole Nahm data are elliptic. Once this is understood, it is possible to seek all multimonopoles with elliptic Nahm data. This search leads to the discovery of a one-parameter family of 4-monopoles and a two-parameter family of 3-monopoles. When some of these new 3-monopoles are examined, it is found that the fields have a surprising characteristic: the Higgs field has anti-zeros.

The reader wishing to learn about BPS monopoles is recommended the introductory material in the thesis of Samols [Sa]. The approximation of low energy dynamics by geodesic flow in the moduli space is very elegantly reviewed there. The book by Atiyah and Hitchin [AH] is essential reading. In addition to the important results it contains concerning the 2-monopole metric, it also reviews the mathematical treatment of BPS monopoles and describes the geometry of moduli spaces. The introductory part of [HMM] also reviews the mathematical tools available to the student of monopoles. The book by Audin [A] is a very rewarding exposition of integrable equations. The use of integrable equation methods in the context of monopoles is explained in [Hi3]. This book also describes the hyperKähler

quotient, another good description of which is given in [GRG].

1.1 Bogomolny-Prasad-Sommerfield monopoles

The Bogomolny equation is

$$D_i \Phi = -\frac{1}{2} \epsilon_{ijk} F_{jk}, \quad (1.1)$$

In the simplest case, $D_i = \frac{\partial}{\partial x_i} + [A_i, \cdot]$ is the \mathbf{R}^3 covariant derivative, A_i is an \mathfrak{su}_2 adjoint representation gauge potential and $F_{ij} = \frac{\partial}{\partial x_i} A_j - \frac{\partial}{\partial x_j} A_i + [A_i, A_j]$. Φ is the Higgs field, an \mathfrak{su}_2 scalar field. The adjoint gauge action is

$$\begin{aligned} \Phi &\rightarrow g \Phi g^{-1} \\ A_i &\rightarrow g A_i g^{-1} + g \frac{\partial g^{-1}}{\partial x_i} \end{aligned} \quad (1.2)$$

where $g \in \text{SU}_2$.

The asymptotic boundary conditions

$$|\Phi| = 1 - \frac{k}{2r} + O(r^{-2}) \quad (1.3)$$

$$\frac{\partial |\Phi|}{\partial \Omega} = O(r^{-2}) \quad (1.4)$$

$$|D\Phi| = O(r^{-2}) \quad (1.5)$$

are imposed. r is the radial coordinate, (1.4) refers to angular derivatives and $|\cdot|$ is the \mathfrak{su}_2 norm: $|\Phi| = \sqrt{-\frac{1}{2} \text{trace} \Phi^2}$. The most striking of these conditions is the first: (1.3), it gives a topological classification of Φ . Φ is a map from \mathbf{R}^3 into $\mathfrak{su}_2 \cong \mathbf{R}^3$ and since (1.3) requires $|\Phi| \sim 1$ for large r , Φ maps the large sphere at large r onto the unit sphere in \mathfrak{su}_2 . The degree of this map is the topological charge, k ; the soliton with this charge is a k -monopole. A k -monopole has energy $4\pi k$ and Φ has k zeros, counted with their multiplicity.

In the 1-monopole case, the explicit solution to the Bogomolny equation is known [PS].

The fields are

$$\Phi^a = \left(\frac{1}{\tanh r} - \frac{1}{r} \right) \frac{x^a}{r} \quad (1.6)$$

$$A^{ia} = -\epsilon^{aij} \frac{x^j}{r^2} \left(1 - \frac{r}{\sinh r}\right).$$

where $\Phi = \Phi^a \tau^a$, $A_\mu = A_\mu^a \tau^a$ and $\tau^a = \frac{i}{2} \sigma^a$ are the generators of \mathfrak{su}_2 . These fields are spherically symmetric, in that a spatial rotation is a gauge transformation. At the origin the Higgs field has a zero and the energy has a maximum. The solution may be translated to give a 1-monopole located at different points in space.

In [JT], it is proved that there are k -monopole solutions which resemble many 1-monopoles at great mutual separations. The corpuscular nature of the solutions is apparent in such well-separated examples. A well-separated k -monopole is composed of k individual monopoles, each being a source of magnetic and scalar forces. The existence of such solutions relies on there being no net static forces: the magnetic force cancels with the scalar force. Historically, the observation by Manton of this cancellation [Ma1] gave the first clue that there exists continuous spaces of k -monopoles .

In fact, there is a $(4k - 1)$ -dimensional space, \mathcal{N}_k , of gauge inequivalent solutions of topological charge k [We1]. When these monopoles are well-separated, the $4k - 1$ parameters can be interpreted as $3k$ parameters giving the positions of the monopoles and a further $k - 1$ parameters corresponding to relative phases of the monopoles. It is easier to understand these phases if the moduli space is extended to the $4k$ -dimensional one \mathcal{M}_k obtained by adding the gauge orbit of $g = e^{-\chi\Phi}$. The 1-monopole moduli space, \mathcal{M}_1 is then four dimensional and for well-separated k -monopoles the $4k$ dimensions of \mathcal{M}_k are made up of these four parameters for each of k 1-monopoles.

In the full \mathfrak{su}_2 Yang-Mills-Higgs theory, the monopoles interact and evolve. It is argued by Manton in [Ma2] that geodesic flow on \mathcal{M}_k is a good approximation to the low energy dynamics of the full theory. The natural metric on the moduli space is induced by the kinetic energy. The calculations of Manton and Samols [MS] provide evidence for the validity of this approximation. Proof of its validity is given in [St]. The approximation is very powerful, it reduces the problem of monopole dynamics from nonlinear field theory to the geometry of a finite-dimensional manifold.

\mathcal{M}_k is an asymptotically flat hyperKähler manifold. A hyperKähler manifold is one

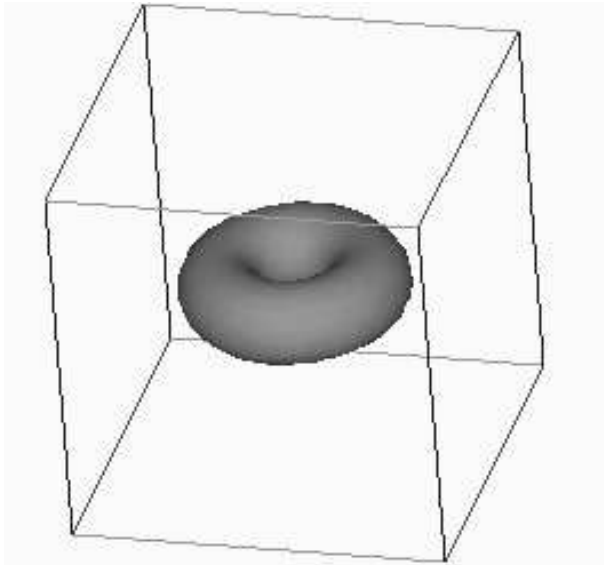


Figure 1.1: A surface of constant energy density for the axially symmetric 2-monopole.

which is Kähler with respect to three complex structures satisfying the quaternion relations. This is a restrictive structure, restrictive enough for Atiyah and Hitchin to calculate the metric on \mathcal{M}_2 [AH].

The nontrivial part of \mathcal{M}_k is contained in the geodesic submanifold, \mathcal{M}_k^0 , of k -monopole with given centre of mass and fixed overall phase. The motion of the overall phase and the centre of mass are trivial.

There is an isometric SO_3 action on \mathcal{M}_k^0 given by rotating the k -monopole about this centre of mass. Finite subgroups of this SO_3 action play a crucial role in this thesis.

Not all k -monopole solutions resemble k individual 1-monopoles. For example, the 2-monopole solution with both zeros of the Higgs field at the origin is axially symmetric and the energy is distributed around a torus. There is no way of distinguishing two individual objects in this monopole and the origin, where the two zeros of the Higgs field are located, is a saddle point of the energy, not a maximum as in the 1-monopole case. Figure 1.1 is a surface of constant energy density of this 2-monopole.

In this thesis are some further examples of k -monopoles that are not well-separated: monopoles where it is impossible to distinguish k individual objects. There are even exam-

ples where there are zeros of negative as well as positive multiplicity. These monopoles are derived from the Nahm equations.

1.2 The Nahm equations

The Nahm equations are

$$\begin{aligned}\frac{dT_1}{dt} &= [T_2, T_3], \\ \frac{dT_2}{dt} &= [T_3, T_1], \\ \frac{dT_3}{dt} &= [T_1, T_2],\end{aligned}\tag{1.7}$$

where (T_1, T_2, T_3) , the Nahm data, are a triplet of skew-Hermitian $k \times k$ matrix functions of t . They are analytic for $t \in (-1, 1)$ and are required to have simple poles at $t = -1$ and $t = 1$. It follows from the equations that the residues at these poles form a representation of \mathfrak{su}_2 and it is imposed, as a boundary condition, that these representations are irreducible.

The Nahm equations are introduced in [Nah]. It is shown there that a solution to the Nahm equations give a solution to the Bogomolny equation. In [Hi2] the moduli spaces are demonstrated to be diffeomorphic. In Sect. 1.5, the relationship of the Nahm equations with BPS monopoles is discussed. Subsequently, the Nahm data are exploited; first to construct new hyperKähler manifolds and afterwards to construct new BPS monopoles.

The Nahm equations are integrable. Their Lax formulation is discussed in Sect. 1.3. It has been noted by Ward [Wa2] that integrable equations are commonly related to the self-dual Yang-Mills equation. The Nahm equations are, in fact, the dimensional reduction of these equations to one dimension. Solutions to the self-duality equations which are independent of three directions satisfy a gauged version of the Nahm equations

$$\begin{aligned}\frac{dT_1}{dt} + [T_0, T_1] &= [T_2, T_3], \\ \frac{dT_2}{dt} + [T_0, T_2] &= [T_3, T_1], \\ \frac{dT_3}{dt} + [T_0, T_3] &= [T_1, T_2],\end{aligned}\tag{1.8}$$

where (T_0, T_1, T_2, T_3) is quadruple of skew-Hermitian matrix functions (T_0, T_1, T_2, T_3) . The gauge action is

$$T_0 \mapsto gT_0g^{-1} - \frac{dg}{dt}g^{-1}, \quad (1.9)$$

$$T_i \mapsto gT_i g^{-1}, \quad (1.10)$$

where $g \in {}_0\mathcal{G}_0$ and

$${}_0\mathcal{G}_0 = \{g \in C^w([-1, 1], U_2) : g(-1) = \mathbf{1}, g(1) = \mathbf{1}\}. \quad (1.11)$$

If T_1, T_2 and T_3 are regular for $t \in (-1, 1)$ and obey the Nahm boundary condition and T_0 is regular for $t \in [-1, 1]$ then the Nahm equations can be recovered from (1.8) by gauging T_0 to zero.

The moduli spaces of Nahm data have an isometric SO_3 action. This action is the tensor product of the natural action of SO_3 on the (T_1, T_2, T_3) triplet as an \mathbf{R}^3 vector and its action on the T_1, T_2 and T_3 as \mathfrak{u}_k matrices. Under the equivalence between $k \times k$ Nahm data and k -monopoles the isometric SO_3 action rotates the whole k -monopole. This action is not triholomorphic; it rotates the Kähler forms.

There is also an isometric \mathbf{R}^3 action on $k \times k$ Nahm data given by translating the trace:

$$T_i \mapsto T_i + i\lambda_i \mathbf{1}_k \quad (1.12)$$

where λ_1, λ_2 and λ_3 are constants. In the k -monopole space, this action translates the centre of gravity of the k -monopole. Just as in the monopole case, where attention is focused on \mathcal{M}_k^0 , it is normal to consider only centred, that is traceless, Nahm data.

1.3 Solving the Nahm equations

A skew-Hermitian 1×1 matrix function is a pure imaginary function and to solve the Nahm equations it must be constant. Therefore the data are a triplet of pure imaginary numbers. The centred data are trivial.

In the 2×2 case, the obvious ansatz is

$$T_i(t) = -\frac{i}{2}f_i(t)\sigma_i \quad (1.13)$$

where σ_i are the Pauli matrices. Substituting into the Nahm equation gives

$$\begin{aligned} \frac{df_1(t)}{dt} &= f_2(t)f_3(t), \\ \frac{df_2(t)}{dt} &= f_3(t)f_1(t), \\ \frac{df_3(t)}{dt} &= f_1(t)f_2(t). \end{aligned} \quad (1.14)$$

It is often noted that these are the Euler-Poinsot equations. The Euler-Poinsot equations for a physical spinning top are

$$\begin{aligned} \frac{d}{d\tau}g_1 &= (\lambda_3 - \lambda_2)g_2g_3, \\ \frac{d}{d\tau}g_2 &= (\lambda_1 - \lambda_3)g_3g_1, \\ \frac{d}{d\tau}g_3 &= (\lambda_2 - \lambda_1)g_1g_2; \end{aligned} \quad (1.15)$$

the λ_i are the moments of inertia and τ is time. To recover (1.14) from (1.15) τ is replaced by it . Taking $\lambda_1 = 1$, $\lambda_2 = 0$ and $\lambda_3 = 2$, (1.14) follows by substituting $f_1 = \sqrt{2}g_1$, $f_2 = \sqrt{2}g_2$ and $f_3 = ig_3$. Although not the equations for the motion of a physical spinning top, (1.14) are nonetheless referred to as Euler-Poinsot equations.

The Euler-Poinsot equations are easy to solve. There are two constants:

$$\begin{aligned} h &= f_3^2 - f_1^2, \\ p &= 2f_3^2 - f_1^2 - f_2^2. \end{aligned} \quad (1.16)$$

These are two surfaces in the \mathbf{R}^3 with coordinates f_1 , f_2 and f_3 . The solutions to (1.14) are the curves along which these surfaces intersect. In the physical case, these surfaces are ellipsoids and so the solutions, which lie at their intersections, have no poles. Here the surfaces are hyperboloids and the solutions have poles; as is required by the boundary conditions.

The equations are solved by substituting the constants into the differential equations. Choosing $f_1^2 \leq f_2^2 \leq f_3^2$ the solutions are

$$\begin{aligned} f_1(t) &= \pm \frac{D \operatorname{cn}_k D(t + \tau)}{\operatorname{sn}_k D(t + \tau)}, \\ f_2(t) &= \pm \frac{D \operatorname{dn}_k D(t + \tau)}{\operatorname{sn}_k D(t + \tau)}, \\ f_3(t) &= \pm \frac{D}{\operatorname{sn}_k D(t + \tau)}, \end{aligned} \tag{1.17}$$

where all the signs are minus or two of them are plus and $D = \sqrt{h}$. The functions $\operatorname{sn}_k u$, $\operatorname{cn}_k u$ and $\operatorname{dn}_k u$ are the Jacobi elliptic functions.

Elliptic functions are meromorphic biperiodic complex functions. Since the quotient of the complex plane by their period lattice is a torus, they may also be regarded as periodic functions over the torus. Nonconstant elliptic function can never be holomorphic. Furthermore, the sum of residues in any period cell must be zero, so the simplest elliptic functions have either two simple poles or one double pole. The Jacobi functions are elliptic functions of the former type, Weierstrass functions of the latter. In calculations involving elliptic functions, the Jacobi or Weierstrass functions are used.

Any elliptic function can be expressed as a rational function of the Weierstrass function and its derivative. One way to define the Weierstrass function is to write down the simplest function with the desired properties: a double pole and two periods, $2\omega_1$ and $2\omega_2$,

$$\wp(z) = \frac{1}{z^2} + \sum_{(n,m) \neq (0,0)} \left[\frac{1}{(z - 2m\omega_1 - 2n\omega_2)^2} - \frac{1}{(2m\omega_1 + 2n\omega_2)^2} \right]. \tag{1.18}$$

This function satisfies the differential equation

$$\left(\frac{d\wp}{dz} \right)^2 = 4\wp^3 - g_2\wp - g_3. \tag{1.19}$$

(\wp, \wp') are (x, y) coordinates on the genus one curve

$$y^2 = 4x^3 - g_2x - g_3. \tag{1.20}$$

The factors of the cubic are named e_1 , e_2 and e_3 . If the discriminant of the cubic is positive these e_i are all real and distinct. They are conventionally ordered $e_1 > e_2 > e_3$. When

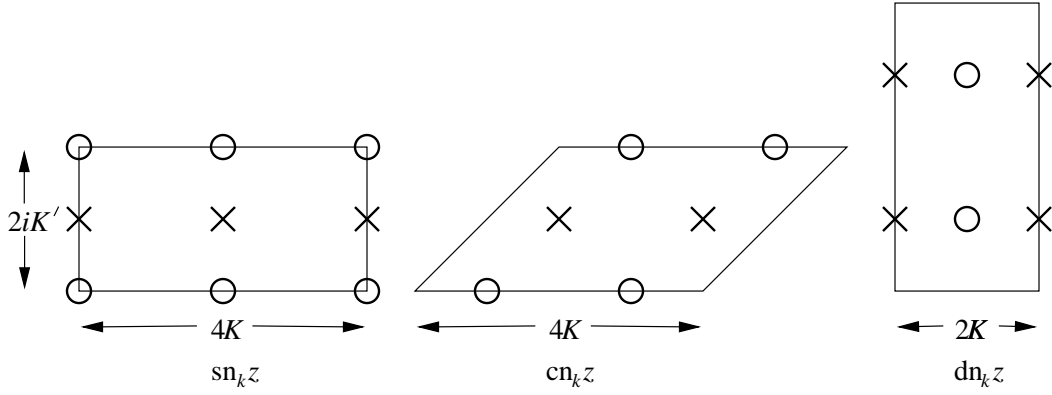


Figure 1.2: Period rectangles for the Jacobi elliptic functions, the crosses mark poles and the circles mark zeros.

$\wp(z) = e_i$ it has vanishing derivative and such points are known to lie on the half periods ω_1 , ω_2 and $\omega_3 = -\omega_1 - \omega_2$. Expressing (1.19) as an integral it follows that

$$\omega_1 = \int_{e_1}^{\infty} \frac{dt}{\sqrt{4t^3 - g_2t - g_3}} \quad (1.21)$$

and

$$\omega_3 = -i \int_{\infty}^{e_3} \frac{dt}{\sqrt{4t^3 - g_2t - g_3}}. \quad (1.22)$$

ω_1 is real and ω_3 is pure imaginary. The discriminant approaches zero as either e_3 approaches e_2 or e_2 approaches e_1 . In the former case the imaginary period becomes infinite and in the latter case the real period becomes infinite. For negative discriminant, two of the e_i are complex and so the period parallelogram is not rectangular.

The Jacobi functions are called $\text{sn}_k z$, $\text{cn}_k z$ and $\text{dn}_k z$. They have the appealing property that $\text{sn}_k z$ and $\text{cn}_k z$ degenerate to the circular functions $\sin z$ and $\cos z$ when the imaginary period is infinite. The parameter k is the elliptic modulus, $0 \leq k \leq 1$ and the imaginary period is infinite when $k = 0$. Figure 1.2 illustrates the location of the poles and zeros of the Jacobi functions in their period parallelograms. The period parallelograms are rectangular and the periods depend on K and K' where

$$K = \int_0^1 \frac{dt}{\sqrt{1-t^2}\sqrt{1-k^2t^2}} \quad (1.23)$$

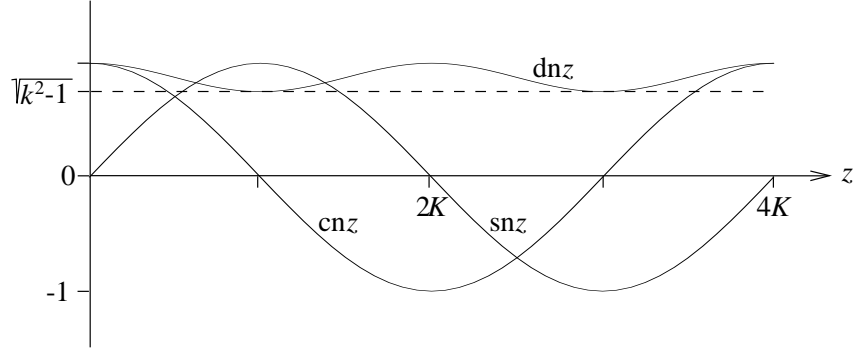


Figure 1.3: The Jacobi elliptic functions with real argument z .

and

$$K' = \int_0^1 \frac{dt}{\sqrt{1-t^2}\sqrt{1-(1-k^2)t^2}}. \quad (1.24)$$

Figure 1.3 represents the Jacobi functions along a real period. The Jacobi elliptic functions satisfy the differential equation

$$\frac{d \operatorname{sn}_k z}{dz} = \operatorname{cn}_k z \operatorname{dn}_k z \quad (1.25)$$

and the identities

$$\begin{aligned} \operatorname{sn}_k^2 z + \operatorname{cn}_k^2 z &= 1, \\ k^2 \operatorname{sn}_k^2 z + \operatorname{dn}_k^2 z &= 1. \end{aligned} \quad (1.26)$$

A classic book concerning elliptic functions is [WW]. [BF] is also useful.

To solve the Nahm equations, it is now necessary to choose τ and h in (1.17) so that the boundary conditions are satisfied. There is a simple pole at $t = -1$ if $\tau = 1$ and a simple pole at $t = 1$ if $D = K(k)$. The residues at the poles are the standard basis of $\underline{2}$, the two-dimensional representation of \mathfrak{su}_2 .

This solves the Euler-Poinsot equations (1.14) to give 2×2 Nahm data. The equations are solvable because of the constants h and p . These constants may be found by inspection. It is more interesting, however, to realise they may be found using the Lax formulation. The Nahm equations are equations of spinning top type. That is, they may be rewritten

as a Lax equation with a spectral parameter. This treatment of the Nahm equations is due to Hitchin [Hil]. From the Nahm equations

$$\frac{d(T_1 + iT_2)}{dt} = [iT_3, T_1 + iT_2]. \quad (1.27)$$

This means that $T_1 + iT_2$ evolves by conjugation. From (1.27), $\text{trace}[(T_1 + iT_2)^n]$ is constant for any n and so the eigenvalues of $T_1 + iT_2$ are constants. In fact, isospectral evolution is a property of the Lax equation; if

$$\left[\frac{d}{dt} + B, A\right] = 0 \quad (1.28)$$

then the eigenvalues of A are constant.

In choosing the combination $T_1 + iT_2$ in equation (1.27) a choice of direction in the triplet (T_1, T_2, T_3) is made. There is a whole sphere of such directions and a Lax equation for each direction. The sphere of directions may be taken as the Riemann sphere \mathbf{P}^1 with inhomogeneous coordinate ζ , ζ then parameterizes a family of Lax equations

$$\left[\frac{d}{dt} - iT_3 - i(T_1 - iT_2)\zeta, -i(T_1 + iT_2) + 2iT_3\zeta + i(T_1 - iT_2)\zeta^2\right] = 0. \quad (1.29)$$

Thus, the eigenvalues of $-i(T_1 + iT_2) + 2iT_3\zeta + i(T_1 - iT_2)\zeta^2$ are constants. For $k \times k$ data there will, in general, be k eigenvalues and so, since ζ is a coordinate over a sphere, the eigenvalues give a k -fold branched covering of the sphere. This is the algebraic curve, P , with equation

$$P(\eta, \zeta) = \det(\eta + i(T_1 + iT_2) - 2iT_3\zeta - i(T_1 - iT_2)\zeta^2) = 0. \quad (1.30)$$

This algebraic curve is independent of t and, since it is a curve of eigenvalues, it is called a spectral curve.

In the 2×2 example considered above the spectral curve is

$$\eta^2 + \frac{1}{4}[(f_2^2 - f_1^2)(\zeta^4 + 1) + 2(f_1^2 + f_2^2 - 2f_3^2)\zeta^2] = 0. \quad (1.31)$$

The coefficients give the constants h and p above. In fact, by substitution, the curve above is

$$\eta^2 + \frac{(1 - k^2)K(k)^2}{4} \left(\zeta^4 - 2\frac{1 + k^2}{1 - k^2}\zeta^2 + 1\right) = 0. \quad (1.32)$$

It is a double covering of the sphere branched at the four solutions of

$$\zeta^4 - 2\frac{1+k^2}{1-k^2}\zeta^2 + 1 = 0. \quad (1.33)$$

These branch points are connected pairwise by branch cuts and the resulting Riemann surface is a torus.

By inspecting the determinant formula (1.30), it is seen that the spectral curve, $P(\eta, \zeta)$, for $k \times k$ data has the form

$$\eta^k + a_1(\zeta)\eta^{k-1} + \dots + a_{k-1}(\zeta)\eta + a_k(\zeta) = 0 \quad (1.34)$$

where $a_i(\zeta)$ is a degree $2i$ polynomial in ζ . If the data are centred, $a_1(\zeta) = 0$. The curve is compact and its genus can be calculated from the Riemann-Hurwitz relation. This relates the genera of two Riemann surfaces M and N between which there is a holomorphic map $f: M \rightarrow N$. If M has genus g , N genus γ and f is a degree n map then

$$2 - 2g = n(2 - 2\gamma) - B \quad (1.35)$$

where B is the branching number of the map. A branch point is a point common to a number of sheets. The branching number of a branch point is one less than number of sheets to which it is common. The branching number of a map is the sum of the branching numbers of all the branch points. The map $(\eta, \zeta) \mapsto \zeta$ from the spectral curve (1.34) to the sphere is degree k and in general has branching points of branching number $k - 1$ at each root of $a_k(\zeta)$, so since the sphere has genus zero, the spectral curve has genus $(k - 1)^2$.

1.4 The eigenvector bundle

There is a distinguished line bundle over the spectral curve, P , given by eigenvectors. There is an eigenvector of $-i(T_1 + iT_2) + 2iT_3\zeta + i(T_1 - iT_2)\zeta^2$ at each point (η, ζ) . This eigenvector is not independent of t and so the eigenvector line bundle evolves with t . What is amazing is that this line bundle evolves linearly with t .

Let $E(t)$ be the eigenvector bundle over $P(\eta, \zeta)$. It is proved in [AvanM1, AvanM2] that

$$E(t) = E(0) \otimes F(t) \quad (1.36)$$

where $F(t)$ is the degree zero line bundle over P defined by the transition function

$$a(\eta, \zeta, t) = e^{\frac{t\eta}{\zeta}} \quad (1.37)$$

on $\mathcal{U}_0 \cap \mathcal{U}_\infty$. \mathcal{U}_0 and \mathcal{U}_∞ are the neighbourhoods of the spectral curve lying over U_0 and U_∞ , the usual $\zeta \neq 0$ and $\zeta \neq \infty$ coordinate neighbourhoods on \mathbf{P}^1 .

The space of degree zero line bundles over a Riemann surface Γ , $\text{Pic}^0 \Gamma$, is known. It is the subject of the classic results of Jacobi and Abel. The space of degree zero line bundles is isomorphic to the Jacobian variety, $\text{Jac } \Gamma$:

$$\text{Pic}^0 \Gamma \cong \text{Jac } \Gamma \quad (1.38)$$

The Jacobian variety of a Riemann surface of genus g is the g -torus \mathbf{C}^g/Λ where Λ is a lattice calculated by integrating the holomorphic one-forms of the surface over its homology cycles.

Thus, the evolution $E(t)$ defines a curve in $\text{Jac } P$ corresponding to $F(t)$. The Jacobian variety is defined by the spectral curve as a quotient of \mathbf{C}^g by a lattice. It derives coordinates from this \mathbf{C}^g . The definition of these coordinates is independent of the eigenbundle flow. Nonetheless, under the natural map into $\text{Jac } P$ from $\text{Pic}^0 \Gamma$, $F(t)$ is linear.

The linearization of the Nahm equations on the Jacobian variety of its spectral curve follows from their having a Lax formulation. It is a feature of many of those nonlinear equations which can be formulated as a Lax equation with a spectral parameter, that they are linearized on the Jacobian variety of their spectral curve. This is the culmination of the research of integrable systems which began with the spinning tops of Euler, Lagrange and Kowalevski. One of the achievements of [Hi2] is the addition of the Nahm equations to the list of such equations. A excellent book concerning spinning tops is [A].

This linearization explains why it is easy to solve the 2×2 Nahm equations. The spectral curve has genus one. Therefore, its Jacobian variety is a one-torus. The solutions to the 2×2 Nahm equations are linear on this Jacobian variety and so the complex coordinate on the Jacobian variety can be identified with the variable t for the Nahm equations if this variable is regarded as complex rather than real. With t complex, the Nahm data

are meromorphic matrix functions with simple poles and so the solutions to the Nahm equations are meromorphic functions over the Jacobian variety. The Jacobian variety is a torus and the meromorphic functions over a torus are elliptic function. Therefore, the solutions to the 2×2 Nahm equations are elliptic. Thus, the 2×2 Nahm equations are integrable, two constants are given by the spectral curve and the solutions are elliptic functions.

1.5 Spectral curves, monopoles and Nahm data

There is also a spectral curve associated with monopoles and it is introduced in [Hi1]. In [Hi2] it is proved that the monopole spectral curve and the Nahm data spectral curve are the same. A useful account is given in [Hi3].

The space of oriented lines in \mathbf{R}^3 is $T\mathbf{P}^1$, the tangent bundle to \mathbf{P}^1 . A tangent has coordinate $\eta \frac{d}{d\zeta}$ and (η, ζ) are coordinates on $T\mathbf{P}^1$. The corresponding line has direction given by ζ and pierces a perpendicular complex plane through the origin at η .

A line bundle is defined over $T\mathbf{P}^1$ by the decaying solution to the Hitchin equation. Let s be the distance along some line u . The Hitchin equation is the one-dimensional Dirac equation along that line:

$$(D_u - i\Phi)\mathbf{v}(s) = 0, \quad (1.39)$$

where, D_u denotes the covariant derivative along u . The space of solutions along the line is two dimensional so, by considering all lines, a rank two vector bundle E is defined over $T\mathbf{P}^1$. The asymptotic boundary conditions on the monopole fields (A_i, Φ) allow this equation to be solved asymptotically. In a suitable gauge, the Hitchin equation is

$$\left[\frac{d}{ds} + \left(1 - \frac{k}{2s}\right) \begin{pmatrix} -1 & 0 \\ 0 & 1 \end{pmatrix} + O(s^{-2}) \right] \mathbf{v}(s) = 0 \quad (1.40)$$

for large s . This has a decaying solution

$$\mathbf{v}(s) = e^{-s} s^{\frac{k}{2}} \begin{pmatrix} 0 \\ 1 \end{pmatrix} \quad (1.41)$$

and so there is a one-dimensional subspace of the solutions along the line which decay for $s \rightarrow \infty$. This distinguishes a holomorphic line subbundle $L^+ \subset E$. In the same way, there is a holomorphic line bundle, $L^- \subset E$, of solutions which decay $s \rightarrow -\infty$. The curve in TP^1 along which these line bundles coincide is the spectral curve of the monopole. It is the curve of lines along which the Hitchin equation has $L^2(-\infty, \infty)$ solutions.

The construction of the monopole fields from their Nahm data also requires the solutions of a Dirac equation. The process of constructing monopole fields from Nahm data is known as the Atiyah-Drinfeld-Hitchin-Manin-Nahm (ADHMN) construction. It is so named because it is Nahm's extension to monopoles of the Atiyah-Drinfeld-Hitchin-Manin construction of self-dual Yang-Mills instantons [Nah, ADHM]. The Dirac equation to be solved is consequently known as the ADHMN equation. It is the ordinary differential equation

$$[\mathbf{1}_{2k} \frac{d}{dt} + \frac{1}{2}(\mathbf{1}_k \otimes x_j \sigma_j + iT_j \otimes \sigma_j)]\mathbf{v}(t) = 0 \quad (1.42)$$

for the complex $2k$ -vector $\mathbf{v}(t)$. (x_1, x_2, x_3) is the point in space at which the monopole fields are being calculated. The solutions of (1.42) are required to be normalizable with respect to the inner product

$$\langle \mathbf{v}_1, \mathbf{v}_2 \rangle = \int_{-1}^1 \mathbf{v}_1^\dagger \mathbf{v}_2 dt. \quad (1.43)$$

It can be shown that the space of normalizable solutions to (1.42) has two complex dimensions. If $\widehat{\mathbf{v}}_1, \widehat{\mathbf{v}}_2$ is an orthonormal basis for this space then the Higgs field Φ is given by

$$\Phi = \frac{i}{2} \begin{pmatrix} \langle t\widehat{\mathbf{v}}_1, \widehat{\mathbf{v}}_1 \rangle & \langle t\widehat{\mathbf{v}}_1, \widehat{\mathbf{v}}_2 \rangle \\ \langle t\widehat{\mathbf{v}}_2, \widehat{\mathbf{v}}_1 \rangle & \langle t\widehat{\mathbf{v}}_2, \widehat{\mathbf{v}}_2 \rangle \end{pmatrix} \quad (1.44)$$

with a similar expression for the gauge potential.

The Hitchin equation and the ADHMN equations are similar. In fact, mirroring the construction of the monopole fields from the Nahm data is a construction, via the Hitchin equation, of Nahm data from the monopole fields. This is discussed by Nahm in [Nah]. It is also discussed by Corrigan and Goddard in [CG] where they refer to the phenomenon as reciprocity.

The spectral curve of a 1-monopole located at (x_1, x_2, x_3) is

$$\eta - (x_1 + ix_2) + 2x_3\zeta + (x_1 - ix_2)\zeta^2 = 0. \quad (1.45)$$

This spectral curve corresponds to all lines through the point (x_1, x_2, x_3) , the centre of the 1-monopole. It is known as the star.

The precise conditions that an algebraic curve in $T\mathbf{P}^1$ must satisfy if it is a spectral curve are given in [Hi2]. The most obvious condition is reality. There is a real structure on $T\mathbf{P}^1$ given by lifting the antipodal map on \mathbf{P}^1 to the tangent bundle. In (η, ζ) coordinates it is

$$\tau : (\eta, \zeta) \mapsto \left(\frac{-\bar{\eta}}{\zeta^2}, \frac{-1}{\bar{\zeta}} \right) \quad (1.46)$$

and it is equivalent in the space of oriented lines in \mathbf{R}^3 to reversing the line orientation. If the Hitchin equation on an oriented line has $L^2(-\infty, \infty)$ solutions, it has $L^2(-\infty, \infty)$ on the same line with the other orientation, this means that the spectral curve is invariant under the reality transformation. As a consequence, the a_i in (1.34) satisfy

$$a_i(\zeta) = (-1)^i \overline{\zeta^{2i} a_i\left(-\frac{1}{\bar{\zeta}}\right)}. \quad (1.47)$$

A general real algebraic curve of the form (1.34) has $(k+1)^2 - 1$ degrees of freedom. However, the requirement that $L^+ = L^-$ on the spectral curve results in $(k-1)^2$ constraints; reducing the number of degrees of freedom to $4k - 1$. There are further conditions on the spectral curve related to the existence of the eigenbundle. These conditions are to be found in [Hi2]. In [Hu1] these conditions are applied to a general $k = 2$ algebraic curve to calculate the 2-monopole spectral curve. It is, of course, the Lax curve (1.32).

1.6 Other gauge groups

BPS monopoles are not unique to SU_2 gauge theory. For SU_n monopoles the Higgs field Φ is an \mathfrak{su}_n valued scalar field and A_i is an \mathfrak{su}_n gauge potential. There is an SU_n gauge action on these fields, broken by the asymptotic Higgs field. If SU_n is broken to the maximal torus U_1^{n-1} the Higgs field at infinity is required to lie in the gauge orbit of

$$\Phi_\infty = i \text{diag}(t_1, t_2, \dots, t_n). \quad (1.48)$$

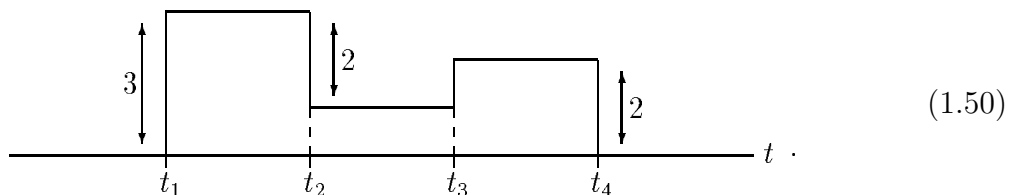
By convention $t_1 < t_2 < \dots < t_n$ and, since Φ is traceless, $t_1 + t_2 + \dots + t_n = 0$. Because of the asymptotic condition on Φ , it gives a map from the large sphere at infinity into the quotient space

$$\text{orbit}_{\text{SU}_n} \Phi_\infty = \text{SU}_n / \text{U}_1^{n-1}. \quad (1.49)$$

Since $\pi_2(\text{SU}_n / \text{U}_1^{n-1}) = \mathbf{Z}^{n-1}$ the moduli space of monopoles is divided, topologically, into sectors labelled by $n - 1$ topological charges, k_i . The maximal torus of SU_n is generated by the Cartan space and the matrix Φ_∞ defines a direction in this Cartan space. This direction picks out a unique set of simple roots in the Cartan space: those whose inner product with Φ_∞ is positive. Each U_1 in the maximal torus is generated by one of these simple roots. The k_i are then ordered by the requirement that adjacent k_i 's correspond to nonorthogonal roots. A monopole with topological charge $(k_1, k_2, \dots, k_{n-1})$ is called a $(k_1, k_2, \dots, k_{n-1})$ -monopole.

In this section the Nahm data corresponding to a $(k_1, k_2, \dots, k_{n-1})$ -monopole are explained. The Nahm description of such monopoles is very useful, it encapsulates how SU_n monopoles differ for different n . This, however, is not discussed in this thesis. The main use made of the general SU_n Nahm formulation is the construction, in Sect. 1.7, of new hyperKähler manifolds. In that section the known 2×2 data is reemployed in the context of SU_3 and SU_4 data to investigate two families of hyperKähler manifolds.

The Nahm data corresponding to a $(k_1, k_2, \dots, k_{n-1})$ -monopole are a triplet of skew-Hermitian matrix functions defined over the interval $[t_1, t_n]$. The t_i 's subdivide the interval into $n - 1$ abutting subintervals. For a $(k_1, k_2, \dots, k_{n-1})$ -monopole a skyline diagram is drawn: a step function over the interval whose height on the i 'th subinterval is k_i . For example, a $(3, 1, 2)$ -monopole in an SU_4 theory has diagram



The Nahm triplet is now a triplet of square matrix functions of t of different size over different subintervals. The size of the Nahm matrices in a subinterval is given by the height

of the skyline in that interval. The matrices must satisfy the Nahm equations (1.7) in each subinterval.

The boundary conditions now relate the Nahm matrices in abutting subintervals. For the purpose of explaining these conditions let us consider the skyline diagram

$$\begin{array}{c}
 \text{---} \\
 \uparrow k_1 \\
 \text{---} \\
 \downarrow k_2 \\
 \text{---} \\
 t = \tau
 \end{array}
 \quad (1.51)$$

The skyline is k_1 high to the left of τ and $k_2 < k_1$ high to the right of it. Thus, the Nahm triplet, (T_1, T_2, T_3) , is a triplet of $k_1 \times k_1$ matrices over the left interval and of $k_2 \times k_2$ matrices over the right interval. As t approaches τ from the left, it is required that

$$T_i(s) = \begin{pmatrix} R_i/s + O(1) & O(s^{(m-1)/2}) \\ O(s^{(m-1)/2}) & T'_i + O(s) \end{pmatrix} \quad (1.52)$$

where $s = \tau - t$, $m = k_1 - k_2$ and the $k_2 \times k_2$ matrix T'_i is the nonsingular limit of the right interval Nahm data at $t = \tau$. The $m \times m$ residue matrices R_i in (1.52) must form the irreducible m -dimensional representation of \mathfrak{su}_2 . Since the one-dimensional representation is trivial, there is no singularity when $m = 1$. When k_1 is less than k_2 the conditions are almost the same. Again there is a pole with residue matrices forming the $m = (k_2 - k_1)$ -dimensional representation of \mathfrak{su}_2 and the $k_1 \times k_1$ data are submatrices of the $k_2 \times k_2$ data at the boundary. The situation when $k_1 = k_2$ is very different and is not discussed in this thesis.

In the SU_2 case the skyline diagram is just

$$\begin{array}{c}
 \uparrow k \\
 \text{---} \\
 \downarrow k \\
 -1 \quad 1
 \end{array}
 \quad (1.53)$$

and the boundary conditions are as described in Sect. 1.2.

When some of the t_i 's in the asymptotic Higgs field are coincident, the residual gauge symmetry is enhanced. If two coincide, one U_1 factor is replaced by an SU_2 factor. If three coincide, two U_1 's are lost and an SU_3 gained. Generally, the unbroken group is $U_1^r \times K$ where K is a rank $n - r - 1$ semisimple Lie group. Since $\pi_2(SU_n/(U_1^r \times K)) = \mathbf{Z}^r$, monopole solutions in theories with nonAbelian residual symmetries have fewer topological charges. However, the monopole solutions still have $n - 1$ integer labels. Some of these integers are the usual topological charges. The rest are what are known as holomorphic charges.

The role of the holomorphic charges is subtle. If two t_i 's are coincident, there is a zero thickness subinterval in the Nahm interval. The boundary conditions for Nahm data in this situation can be described in terms of those explained above, by formally imagining the zero thickness subinterval as the zero thickness limit of a subinterval of finite thickness. The Nahm data on this subinterval become irrelevant in the limit, but the height of the skyline on vanishing subintervals affects the matching condition between the Nahm matrices over the subintervals on either side.

An example is SU_3 broken to U_1^2 . A $(2, 1)$ -monopole has skyline

The Nahm data are 2×2 in the left interval and 1×1 in the right interval. Thus, the right interval triplet is a triplet of imaginary numbers. These numbers are i times the Cartesian coordinates of the $(, 1)$ part of the $(2, 1)$ -monopole. The boundary conditions imply that the 2×2 data are nonsingular at the boundary, $t = \tau$, between the two intervals and, further, that their entries $T_i(\tau)_{2,2}$ are the 1×1 data. The 2×2 data are singular on the left boundary of the interval and the residues there form an irreducible representation of \mathfrak{su}_2 . Letting the right hand interval vanish, an SU_3 monopole with topological charge two and holomorphic charge one is obtained. Holomorphic charges are distinguished from topological charges by square bracketing them. Thus, this monopole is a $(2, [1])$ -monopole

and it has skyline

$$(1.55)$$

The Nahm data are 2×2 matrices with a pole on the left boundary but not on the right one.

In contrast, a $(2, 0)$ -monopole has skyline

$$(1.56)$$

The Nahm data are 2×2 matrices over the left hand subinterval and have poles at t_1 and t_2 . There are no data over the right hand subinterval. These data are identical to SU_2 2-monopole data and correspond to the embedding of an SU_2 2-monopole in SU_3 . The length of the right hand subinterval does not affect the Nahm data. There is a pole at both t_1 and t_2 irrespective of whether $t_2 = t_3$ or not. If $t_2 = t_3$ the Nahm data correspond to a $(2, [0])$ -monopole.

These examples demonstrate how the holomorphic charges determine the boundary conditions and how these boundary conditions can be derived by imagining the nonAbelian case as the zero interval thickness limit of the Abelian case. It should be noted that different holomorphic charges do not necessarily correspond to different monopoles or to different Nahm data. For example, $(3, [1])$ -monopoles are also $(3, [2])$ -monopoles. This ambiguity is discussed, for example, in [We2].

1.7 New hyperKähler manifolds

New hyperKähler manifolds can be constructed using SU_n Nahm data. In this section, the one-parameter family of hyperKähler manifolds due to Dancer is shown to be an infinite mass limit of the moduli space of $(2, 1)$ -monopoles. A new family of fixed monopole spaces

is also constructed. They are the moduli spaces of $(1, 2, 1)$ -monopoles, in the infinite mass limit of the two distinct monopoles.

It is imagined that many new hyperKähler manifolds might be constructed by fixing monopole masses. Because the Nahm equations for 2×2 data are known, it is possible to demonstrate nonsingularity in the $(2, 1)$ case and in the $(1, 2, 1)$ case for generic fixed monopole positions. Without general solutions of the Nahm equations, only the $(2, 1)$ and $(1, 2, 1)$ cases are amenable to this investigation.

This section is divided into subsections. In Subsect. 1.7.1 Dancer's one-parameter family of hyperKähler manifolds is discussed. They are seen to be fixed monopole spaces with one fixed monopole. Spaces with two fixed monopoles are introduced in Subsect. 1.7.2 and their nonsingularity is demonstrated in Subsect. 1.7.3. Other fixed monopole spaces are described in Subsect. 1.7.4. The discussion of fixed monopole spaces concludes in Subsect. 1.7.5 with some remarks about the applications of the new hyperKähler manifolds to three-dimensional supersymmetric theories. Subsection 1.7.6 is an aside concerning SU_4 monopoles.

1.7.1 Dancer's family of hyperKähler manifolds

In [Da2] the moduli space of centred $(2, [1])$ -monopoles is constructed. They have the skyline diagram (1.55). The moduli space, $\mathcal{M}_{(2,[1])}^0$, is eight dimensional. The Nahm data for such monopoles are a triplet of 2×2 traceless skew-Hermitian matrix functions over the interval $[-2, 1]$. There is a simple pole at $t = -2$ and the residues there form the irreducible two-dimensional representation of \mathfrak{su}_2 . The space of such Nahm triplets, $\mathcal{N}_{(2,[1])}$, is five dimensional. The whole of $\mathcal{M}_{(2,[1])}^0$ is generated by the action of SU_2 on these Nahm data. To describe this group action, the gauged version of the Nahm equations (1.8) must be used.

A group action is defined on the space of $(2, [1])$ Nahm data. The group

$${}_0\mathcal{G} = \{g \in C^w([-2, 1], U_2) : g(-2) = \mathbf{1}\} \quad (1.57)$$

contains the gauge action

$${}_0\mathcal{G}_0 = \{g \in C^w([-2, 1], U_2) : g(-2) = g(1) = \mathbf{1}\} \quad (1.58)$$

as a subgroup. The action of $g \in {}_0\mathcal{G}$ on (T_0, T_1, T_2, T_3) is defined as in the SU_2 case (1.9). The moduli space of uncentred Nahm data, $\mathcal{M}_{(2,[1])}$, is the space of gauge inequivalent data. However, $U_2 = {}_0\mathcal{G}/{}_0\mathcal{G}_0$ and, so, a U_2 action on the data is given by $g \in {}_0\mathcal{G}$ acting as in (1.9). A hyperKähler quotient by the centre of this U_2 on $\mathcal{M}_{(2,[1])}$ centres the Nahm data, giving $\mathcal{M}_{(2,[1])}^0$. The remaining SU_2 action can be fixed by setting T_0 to zero, reducing (1.8) to (1.7) and $\mathcal{M}_{(2,[1])}^0$ to $\mathcal{N}_{(2,[1])}$.

The SU_2 action on $\mathcal{N}_{(2,[1])}$ is triholomorphic and isometric. This means that there is an induced moment map, μ , from $\mathcal{M}_{(2,[1])}^0$ to \mathbf{R}^3 formed by the action of a U_1 subgroup of SU_2 . Dancer's family of hyperKähler manifolds is the family of hyperKähler four-manifolds

$$M(\boldsymbol{\lambda}) = \mu^{-1}(\boldsymbol{\lambda})/U_1, \quad (1.59)$$

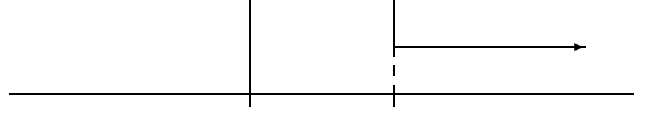
where $\boldsymbol{\lambda} \in \mathbf{R}^3$. The SO_3 action on $\mathcal{M}_{(2,[1])}^0$ is not an isometry of $M(\boldsymbol{\lambda})$, rather, it acts on $\boldsymbol{\lambda}$ to give an isometry between $M(\boldsymbol{\lambda})$ and $M(R\boldsymbol{\lambda})$ where R is an SO_3 matrix. $M(\mathbf{0})$ is a double cover of the Atiyah-Hitchin manifold.

The hyperKähler manifolds $M(\boldsymbol{\lambda})$ are hyperKähler quotients of a monopole moduli space. It is now shown that they are the infinite mass limit of another monopole space. The moment map μ is known explicitly. If the U_1 subgroup is the subgroup which fixes $i\sigma_3$ when SU_2 acts on \mathfrak{su}_2 in the adjoint representation, the moment map $\mu : \mathcal{M}_{(2,[1])}^0 \rightarrow \mathbf{R}^3$ given by this U_1 action is

$$\mu : (T_0, T_1, T_2, T_3) \mapsto (-\text{trace}(T_1(1)i\sigma_3), -\text{trace}(T_2(1)i\sigma_3), -\text{trace}(T_3(1)i\sigma_3)). \quad (1.60)$$

The level set $\mu^{-1}(\boldsymbol{\lambda})$ consists of Nahm data whose entries $T_i(1)_{2,2}$ are $i\lambda_i/2$ at $t = 1$. For $(2, 1)$ -monopoles, (1.54), the data in the right-hand interval are given by the $T_i(1)_{2,2}$, that is, the $(2, 2)$ entries from the Nahm data on the left-hand interval. Thus, the hyperKähler manifolds $M(\boldsymbol{\lambda})$ are the moduli spaces of $(2, 1)$ -monopoles with the $(, 1)$ -monopole fixed. The $(, 1)$ -monopole can be fixed by taking its infinite mass limit. The monopole mass is

proportional to the length of the corresponding interval, so this limit is



$$(1.61)$$

The vector $\boldsymbol{\lambda}$ is now related to the position of the $(, 1)$ -monopole: the monopole whose position is fixed. When the position of the $(, 1)$ -monopole is fixed in the centre, the relative metric of the $(2,)$ -monopole is Atiyah-Hitchin.

An advantage of this description of $M(\boldsymbol{\lambda})$ is that its asymptotic behaviour may be calculated using the methods of [Ma2, GM2, LWY2]. That is, by approximating the monopoles by point particles and calculating their long range interactions. This yields a purely kinetic Lagrangian for the motion of the well-separated monopoles and, hence, an asymptotic metric. This metric is

$$ds^2 = g_{ij}d\mathbf{x}_i \cdot d\mathbf{x}_j + g_{ij}^{-1}(d\chi_i + \mathbf{W}_{ik} \cdot d\mathbf{x}_k)(d\chi_j + \mathbf{W}_{jl} \cdot d\mathbf{x}_l), \quad (1.62)$$

where,

$$\begin{aligned} g_{jj} &= m_j - \sum_{i \neq j} \frac{\alpha_{ij}}{r_{ij}}, \\ g_{ij} &= \frac{\alpha_{ij}}{r_{ij}}, \quad (i \neq j) \\ \mathbf{W}_{jj} &= - \sum_{i \neq j} \mathbf{w}_{ij}, \\ \mathbf{W}_{ij} &= \mathbf{w}_{ij}, \quad (i \neq j) \end{aligned} \quad (1.63)$$

and \mathbf{x}_i , χ_i and m_j are the spatial coordinates, phases and masses of the monopoles; these are all well defined in the point particle approximation. A Dirac potential $\mathbf{w}(\mathbf{r})$ satisfies

$$\nabla_{\mathbf{r}} \times \mathbf{w} = -\frac{\mathbf{r}}{r^3}. \quad (1.64)$$

In (1.63) $r_{ij} = |\mathbf{x}_i - \mathbf{x}_j|$ and \mathbf{w}_{ij} is the corresponding Dirac potential. If the i and j monopoles have the same U_1 charge then $\alpha_{ij} = 1$ and, if they correspond to adjacent U_1 's, $\alpha_{ij} = -1/2$, otherwise it is zero.

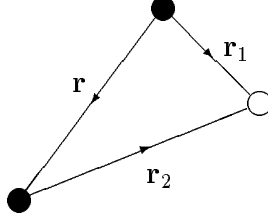


Figure 1.4: Two unfixed monopoles and a fixed one. The unfixed monopoles are the solid dots.

For $(2, 1)$ -monopoles the mass of the two $(2, \)$ -monopoles, is chosen to be one and that of the $(\ , 1)$ -monopole to be m . Then, in the notation of Fig. 1.4,

$$g_{ij} = \begin{pmatrix} 1 - \frac{1}{r} + \frac{1}{2r_1} & \frac{1}{r} & -\frac{1}{2r_1} \\ \frac{1}{r} & 1 - \frac{1}{r} + \frac{1}{2r_2} & -\frac{1}{2r_2} \\ -\frac{1}{2r_1} & -\frac{1}{2r_2} & m + \frac{1}{2r_1} + \frac{1}{2r_2} \end{pmatrix}. \quad (1.65)$$

In the $(\mathbf{r}, \frac{1}{2}(\mathbf{x}_1 + \mathbf{x}_2), \mathbf{x}_3 - \frac{1}{2}(\mathbf{x}_1 + \mathbf{x}_2))$ basis this becomes

$$g'_{ij} = \begin{pmatrix} \frac{1}{2} - \frac{1}{r} + \frac{1}{8r_1} + \frac{1}{8r_2} & 0 & \frac{1}{4r_2} - \frac{1}{4r_1} \\ 0 & m + 2 & m \\ \frac{1}{4r_2} - \frac{1}{4r_1} & m & m + \frac{1}{2r_1} + \frac{1}{2r_2} \end{pmatrix}. \quad (1.66)$$

Thus, taking the infinite mass limit, the asymptotic metric on $M(\boldsymbol{\lambda})$ is

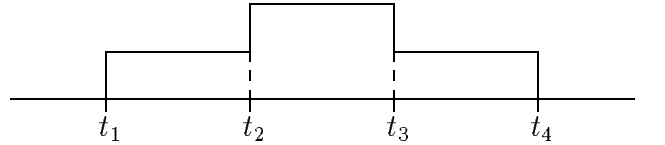
$$\begin{aligned} ds^2 &= V_1 d\mathbf{r} \cdot d\mathbf{r} + V_2^{-1} (d\chi + \mathbf{W} \cdot d\mathbf{r})^2, \\ V_1 &= \frac{1}{2} - \frac{1}{r} + \frac{1}{8r_1} + \frac{1}{8r_2}, \\ V_2 &= 1 - \frac{1}{r} + \frac{1 - 4r_1 r_2}{8r_1 r_2 + 2r_1 + 2r_2}, \\ \mathbf{W} &= -\mathbf{w} + \frac{1}{8}\mathbf{w}_1 + \frac{1}{8}\mathbf{w}_2. \end{aligned} \quad (1.67)$$

This metric is singular as $r \rightarrow 0$. It is only valid for large r .

The asymptotic metric for $M(\mathbf{0})$ is found by placing the fixed monopole at the centre of mass of the two unfixed monopoles and, thus, by substituting $r_1 = r_2 = r/2$ and $\mathbf{w}_1 = \mathbf{w}_2 = 2\mathbf{w}$ in (1.67). Making these substitutions reduces (1.67) to the asymptotic form of the Atiyah-Hitchin metric.

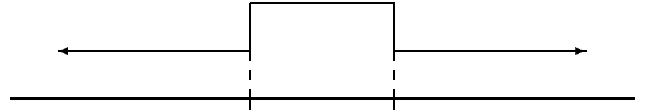
1.7.2 A new family of hyperKähler manifolds

Another advantage of this description is that it immediately suggests the new family of four-dimensional hyperKähler manifolds, $N(\boldsymbol{\lambda}, \boldsymbol{\mu})$. $M(\boldsymbol{\lambda})$ is a fixed monopole space derived from the moduli space of charge $(2, 1)$ SU_3 monopoles. This suggests that a new family of hyperKähler manifolds could be constructed by fixing monopoles in the moduli space of charge $(1, 2, 1)$ SU_4 monopoles. A $(1, 2, 1)$ -monopole has skyline


(1.68)

The corresponding Nahm data are 2×2 matrices in the middle subinterval and 1×1 matrices in the left and right subintervals. The Nahm data in the left subinterval are equal to the entries $T_i(t_2)_{2,2}$ of the 2×2 data. The Nahm data in the right subinterval are equal to the entries $T_i(t_3)_{2,2}$. All the Nahm data are regular.

The limit where the subintervals $[t_1, t_2]$ and $[t_3, t_4]$ become infinitely long gives the $(1, 2, 1)$ fixed monopole spaces:


(1.69)

They are labelled by two vectors, $\boldsymbol{\lambda}$ and $\boldsymbol{\mu}$, the positions of the two fixed monopoles: the $(1, \ , \)$ -monopole and the $(\ , \ , 1)$ -monopole. These spaces are denoted $N(\boldsymbol{\lambda}, \boldsymbol{\mu})$. The SO_3 action on the charge $(1, 2, 1)$ moduli space is isometric and rotates the two vectors $\boldsymbol{\lambda}$ and $\boldsymbol{\mu}$. In the infinite mass limit of the $(1, \ , \)$ -monopole and the $(\ , \ , 1)$ -monopole, the action of some $R \in SO_3$ gives an isomorphism between $N(\boldsymbol{\lambda}, \boldsymbol{\mu})$ and $N(R\boldsymbol{\lambda}, R\boldsymbol{\mu})$. Thus, $N(\boldsymbol{\lambda}, \boldsymbol{\mu})$ is a three-parameter family of hyperKähler manifolds. If $\boldsymbol{\lambda}$ and $\boldsymbol{\mu}$ are parallel, then a U_1 subgroup of the SO_3 action fixes $N(\boldsymbol{\lambda}, \boldsymbol{\mu})$ and so $N(\boldsymbol{\lambda}, \boldsymbol{\mu})$ has a U_1 isometry.

Using the same methods as for the Dancer family, the asymptotic form of the $N(\boldsymbol{\lambda}, \boldsymbol{\mu})$

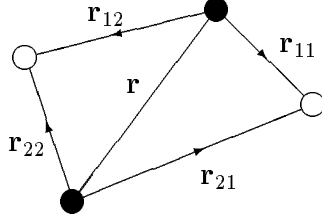


Figure 1.5: Two unfixed monopoles and two fixed ones. The unfixed monopoles are the solid dots.

metric can be calculated. It is

$$\begin{aligned}
 ds^2 &= V_1 d\mathbf{r} \cdot d\mathbf{r} + V_2^{-1} (d\chi + \mathbf{W} \cdot d\mathbf{r})^2, \\
 V_1 &= \frac{1}{2} - \frac{1}{r} + \frac{1}{8r_{11}} + \frac{1}{8r_{12}} + \frac{1}{8r_{21}} + \frac{1}{8r_{22}}, \\
 V_2 &= 1 - \frac{1}{r} + \frac{1}{2} \frac{r_{11}r_{21} + r_{11}r_{22} + r_{12}r_{21} + r_{12}r_{22} - 4r_{11}r_{12}r_{21}r_{22}}{4r_{11}r_{12}r_{21}r_{22} + r_{11}r_{12}r_{21} + r_{11}r_{12}r_{22} + r_{11}r_{21}r_{22} + r_{12}r_{21}r_{22}}, \\
 \mathbf{W} &= -\mathbf{w} + \frac{1}{8}\mathbf{w}_{11} + \frac{1}{8}\mathbf{w}_{12} + \frac{1}{8}\mathbf{w}_{21} + \frac{1}{8}\mathbf{w}_{22},
 \end{aligned} \tag{1.70}$$

where everything is defined as before; except that now, there are two fixed monopoles and the distances from the two $(, 2,)$ -monopoles to the first of these have been denoted by r_{11} and r_{21} and the distances to the second by r_{12} and r_{22} . This notation is illustrated in Fig. 1.5. Examining the asymptotic formula, it is interesting to see how flat the $N(\boldsymbol{\lambda}, \boldsymbol{\mu})$ metrics are. All the metrics are flat up to the second order in $1/r$.

1.7.3 Nonsingularity of the new hyperKähler manifolds

It is not clear, however, that the $(1, 2, 1)$ -moduli space remains nonsingular as the masses of the $(1, ,)$ -monopole and the $(, , 1)$ -monopole become infinite. Dancer's family, $M(\boldsymbol{\lambda})$, is known to be nonsingular because it can be constructed using a hyperKähler quotient. In imitation of this, $N(\boldsymbol{\lambda}, \boldsymbol{\mu})$ is constructed in this section by hyperKähler quotient of the moduli space of $([1], 2, [1])$ -monopoles. These monopoles are SU_4 monopoles of

topological charge two with the SU_4 broken to $SU_2 \times U_1 \times SU_2$. The skyline diagram is



$$(1.71)$$

The Nahm data are 2×2 matrices analytic over the whole interval $[-2, 2]$. There are two commuting SU_2 actions, one at each boundary. These data correspond to $([1], 2, [1])$ -monopoles. The moduli space of $([1], 2, [1])$ -monopoles is used to construct $N(\boldsymbol{\lambda}, \boldsymbol{\mu})$ in the same way as the moduli space of $(2, [1])$ -monopole is used to construct $M(\boldsymbol{\lambda})$. It is found that the manifold $N(\boldsymbol{\lambda}, \boldsymbol{\mu})$ is free of singularities as long as $\boldsymbol{\lambda} \neq \boldsymbol{\mu}$.

The charge $([1], 2, [1])$ Nahm data are quadruplets (T_0, T_1, T_2, T_3) satisfying the Nahm equations (1.8) and acted on by the gauge group

$${}_0\mathcal{G}_0 = \{g \in C^w([-2, 2], U_2) : g(-2) = g(2) = \mathbf{1}\}. \quad (1.72)$$

The two larger groups,

$${}_0\mathcal{G} = \{g \in C^w([-2, 2], U_2) : g(-2) = \mathbf{1}\}, \quad (1.73)$$

$$\mathcal{G}_0 = \{g \in C^w([-2, 2], U_2) : g(2) = \mathbf{1}\} \quad (1.74)$$

are defined. These are subgroups of $\mathcal{G} = \{g \in C^w([-2, 2], U_2)\}$.

Two U_2 actions are given by ${}_0\mathcal{G}/{}_0\mathcal{G}_0$ and $\mathcal{G}_0/{}_0\mathcal{G}_0$. These actions commute. The whole $U_2 \times U_2$ action is the $\mathcal{G}/{}_0\mathcal{G}_0$ action. The centre is $U_1 \times U_1$. The Nahm data are fixed under the central element represented by the constant function $g(t) = e^{i\theta} \mathbf{1}_2$. The element represented by $g(t) = e^{i\theta t} \mathbf{1}_2$ sends (T_0, T_1, T_2, T_3) to $(T_0 - i\theta \mathbf{1}_2, T_1, T_2, T_3)$ and generates the vector field $(-i\mathbf{1}_2, 0, 0, 0)$. The hyperKähler quotient by this action centres the Nahm data. This space of centred data, $\mathcal{M}_{([1], 2, [1])}^0$, is twelve dimensional. It has an isometric triholomorphic $SU_2 \times SU_2$ action. There is also an SO_3 action, which rotates (T_1, T_2, T_3) as a three-vector and commutes with the $SU_2 \times SU_2$ action.

A $U_1 \times U_1$ subgroup of the $SU_2 \times SU_2$ is represented by the elements

$$\alpha(t) = e^{\frac{i\theta}{4}(t+2)\sigma_3}, \quad \beta(t) = e^{\frac{i\theta}{4}(2-t)\sigma_3}. \quad (1.75)$$

The moment map, $\mu : \mathcal{N}_{([1],2,[1])}^0 \rightarrow \mathbf{R}^3 \times \mathbf{R}^3$, for the action of this subgroup is

$$\mu : (T_0, T_1, T_2, T_3) \mapsto (\boldsymbol{\lambda}, \boldsymbol{\mu}) \quad (1.76)$$

where

$$\boldsymbol{\lambda} = (-\text{trace}(T_1(-2)i\sigma_3), -\text{trace}(T_2(-2)i\sigma_3), -\text{trace}(T_3(-2)i\sigma_3)) \quad (1.77)$$

and

$$\boldsymbol{\mu} = (-\text{trace}(T_1(2)i\sigma_3), -\text{trace}(T_2(2)i\sigma_3), -\text{trace}(T_3(2)i\sigma_3)). \quad (1.78)$$

By the same argument as before $\mathcal{N}_{([1],2,[1])}^0$ reduces to $N(\boldsymbol{\lambda}, \boldsymbol{\mu})$ under the hyperKähler quotient:

$$N(\boldsymbol{\lambda}, \boldsymbol{\mu}) = \mu^{-1}(\boldsymbol{\lambda}, \boldsymbol{\mu})/\text{U}_1 \times \text{U}_1 \quad (1.79)$$

The condition that $\boldsymbol{\lambda}$ and $\boldsymbol{\mu}$ must satisfy, in order for the $\text{U}_1 \times \text{U}_1$ action to be free, are now needed. These are the conditions for the nonsingularity of the $N(\boldsymbol{\lambda}, \boldsymbol{\mu})$.

To apply these conditions, it is necessary to solve the Nahm equations. Using the \mathcal{G} action, T_0 is gauged to zero. This leaves an eight-dimensional space acted on by constant elements of \mathcal{G} and by the SO_3 action. $\text{trace}(T_1T_2)$, $\text{trace}(T_2T_3)$ and $\text{trace}(T_3T_1)$ are independent of t . By acting SO_3 they can be set to zero. This means that if the T_i are written as

$$T_i = -\frac{i}{2}f_i\mathbf{n}_i \cdot \boldsymbol{\sigma}, \quad (1.80)$$

where the \mathbf{n}_i are constant orthonormal vectors. The f_i 's satisfy the Euler-Poinsot equations (1.14). The SO_3 action are completely fixed by requiring that

$$f_1^2 \leq f_2^2 \leq f_3^2. \quad (1.81)$$

The f_i are then those given in (1.17)

The remaining group action is that of constant elements of \mathcal{G} . It is fixed by setting $\mathbf{n}_1 = (1, 0, 0)$, $\mathbf{n}_2 = (0, 1, 0)$ and $\mathbf{n}_3 = (0, 0, 1)$. The resulting subspace of the moduli space $\mathcal{N}_{([1],2,[1])}^0$ is called \mathcal{N}^3 . Since the SO_3 action on $\mathcal{N}_{([1],2,[1])}^0$ is not free, \mathcal{N}^3 is not a manifold. In the SU_2 case, the boundary conditions fixed the constants τ and D in (1.17). Here the only constraints are that the poles do not fall in the $[-2, 2]$ interval. This requires that

$\tau > 2$ and $D(\tau + 2) < 2K(k)$. Further solutions are found by changing the sign of all three f_i 's and sending t to $-t$. The analyticity requirements on these further solutions are that $\tau < 2$ and $D(\tau + 2) < 2K(k)$. This exhausts all the solutions consistent with the various conditions which have been imposed.

The action of $\alpha(t)$ and $\beta(t)$ is given by (1.75). A fixed point of $\alpha(t)$ is diagonal at $t = 2$ and so for $\alpha(t)$ to have a fixed point in \mathcal{N}^3 it is necessary and sufficient that $f_1(2) = f_2(2) = 0$. This only occurs if $k = 1$ and $\tau = \infty$. The solutions (1.17) are then $f_1(t) = 0$, $f_2(t) = 0$ and $f_3(t) = D$ and the hyperKähler quotient gives the space $N((0, 0, D), (0, 0, D))$. This means $N(\boldsymbol{\lambda}, \boldsymbol{\mu})$ with $\boldsymbol{\lambda} = \boldsymbol{\mu} = (0, 0, D)$ may have a singularity. A point in \mathcal{N}^3 with $f_1(t) = 0$, $f_2(t) = 0$ is also a fixed point of $\beta(t)$ and these are all the fixed points of $\beta(t)$ in \mathcal{N}_3 .

To find all the fixed points of the $U_1 \times U_1$ action the whole of $\mathcal{N}_{([1], 2, [1])}^0$ must be examined and those points whose data are diagonal at either end found. Acting on the $t = 2$ data with a general element of U_2 demonstrates that the only data which are diagonal at $t = 2$ have $f_1(t) = 0$ and $f_2(t) = 0$. The corresponding quotient space has both the fixed monopoles lying on the x_3 -axis. In $\mathcal{N}_{([1], 2, [1])}^0$ the only fixed points are those for which the fixed monopoles are collinear with the origin. This means that the only potentially singular $N(\boldsymbol{\lambda}, \boldsymbol{\mu})$ manifolds have $\boldsymbol{\lambda}$ parallel to $\boldsymbol{\mu}$.

The manifold $N(\mathbf{0}, \mathbf{0})$ is singular. This is in contrast with $M(\mathbf{0})$ which is a double cover of the Atiyah-Hitchin manifold. The $N(\boldsymbol{\lambda}, \boldsymbol{\mu})$ spaces are not deformations of a smooth SO_3 isometric hyperKähler manifold.

1.7.4 Other fixed monopole spaces

Following the example of $M(\boldsymbol{\lambda})$ and $N(\boldsymbol{\lambda}, \boldsymbol{\mu})$, it is natural to ask whether further non-singular fixed monopole spaces might be constructed by fixing larger numbers of monopoles. For example, a large class of four-dimensional hyperKähler manifolds might be derived from the $(k_1, 2, k_2)$ -monopole moduli spaces. One might conjecture that, as long as the (k_1, \cdot) -monopoles and the (\cdot, k_2) -monopoles are not fixed in collinear positions, new multi-parameter families of four-dimensional hyperKähler manifolds could result.

More complicated mixtures of fixed and unfixed monopoles could be used to give fixed monopole spaces of dimensions higher than four. Fixed charges are distinguished from other charges by enclosing them in curly brackets. It could be conjectured that for $r > 1$ the $(\{k_1\}, l_1, l_2, \dots, l_r, \{k_2\})$ spaces are nonsingular when the $(k_1, \dots,)$ -monopoles and the $(, \dots, , k_2)$ -monopoles are each fixed so they are not collinear with monopoles of the same type.

The asymptotic metrics can always be constructed for fixed monopole spaces using the point monopole methods of [Ma3, GM2, LWY2]. Generally, these asymptotic fixed monopole metrics are singular. This is not the case for the $(\{k\}, 1)$ space. In the limit of infinite $(k,)$ -monopole mass the $(k, 1)$ -monopole asymptotic metric is the k centre multi-Taub-NUT metric of Hawking [Ha]. The positions of the k centres are the k fixed monopole positions. Since the multi-Taub-NUT metric is generically nonsingular and is the same asymptotically as the $(k, 1)$ metric, it seems likely that they are the same everywhere. Certainly, the $(1, 1)$ -monopole metric is known explicitly [C, GL, LWY1] and the $(\{1\}, 1)$ metric is Taub-NUT. The $(1, 1, 1)$ metric is also known [LWY2, Mu] and the infinite mass limit $(\{1\}, 1, \{1\})$ is two centre multi-Taub-NUT.

Mixtures of fixed, topological and holomorphic charges might also be considered. An example is the eight-dimensional space $(\{1\}, 2, [1])$:

It is an interesting space, it has a triholomorphic SU_2 isometry and an isometric U_1 action which rotates the complex structures.

1.7.5 Applications

The $N(\lambda, \mu)$ are gravitational instantons. Gravitational instantons are asymptotically flat solutions of the vacuum Einstein equations. All asymptotically flat four-dimensional

	1	2	3	4	5	6	7	8	9
fivebranes	X	X	X	X	X	t_i	\leftarrow	$\mathbf{0}$	\rightarrow
threebranes	X	X	\leftarrow	λ_i	\rightarrow	X	\leftarrow	$\mathbf{0}$	\rightarrow

Figure 1.6: The threebrane and fivebrane configuration. An X marks an extended direction.

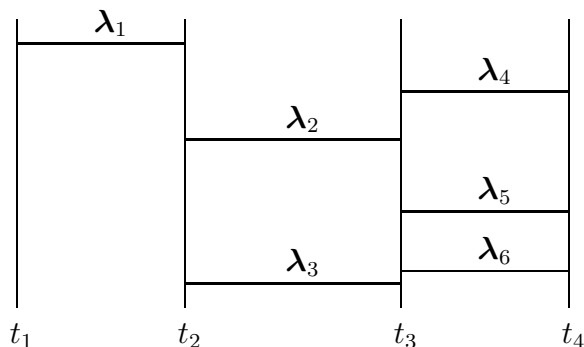
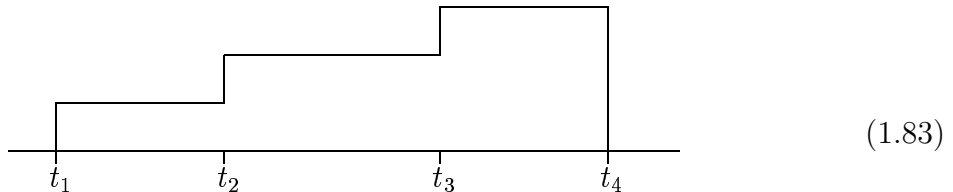


Figure 1.7: A typical configuration. The horizontal lines are threebranes and the vertical lines are fivebranes.

hyperKähler manifolds are gravitational instantons. As noted earlier, $N(\boldsymbol{\lambda}, \boldsymbol{\mu})$ rapidly approaches flat space.

Fixed monopole spaces are relevant to (2+1)-dimensional quantum field theories. In a celebrated recent paper Hanany and Witten [HW] propose a correspondence between three-dimensional supersymmetric gauge theories and moduli spaces of magnetic monopoles. Hanany and Witten consider the theory of type IIB superstrings. In this theory there are threebranes and fivebranes, that is, objects extended in, respectively, three and five spatial dimensions. A number of fivebranes are placed so that they are extended in the x_0 and x_1 to x_5 directions, are at the origin in the x_7 to x_9 directions and are at positions t_i along the x_6 directions. Threebranes are placed so that they are extended in the x_0 , x_1 and x_2 directions and stretch between fivebranes in the x_6 direction. Like the fivebranes they are at the origin in the x_7 to x_9 directions. In the x_3 to x_5 directions each threebrane is at some position λ_i . Figure 1.6 recapitulates this assignment. Figure 1.7 illustrates a typical configuration.

In their paper Hanany and Witten consider a given brane configuration in two different ways. The ends of the threebranes in the fivebranes are infinitely extended in two spatial directions and positioned at λ_i in the remaining three spatial dimensions. It is argued that the ends of the threebranes in the fivebranes are BPS monopoles in their three codimensions. In fact, it is argued that the theory of the threebranes as objects is a BPS monopole theory. For the configuration pictured in Fig. 1.7, for example, this BPS monopole theory has skyline diagram



There is also a theory in the threebranes themselves. It is argued by Hanany and Witten that, in the x_0 , x_1 and x_2 directions of the threebranes, there is a (2+1)-dimensional $N = 4$ supersymmetric quantum field theory. The matter content of this field theory can be deduced from the precise configuration of branes. Thus, a given brane configuration contains a BPS monopole configuration and a (2+1)-dimensional supersymmetric quantum field theory. This pairing is conjectured to give a correspondence between BPS moduli spaces and the moduli spaces of supersymmetric theories. It is thought that, along the x_6 direction the theory reduces to the Nahm equations [Dia].

In the language of [HW], the fixed monopole spaces correspond to brane configurations in which some of the threebranes are infinitely extended in the direction along which the fivebranes are separated. Thus, $N(\lambda, \mu)$ corresponds to the configuration of Fig. 1.8. The quantum field theories in this case have hypermultiplets of masses λ and μ . The Dancer space $M(\lambda)$ corresponds to Fig. 1.9 and to quantum field theories with hypermultiplets of mass λ .

The brane configurations of Hanany and Witten are not the only evidence for the correspondences thereby constructed. (2+1)-dimensional $N = 4$ supersymmetric quantum field theories are studied by compactifying (3+1)-dimensional $N = 2$ supersymmetric quantum field theories; the theories which are parametrized by the Seiberg-Witten curves. In [AH] the Atiyah-Hitchin manifold is described as the quotient by $(x, y, z) \rightarrow (-x, -y, z)$ of the

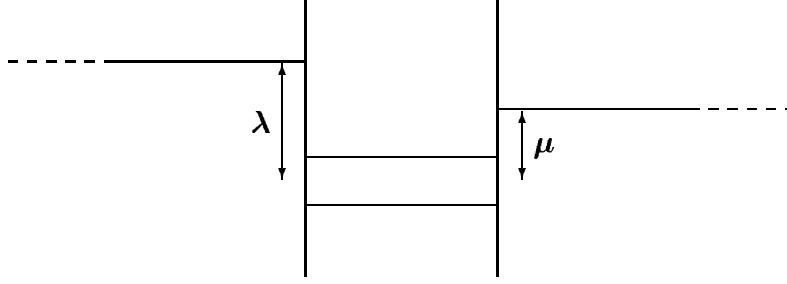


Figure 1.8: The fivebrane and threebrane configuration equivalent to $N(\boldsymbol{\lambda}, \boldsymbol{\mu})$.

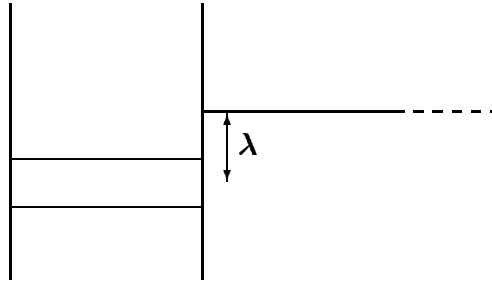


Figure 1.9: The fivebrane and threebrane configuration equivalent to $M(\boldsymbol{\lambda})$.

surface

$$x^2 - zy^2 = 1, \tag{1.84}$$

in \mathbf{C}^3 . In [SW] this curve is derived from the Seiberg-Witten curve by compactifying a suitable (3+1)-dimensional theory to give a (2+1)-dimensional theory with no hypermultiplets. $M(\boldsymbol{\lambda})$ also has a complex surface description [Da3] and in [SW] the same compactification procedure shows that this surface is the surface of theories with one hypermultiplet of mass $\boldsymbol{\lambda}$. The reinterpretation of $M(\boldsymbol{\lambda})$ as a fixed monopole moduli space gives an explanation of this, in the spirit of [HW].

1.7.6 A note on $([1], 2, [1])$ -monopoles

The moduli space of $([1], 2, [1])$ -monopoles is used to prove the nonsingularity of $N(\boldsymbol{\lambda}, \boldsymbol{\mu})$. The discussion of it is also be useful in studying $([1], 2, [1])$ -monopoles *per se*. The metric on the moduli space is unknown, but could be calculated using methods similar to those used to calculate the $(2, [1])$ -monopole metric [Da1, I]. In fact, since [Ho] appeared Lee and Lu have calculated the metric on a specific submanifold of the $([1], 2, [1])$ moduli space [LL].

The Coxeter-Dynkin diagram for \mathfrak{su}_4 is

$$\begin{array}{c} \circ \text{---} \circ \text{---} \circ \\ \vec{\alpha} \quad \vec{\beta} \quad \vec{\gamma} \end{array} \quad (1.85)$$

and there are three simple roots, $\vec{\alpha}$, $\vec{\beta}$ and $\vec{\gamma}$. If the roots are $\vec{\alpha} = (1, 0, 0)$, $\vec{\beta} = (-\frac{1}{2}, -\frac{1}{2}, \frac{1}{\sqrt{2}})$ and $\vec{\gamma} = (0, 1, 0)$ then the theory with residual symmetry $SU_2 \times U_1 \times SU_2$ has Φ_∞ along the x_3 -axis. Some $([1], 2, [1])$ -monopoles have a very simple form. There is an embedding of \mathfrak{su}_2 in \mathfrak{su}_4 corresponding to any root. If a SU_2 1-monopole is embedded in \mathfrak{su}_4 along the root $\vec{\alpha} + \vec{\beta}$ it is a $([1], 1, [0])$ -monopole. Similarly, a SU_2 1-monopole embedded along the root $\vec{\gamma} + \vec{\beta}$ is a $([0], 1, [1])$ -monopole. Since $\vec{\alpha} + \vec{\beta}$ and $\vec{\gamma} + \vec{\beta}$ are orthogonal, these two monopoles can be superimposed to give a $([1], 2, [1])$ -monopole, they occupy different 2×2 blocks of the 4×4 \mathfrak{su}_4 fields. These embedded monopoles are exceptional, not all $([1], 2, [1])$ -monopoles are of this form.

All $([1], 2, [1])$ -monopoles are D_2 symmetric about some axes. The monopole can be orientated by imposing D_2 symmetry about particular axes. By imposing D_2 symmetry about the Cartesian axes, the monopoles are restricted to a three-dimensional geodesic submanifold of the moduli space: \mathfrak{K} . The space \mathcal{N}^3 of Nahm data described above, is the quotient of the full moduli space by the full SO_3 action and since this action is not free, \mathcal{N}^3 is not a manifold. The orientation of the monopole is fixed by imposing D_2 symmetry on it. Unlike the quotient space, this space, \mathfrak{K} , is not singular and imposing D_2 symmetry is a good way to fix the SO_3 action. The D_2 symmetry conditions are identical to (1.80) but without the ordering condition (1.81). Thus, \mathfrak{K} is composed of the six copies of \mathcal{N}^3 obtained by permuting the inequality (1.81). These copies are joined at the planes where

two of the f_i 's are equal. These data, where two of the f_i 's are equal, correspond to axially symmetric monopoles. The planes intersect on the lines of spherical symmetry. An example of a line of spherical symmetry is

$$f_1(t) = f_2(t) = f_3(t) = -\frac{1}{t + \tau} \quad (1.86)$$

where $\tau > 2$.

There are exceptional lines in \mathfrak{K} given by letting $k = 1$ and taking τ to infinity. These lines are notable as the fixed points of the $U_1 \times U_1$ action. These are the lines where one f_i is constant and the other two are zero. These lines correspond to the exceptional $([1], 2, [1])$ -monopoles produced by embedding two SU_2 1-monopoles. They meet at the point where all three f_i are zero. This monopole is the embedding of two coincident \mathfrak{su}_2 1-monopoles.

In their paper [DL], Dancer and Leese studied the head on collision of $(2, [1])$ -monopoles. These collisions are described by geodesics on a two-dimensional manifold that they call Y . \mathfrak{K} is the analogue of Y for $([1], 2, [1])$ -monopoles. The Y space looks like the letter Y , the \mathfrak{K} space has been called \mathfrak{K} because it resembles that symbol. The boundaries of \mathfrak{K} occur when (D, τ) attain the bounds imposed by analyticity. When (D, τ) attain these bounds, the Nahm data has a pole at one or the other end. This means these boundaries are actually copies of the space Y . In fact, the whole of \mathfrak{K} has eight copies of Y at its boundaries.

\mathfrak{K} can be pictured. Take the \mathbf{R}^3 Cartesian axes and thicken them. Divide the surfaces of these thickened axes by tracing their intersections with the x_1x_2 , x_2x_3 and x_3x_1 planes. The eight surface elements bounded by these lines are the eight copies of Y . The interior of the thickened axes is \mathfrak{K} . The Cartesian axes themselves are the lines of embedded monopoles. The origin is the spherical embedded monopole. The intersections of the six planes $x_1 = \pm x_2$, $x_2 = \pm x_3$ and $x_3 = \pm x_1$ with \mathfrak{K} are the planes of axially symmetric monopoles. The lines $x_1 = \pm x_2 = \pm x_3$ are the lines of spherically symmetric monopoles. This picture of \mathfrak{K} is not metrically correct.

In Fig. 1.10 some attempt has been made at illustrating the picture of \mathfrak{K} described above. In Fig. 1.10a \mathfrak{K} itself is drawn. It resembles thickened Cartesian axes, the dashed

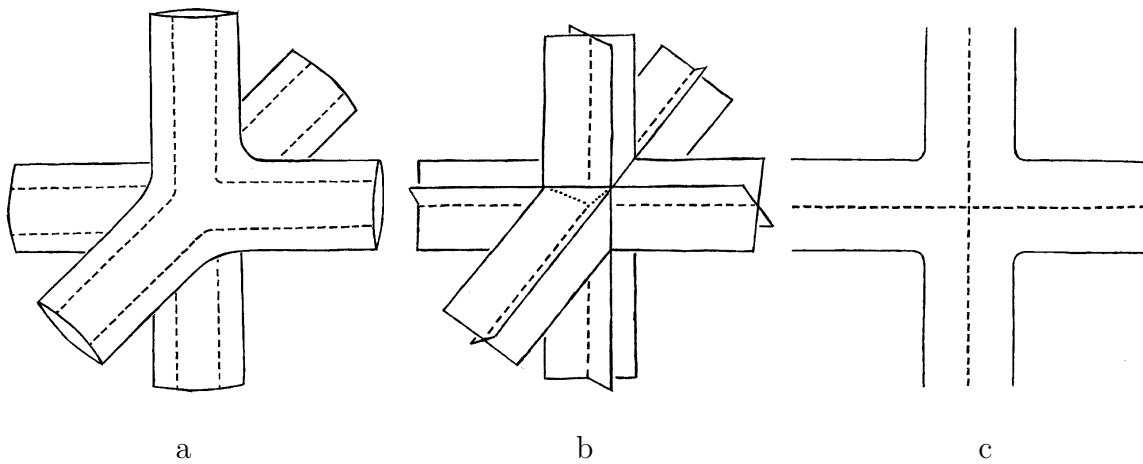


Figure 1.10: The space \mathcal{K} .

line along its surface marks the boundary between different copies of Y on its asymptotic boundary. In Fig. 1.10b are drawn the planes of axially symmetric monopoles. The Cartesian axes are marked by the dashed lines and correspond to embedded monopoles; the dotted lines mark the intersections of three planes and correspond to spherically symmetric monopoles. In Fig. 1.10c is drawn the x_1x_2 -plane slice of \mathcal{K} . These are the data considered by Lee and Lu [LL]. SO_5 can be embedded in SU_4 and those $([1], 2, [1])$ -monopoles in Fig. 1.10c have fields in the image of this embedding SO_5 and so may be reinterpreted as SO_5 monopoles.

Chapter 2

Symmetric Monopoles

The \mathfrak{su}_2 1-monopole is spherically symmetric and its fields are known explicitly [PS]. For charges higher than one, the most symmetric \mathfrak{su}_2 monopoles are axially symmetric. The axially symmetric 2-monopole was discovered by Ward [Wa1] and by Forgács, Horváth and Palla [FHP]. It was quickly realised that there are axially symmetric k -monopoles for each k [Pr, PR, Hi2]. Also, at this time, the ADHMN construction was used to construct general 2-monopoles [BPP, Pa]. No new multimonopoles were discovered until the paper of Hitchin, Manton and Murray [HMM]. In this paper, there is a tetrahedrally symmetric 3-monopole and a cubic 4-monopole.

In their paper, Hitchin, Manton and Murray solve the Nahm equations for the tetrahedral 3-monopole and the cubic 4-monopole. The Nahm equations for these symmetric multimonopoles are much simpler than the general Nahm equations. By imposing symmetry the intractable general problem is reduced to a tractable special case. This approach is very fruitful. In this chapter it is explained how the methods of Hitchin, Manton and Murray are extended and exploited, leading to the discovery of further multimonopoles. There is a dodecahedral 7-monopole, described in Sect. 2.3 and an octahedral 5-monopole, described in Sect 2.4. These monopoles are the subject of [HS2]. Before these new multimonopoles are described, the tetrahedral 3-monopoles and cubic 4-monopole are discussed in Sect. 2.1. In this section are the pictures of these monopoles which first appeared in [HS1]. These pictures are the result of a numerical implementation of the ADHMN

construction. The method for applying symmetry to Nahm data is described in Sect. 2.2.

Sections 2.1 to 2.4 demonstrate how useful it is to apply symmetry to find new multimonopoles. The calculations themselves, however, are tedious. Sections 2.3 and 2.4 contain some large matrices. It is very satisfactory to have explicit solutions to the Nahm equations and thus pictures of the multimonopoles themselves. However, it is also satisfying to find that because of the rational map descriptions it is possible to understand something of symmetric multimonopoles without having to solve the corresponding symmetric Nahm equations. These rational map descriptions are discussed in Sect. 2.5 to 2.7.

There are two rational map descriptions, that of Donaldson and that of Jarvis. Each description has different advantages. The Donaldson rational maps are introduced in Sect. 2.5. It is not possible to study all symmetries with these maps. However, it is easy to deduce qualitative features of a monopole from the corresponding Donaldson rational map. As an example, it is demonstrated that there is a one-parameter family of C_{4h} 5-monopoles which pass through the octahedral 5-monopole. This one-parameter family is a geodesic and the qualitative features of the corresponding scattering process are derived from the rational maps.

In Sect. 2.6, the Donaldson rational map description is used to discover a large family of geodesics. These scattering processes have rotary-reflection symmetries: they were named twisted line scattering geodesics in [HS3]. The methods of Sect. 2.5 reveal how the monopoles behave during twisted line scattering. Twisted line scattering is revisited in Chapter 3 where the Nahm equations are solved in the 3-monopole case.

The Jarvis rational map description permits the investigation of any symmetry. It can determine the existence or nonexistence of any putative symmetric multimonopole. To prove the existence of a symmetric multimonopole the corresponding symmetric rational map must be constructed. This construction is explained in Sect. 2.7.

At the start of this chapter, symmetry is introduced as a way of simplifying the Nahm equations. The rational map descriptions are then used to study symmetric multimonopoles in a general way. It is now possible to tell which symmetric multimonopoles exist. The Nahm equations are not usually solvable for a general multimonopole and it is interesting to

ask for which symmetric multimonopoles can the Nahm equations be solved. This problem is addressed in Chapter 3 and solving it leads to several further solutions to the Nahm equations, including the 3-monopole twisted line scattering mentioned above.

2.1 Tetrahedral and cubic monopoles

In [HMM], Hitchin, Manton and Murray demonstrate that there exists a 3-monopole with tetrahedral symmetry and a 4-monopole with octahedral symmetry. Their approach combines the spectral curve and Nahm data formulations.

A rotation in space maps lines into one another. As a monopole is rotated, there is an equivalent transformation of the spectral curve resulting from the transformation of (η, ζ) . An SO_3 rotation in \mathbf{R}^3 of 2θ about the unit vector (n_1, n_2, n_3) corresponds to the Möbius transformation $\zeta \rightarrow \zeta'$ where

$$\zeta' = \frac{(\cot \theta + in_3)\zeta + (n_2 - in_1)}{-(n_2 + in_1)\zeta + (\cot \theta - in_3)}. \quad (2.1)$$

It follows from the definition of η that it transforms as $\eta \rightarrow \eta'$ where

$$\eta' = \frac{\eta}{[-(n_2 + in_1)\zeta + (\cot \theta - in_3)]^2}. \quad (2.2)$$

An algebraic curve $P(\eta, \zeta) = 0$ is then invariant under an element of SO_3 if $P(\eta', \zeta') = 0$ is the same algebraic curve. In [HMM], this is extended to reflection in the x_1x_2 -plane:

$$\begin{aligned} \sigma : \mathbf{R}^3 &\rightarrow \mathbf{R}^3 \\ (x_1, x_2, x_3) &\mapsto (x_1, x_2, -x_3). \end{aligned} \quad (2.3)$$

This corresponds to the map

$$\sigma : (\eta, \zeta) \mapsto \left(\frac{-\bar{\eta}}{\zeta^2}, \frac{1}{\bar{\zeta}} \right) \quad (2.4)$$

on TP^1 . Combining this involution with the reality transformation (1.46) gives

$$\sigma \circ \tau : (\eta, \zeta) \rightarrow (\eta, -\zeta). \quad (2.5)$$

Thus, if an algebraic curve $P(\eta, \zeta) = 0$ of the form (1.34), satisfying the reality condition (1.47), is invariant under the reflection σ , $P(\eta, -\zeta) = 0$ is the same curve as $P(\eta, \zeta) = 0$.

This allows algebraic curves symmetric under a given finite subgroup G of O_3 to be calculated. Consider $G = C_2$, the group generated by a rotation of π . The axis of rotation is taken to be the x_3 -axis. C_2 is generated in $T\mathbf{P}^1$ by

$$\zeta' = e^{\pi i} \zeta \tag{2.6}$$

$$\eta' = e^{\pi i} \eta. \tag{2.7}$$

The degree two centred algebraic curve

$$\eta^2 + \alpha_4 \zeta^4 + \alpha_3 \zeta^3 + \alpha_2 \zeta^2 + \alpha_1 \zeta + \alpha_0 = 0 \tag{2.8}$$

satisfies the reality condition (1.47) provided α_2 is real, $\alpha_1 = -\bar{\alpha}_3$ and $\alpha_0 = \bar{\alpha}_4$. This transforms under (2.7) into

$$\eta^2 + \alpha_4 \zeta^4 - \alpha_3 \zeta^3 + \alpha_2 \zeta^2 - \alpha_1 \zeta + \alpha_0 = 0 \tag{2.9}$$

and so this algebraic curve is C_2 symmetric about the x_3 -axis if $\alpha_3 = \alpha_1 = 0$.

2.1.1 Platonic symmetries

The tetrahedral group T is the group of rotational symmetries of a tetrahedron. It has twelve elements and is isomorphic to the permutation group \mathfrak{A}_4 . The octahedral group O is the group of rotational symmetries of the octahedron or, equivalently, the cube. It has 24 elements and is isomorphic to \mathfrak{S}_4 . The icosahedral group Y is the group of rotational symmetries of the icosahedron or, equivalently, the dodecahedron. It has sixty elements and is isomorphic to \mathfrak{A}_5 . As pointed out in [HMM], the simplest way to construct algebraic curves invariant under these groups is to exploit the work presented by Klein in his classic book [K].

Let (ζ_0, ζ_1) be homogeneous coordinates on the Riemann sphere such that $\zeta = \zeta_1/\zeta_0$. If $q_{2r}(\zeta_0, \zeta_1)$ is a degree $2r$ homogeneous polynomial invariant under the finite rotation group G then the corresponding inhomogeneous polynomial

$$q_{2r}(\zeta) = \frac{1}{\zeta_0^{2r}} q_{2r}(\zeta_0, \zeta_1) \tag{2.10}$$

transforms identically to η^r under G . Thus, an algebraic curve of the form (1.34) is G -invariant if any nontrivial polynomial coefficient $a_{2r}(\zeta)$ is derived from a G -invariant degree $2r$ homogeneous polynomial as in (2.10). These G -invariant homogeneous polynomials are known as Klein polynomials. They are given in [K] for $G = T, O, Y$. In [HMM] they are presented in a convenient table form. That table is reproduced here as Fig. 2.1.

In Fig. 2.1 are given the homogeneous polynomials q_V , q_E and q_F for $G = T, O, Y$. The polynomials q_V have zeros on the vertices of the relevant polyhedron, the polynomials q_E have zeros on the midpoints of the edges and the polynomials q_F have zeros on the midpoints of the faces. These polynomials are obviously dependent on orientation. The tetrahedron is oriented so that its vertices lie on $(1/\sqrt{3})(\pm 1, \pm 1, \pm 1)$ with either two or no signs negative. It is also useful to know the q_E polynomial for a tetrahedron oriented so that one vertex is on the positive x_3 -axis and one edge intersects the positive x_1 -axis. It is

$$\zeta_1^6 + 5\sqrt{2}\zeta_1^3\zeta_0^3 - \zeta_0^6. \quad (2.11)$$

The octahedron has its vertices on the Cartesian axes. The icosahedron has its uppermost vertex on the x_3 -axis and one of the five edges leaving it is in the $(x_1 > 0)x_3$ -halfplane.

Only some of the inhomogeneous polynomials are strictly invariant. These polynomials are marked with a star. The tetrahedral polynomials q_V and q_F acquire factors of $e^{\pm 2\pi i/3}$ respectively under rotations of $2\pi/3$ about a three-fold axes. The octahedral polynomials q_V and q_E acquire factors of -1 under a rotation by $\pi/2$ about a four-fold symmetry axis. These polynomials can be combined together to form invariant polynomials of higher degree.

2.1.2 Tetrahedral 3-monopole and cubic 4-monopole

In the edge-upward orientation, a tetrahedrally invariant degree three algebraic curve is

$$\eta^3 + ia_T\zeta(\zeta^4 - 1) = 0 \quad (2.12)$$

or, in the vertex-upward orientation (2.11),

$$\eta^3 + \frac{\sqrt{2}}{3^{3/2}}a_T(\zeta^6 + 5\sqrt{2}\zeta^3 - 1) = 0, \quad (2.13)$$

G	q_V	q_E	q_F
T	$\zeta_1^4 + 2\sqrt{3}i\zeta_1^2\zeta_0^2 + \zeta_0^4$	$\zeta_1\zeta_0(\zeta_1^4 - \zeta_0^4) \star$	$\zeta_1^4 - 2\sqrt{3}i\zeta_1^2\zeta_0^2 + \zeta_0^4$
O	$\zeta_1\zeta_0(\zeta_1^4 - \zeta_0^4)$	$\zeta_1^{12} - 33\zeta_1^8\zeta_0^4$ $-33\zeta_1^4\zeta_0^8 + \zeta_0^{12}$	$\zeta_1^8 + 14\zeta_1^4\zeta_0^4 + \zeta_0^8 \star$
Y	$\zeta_1\zeta_0(\zeta_1^{10} + 11\zeta_1^5\zeta_0^5 - \zeta_0^{10}) \star$	$\zeta_1^{30} + 522\zeta_1^{25}\zeta_0^5$ $-10005\zeta_1^{20}\zeta_0^{10} - 10005\zeta_1^{10}\zeta_0^{20}$ $-522\zeta_1^5\zeta_0^{25} + \zeta_0^{30} \star$	$\zeta_1^{20} - 228\zeta_1^{15}\zeta_0^5$ $+494\zeta_1^{10}\zeta_0^{10}$ $+228\zeta_1^5\zeta_0^{15} + \zeta_0^{20} \star$

Figure 2.1: Invariant homogeneous polynomials.

where a_T is real. These algebraic curves can be obtained one from the other by rotation and the factor of $-i\sqrt{2}/3^{3/2}$ results from that rotation. Up to orientation, this is the lowest degree tetrahedral algebraic curve. The lowest degree octahedrally invariant degree four algebraic curve is

$$\eta^4 + a_O(\zeta^8 + 14\zeta^4 + 1) = 0, \quad (2.14)$$

where a_O is real. Finally, the lowest degree icosahedral curve is

$$\eta^6 + a_Y\zeta(\zeta^{10} + 11\zeta^5 - 1) = 0, \quad (2.15)$$

with a_Y real. These are simply G -invariant algebraic curves in TP^1 . It is not obvious for which values of a_T , a_O or a_Y , if any, they are the spectral curves of monopoles. In [HMM], the ADHMN construction is used to prove that

$$\eta^3 + i\frac{\Gamma(1/6)^3\Gamma(1/3)^3}{48\sqrt{3}\pi^{3/2}}\zeta(\zeta^4 - 1) = 0 \quad (2.16)$$

$$\eta^4 + \frac{3\Gamma(1/4)^8}{1024\pi^2}(\zeta^8 + 14\zeta^4 + 1) = 0 \quad (2.17)$$

are spectral curves and, thus, that there is a tetrahedral 3-monopole and an octahedral 4-monopole. It is also proved that there is no value of a_Y such that the icosahedral curve of degree six is a spectral curve. Therefore, there is no 6-monopole with icosahedral symmetry.

Since the Nahm data of the tetrahedral 3-monopole and octahedral 4-monopole are known, it is interesting to examine surfaces of constant energy density for these monopole configurations. The easiest way to calculate energy density is to use the Ward's formula [Wa1],

$$\mathcal{E} = \Delta|\Phi|^2. \tag{2.18}$$

Thus, only the Higgs field Φ is required. The ADHMN construction has been described in Chapter 1. It allows the monopole fields to be calculated from their Nahm data. The Nahm data which correspond to monopoles with Platonic symmetry are sufficiently complicated to preclude the calculation of a closed expression for Φ . A numerical implementation of the procedure is required and one is presented in [HS1].

Figure 2.2 displays the output of this numerical implementation for the tetrahedral 3-monopole. The plot shows a surface of constant energy density. The tetrahedral symmetry of this surface is clearly evident and plots for other values of energy density close to this one are qualitatively similar. For large energy density, the surface breaks up into four disconnected pieces centred on the vertices of a tetrahedron.

Figure 2.3 displays the output of the numerical ADHMN construction for the octahedral 4-monopole. The plot shows a surface of constant energy density. Note that for the monopole with octahedral symmetry, a constant energy density surface could have resembled an octahedron or a cube: it is the latter. For large values of \mathcal{E} , the surface breaks up into eight disconnected pieces on the vertices of a cube.

2.1.3 Tetrahedral $(3, [2], [1])$ -monopoles

It is noted, as an aside, that SU_2 data are easily adapted to other gauge groups. This is done in Chapter 1; the 2×2 data is adapted to give $([1], 2, [1])$ data. In the same way, the symmetric data corresponding to the tetrahedral 3-monopole can be adapted to give data

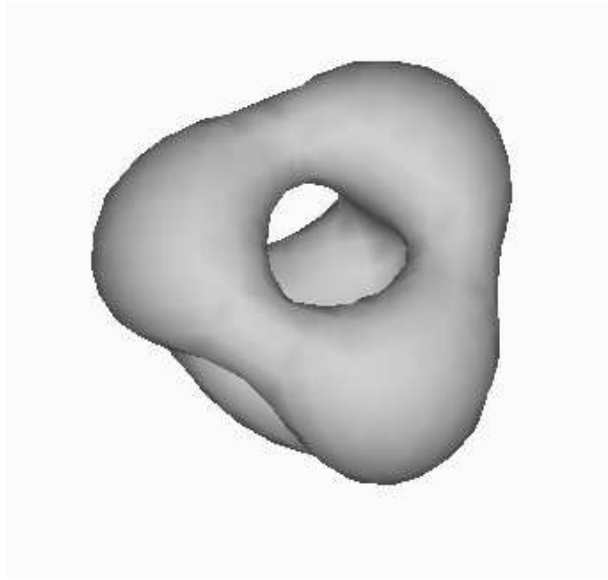
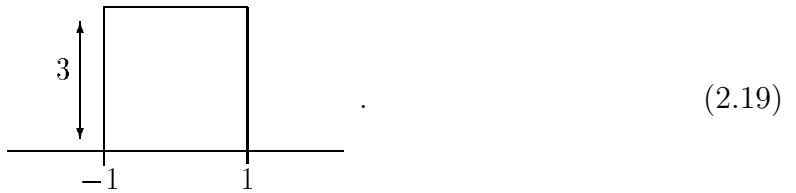
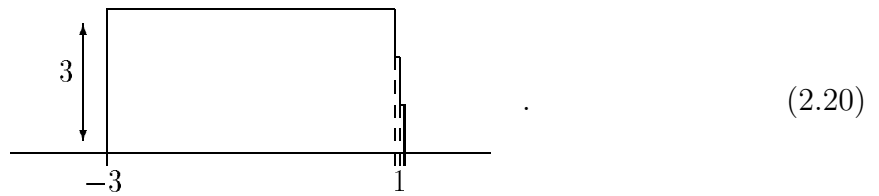


Figure 2.2: Tetrahedral 3-monopole; surface of constant energy density.

for a tetrahedral $(3, [2], [1])$ -monopole or even a tetrahedral $([1], [2], 3, [2], [1])$ -monopole. The tetrahedral 3×3 data have skyline diagram



The data have poles at $t = 1$ and $t = -1$. $(3, [2], [1])$ data have skyline



There is a pole at $t = -3$ and none at $t = 1$. This is a weaker condition and, moving from the 3-monopole case to the $(3, [2], [1])$ -monopole case, the unique tetrahedral data spawn a one-parameter family of tetrahedral data [HS5].

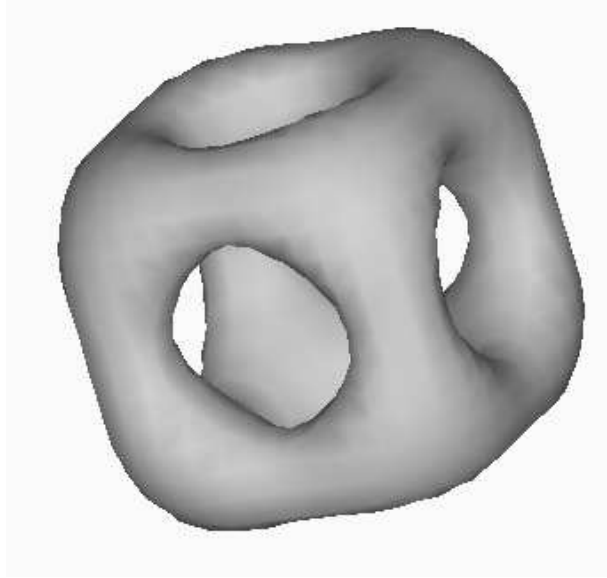


Figure 2.3: Cubic 4-monopole; surface of constant energy density.

Since the fixed point set of a group action gives a totally geodesic submanifold, this one-parameter family is a geodesic in $\mathcal{M}_{(3,[2],[1])}^0$. Within the moduli space approximation, this family of monopoles may be interpreted as describing the low energy dynamics of three deforming monopoles. Surfaces of constant energy density for monopoles along the geodesic are plotted in Fig. 2.4. During the course of the motion, a tetrahedron gets smoothed out into a sphere and then deforms into the dual tetrahedron. This is an example of dynamics in which the monopoles never become separated: a feature of monopole dynamics in theories with nonAbelian residual symmetry.

In Chapter 3 a one-parameter family of tetrahedral 4×4 data is presented, the above construction would derive from the same solutions to the Nahm equations a two-parameter family of tetrahedral $(4, [3], [2], [1])$ -monopoles. In the same way it is noted that in [HMS] putative icosahedral 6×6 data are examined. These data satisfy the correct boundary condition at $t = -1$: the residue is the irreducible representation $\underline{6}$. However it is not SU_2 monopole data because at $t = 1$ the matrix residues are a reducible representation: $\underline{2} + \underline{2} + \underline{2}$. This means that, with t rescaled, the data are data for an icosahedral $(6, [4], [2])$ -monopole and, so, contained in the proof that no 6-monopole has icosahedral symmetry is a proof

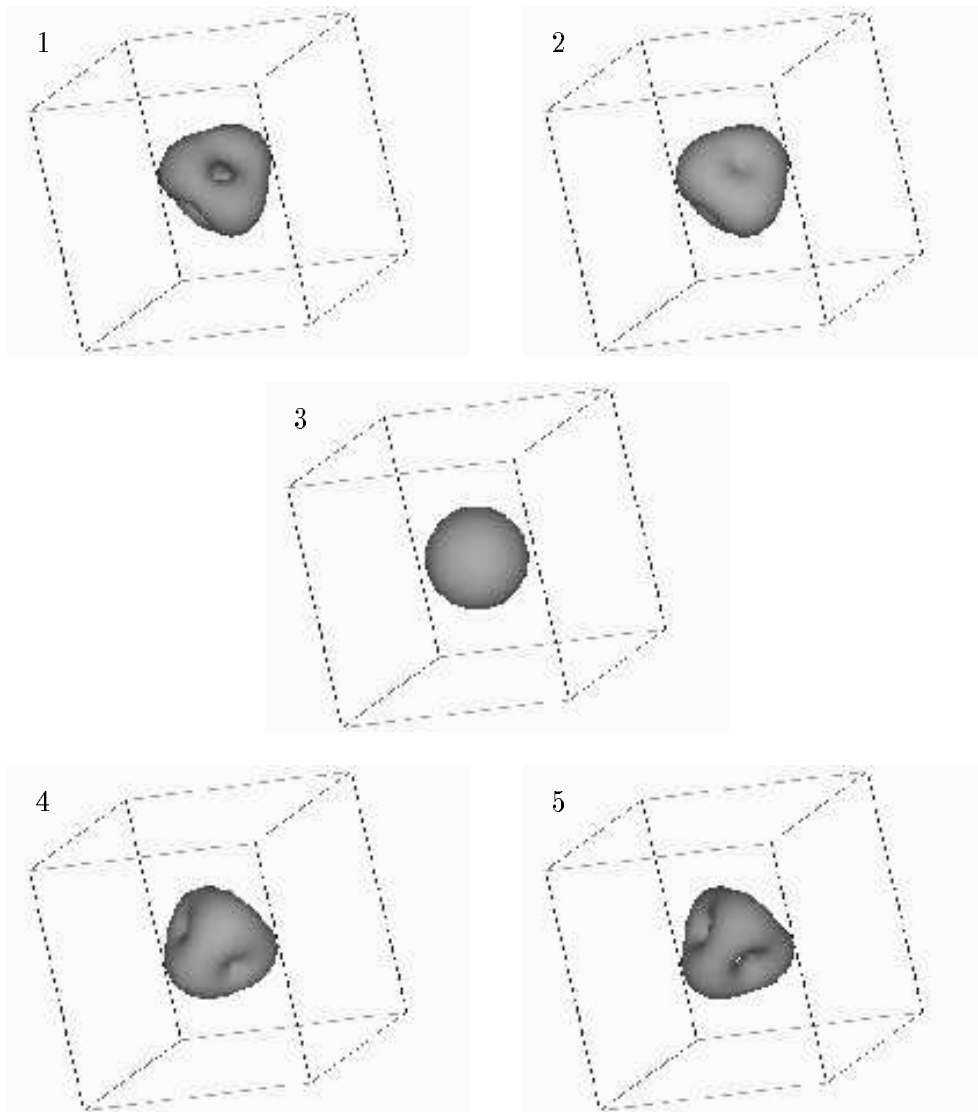


Figure 2.4: Tetrahedral scattering of a $(3, [2], [1])$ -monopole.

that there is an icosahedrally symmetric $(6, [4], [2])$ -monopole. Many opportunities exist to derive higher gauge group data like this from the data for SU_2 monopoles. It is more interesting to find new SU_2 Nahm data. In the next section the construction of symmetric Nahm data is explained and in Sect. 2.3 this construction will be used show that there is an icosahedrally symmetric 7-monopole.

2.2 Symmetric Nahm data

The combined spectral curve and Nahm data approach of Hitchin, Manton and Murray [HMM] can be adapted and extended to apply to other symmetric monopoles.

The Nahm data are an $\mathbf{R}^3 \times \mathfrak{sl}_k \mathbf{C}$ valued function of s , which transform under the rotation group SO_3 as

$$\underline{3} \times \mathfrak{sl}(\underline{k}). \quad (2.21)$$

Since $\mathfrak{gl}(\underline{k}) \cong \underline{k} \times \underline{k}$ Clebsh-Gordon decomposition gives

$$\mathfrak{gl}(\underline{k}) \cong \underline{2k-1} + \underline{2k-3} + \dots + \underline{3} + \underline{1} \quad (2.22)$$

and, so,

$$\mathfrak{sl}(\underline{k}) \cong \underline{2k-1} + \underline{2k-3} + \dots + \underline{3}. \quad (2.23)$$

Substituting into (2.21)

$$\begin{aligned} \underline{3} \times \mathfrak{sl}(\underline{k}) &\cong \underline{3} \times (\underline{2k-1} + \underline{2k-3} + \dots + \underline{3}) \\ &\cong (\underline{2k+1} + \underline{2k-1} + \underline{2k-3}) + \dots + (\underline{5} + \underline{3} + \underline{1}). \end{aligned} \quad (2.24)$$

Thus, for example, the Nahm data corresponding to 4-monopoles are in the carrier space $(\underline{9} + \underline{7} + \underline{5}) + (\underline{7} + \underline{5} + \underline{3}) + (\underline{5} + \underline{3} + \underline{1})$. It is convenient to write this as $(\underline{9}_u + \underline{7}_m + \underline{5}_l) + (\underline{7}_u + \underline{5}_m + \underline{3}_l) + (\underline{5}_u + \underline{3}_m + \underline{1}_l)$ where the subscripts u, m and l , standing for upper, middle and lower allow isomorphic representations with different pedigrees to be distinguished. The $\underline{1}_l$ representation is invariant under all of SO_3 .

X, Y and H satisfying the commutation relations

$$\begin{aligned} [X, Y] &= H, \\ [H, X] &= 2X, \\ [H, Y] &= -2Y \end{aligned} \tag{2.25}$$

are a basis for \mathfrak{su}_2 . They may be represented by the principal \mathfrak{su}_2 subalgebra of $\mathfrak{sl}(\underline{k})$ which in turn acts on the algebra by the adjoint action. In this representation, X is a rank $k - 1$ nilpotent element and a basis of $\mathfrak{sl}(\underline{k})$ can be generated by acting with Y on X^r , for $r = 1, 2, \dots, k - 1$. Thus,

$$\begin{array}{ccccccc} X^{k-1} & (\text{ad}Y)X^{k-1} & (\text{ad}Y)^2X^{k-1} & \dots & \dots & (\text{ad}Y)^{2k-2}X^{k-1} \\ \vdots & \dots & & & & \\ X^r & (\text{ad}Y)X^r & (\text{ad}Y)^2X^r & \dots & (\text{ad}Y)^{2r}X^r \\ \vdots & \dots & & & \\ X & (\text{ad}Y)X & (\text{ad}Y)^2X \end{array}$$

is a basis of $\mathfrak{sl}(\underline{k})$ where $\text{ad}Y$ denotes the adjoint action of Y and is given on a general matrix M by $\text{ad}YM = [M, Y]$. The element X^r of the Abelian nilpotent subalgebra $\langle X, X^2, \dots, X^{k-1} \rangle$ is the highest weight vector for the \mathfrak{su}_2 representation $\underline{2r + 1}$ lying in the decomposition (2.24) of $\mathfrak{sl}(\underline{k})$.

Since the invariant polynomials are known, it is convenient to exploit the representations of \mathfrak{su}_2 on homogeneous polynomials over \mathbf{P}^1 . $\underline{r + 1}$ is defined on degree r homogeneous polynomials by the identification

$$\begin{aligned} X &= \zeta_1 \frac{\partial}{\partial \zeta_0}, \\ Y &= \zeta_0 \frac{\partial}{\partial \zeta_1}, \\ H &= -\zeta_0 \frac{\partial}{\partial \zeta_0} + \zeta_1 \frac{\partial}{\partial \zeta_1}. \end{aligned} \tag{2.26}$$

In the case of degree r homogeneous polynomials, the highest weight vector is ζ_1^r and the basis is $\{\zeta_1^r, (\zeta_0 \frac{\partial}{\partial \zeta_1})\zeta_1^r, \dots, (\zeta_0 \frac{\partial}{\partial \zeta_1})^r \zeta_1^r\}$. Thus, a degree $2r$ homogeneous polynomial

$q_{2r}(\zeta_0, \zeta_1)$ is related to a matrix S in the $\underline{2r+1}$ representation of the decomposition of $\mathfrak{sl}(k)$ by rewriting $q_{2r}(\zeta_0, \zeta_1)$ as $q_{2r}(\zeta_0 \frac{\partial}{\partial \zeta_1}) \zeta_1^{2r}$ and then letting

$$S = q_{2r}(\text{ad}Y)X^r. \quad (2.27)$$

It is now possible to construct G symmetric $\underline{2r+1}_u$ $k \times k$ Nahm data corresponding to the G symmetric homogeneous polynomial $p(\zeta_0, \zeta_1)$. The inclusion

$$\underline{2r+1} \hookrightarrow \underline{3} \times \underline{2r-1} \cong \underline{2r+1}_u + \underline{2r-1}_m + \underline{2r-3}_l \quad (2.28)$$

is given on polynomials by

$$p(\zeta_0, \zeta_1) \mapsto \xi_1^2 \times p_{11}(\zeta_0, \zeta_1) + 2\xi_0 \xi_1 \times p_{10}(\zeta_0, \zeta_1) + \xi_0^2 \times p_{00}(\zeta_0, \zeta_1) \quad (2.29)$$

where

$$p_{ab}(\zeta_0, \zeta_1) = \frac{\partial^2 p}{\partial \zeta_a \partial \zeta_b}(\zeta_0, \zeta_1). \quad (2.30)$$

The polynomial expression $\xi_1^2 \times p_{11}(\zeta_0, \zeta_1) + 2\xi_0 \xi_1 \times p_{10}(\zeta_0, \zeta_1) + \xi_0^2 \times p_{00}(\zeta_0, \zeta_1)$ is rewritten in the form

$$\xi_1^2 \times p_{11}(\zeta_0 \frac{\partial}{\partial \zeta_1}) \zeta_1^{2r} + (\xi_0 \frac{\partial}{\partial \xi_1}) \xi_1^2 \times p_{10}(\zeta_0 \frac{\partial}{\partial \zeta_1}) \zeta_1^{2r} + \frac{1}{2} (\xi_0 \frac{\partial}{\partial \xi_1})^2 \xi_1^2 \times p_{00}(\zeta_0 \frac{\partial}{\partial \zeta_1}) \zeta_1^{2r}. \quad (2.31)$$

This defines a triplet of $k \times k$ matrices. Given a $k \times k$ representation of X, Y and H above, the invariant Nahm triplet is

$$(S'_1, S'_2, S'_3) = (q_{11}(\text{ad}Y)X^r, q_{10}(\text{ad}Y)X^r, q_{00}(\text{ad}Y)X^r). \quad (2.32)$$

The Nahm isospace basis is transformed. This transformation is given by

$$(S_1, S_2, S_3) = (\frac{1}{2}S'_1 + S'_3, -\frac{i}{2}S'_1 + iS'_3, -iS'_2). \quad (2.33)$$

Relative to this basis the SO_3 -invariant Nahm triplet corresponding to the $\underline{1}_l$ representation in (2.23) is given by (ρ_1, ρ_2, ρ_3) where

$$\begin{aligned} \rho_1 &= X - Y, \\ \rho_2 &= i(X + Y), \\ \rho_3 &= iH. \end{aligned} \quad (2.34)$$

In applying this method to cases other than those considered in [HMM], it is sometimes also necessary to construct invariant Nahm triplets lying in the $\underline{2r+1}_m$ representations. This problem is similar to that of finding the spin states of two particles in quantum mechanics. The corresponding $\underline{2r+1}_u$ triplet is constructed first. This triplet is then written in the canonical form

$$[c_0 + c_1(\text{ad}Y \times 1 + 1 \times \text{ad}Y) + \dots + c_i(\text{ad}Y \times 1 + 1 \times \text{ad}Y)^i + \dots + c_{2r}(\text{ad}Y \times 1 + 1 \times \text{ad}Y)^{2r}] X \times X^r \quad (2.35)$$

and mapped isomorphically into $\underline{2r+1}_m$ by mapping the highest weight vector $X \times X^r$ to the highest weight vector

$$X \times \text{ad}Y X^{r+1} - \frac{1}{r+1} \text{ad}Y X \times X^{r+1}. \quad (2.36)$$

This highest weight vector is derived by requiring it to be annihilated by the ladder operator $\text{ad}X \times 1 + 1 \times \text{ad}X$. A $\underline{2r+1}_l$ invariant can also be constructed by this method but by using the highest weight vector

$$X \times (\text{ad}Y)^2 X^{r+2} - (2r+3) \text{ad}Y X \times \text{ad}Y X^{r+2} - (2r+3)(r+2) (\text{ad}Y)^2 X \times X^{r+2}. \quad (2.37)$$

This means the construction of symmetric Nahm triplets is known. In the next two sections this method will be applied to construct icosahedral 7×7 data and octahedral 5×5 triplets. Substituting these symmetric Nahm triplets into the Nahm equations simplifies the Nahm equations; the Nahm equations are solvable in both these cases. This means the numerical ADHMN construction mentioned in Sect. 2.1 can be used to produce pictures of these monopoles. At the end of Sect. 2.3 it is seen that the icosahedral 7-monopole looks like a dodecahedron. At the end of Sect. 2.4 it is seen that the octahedral 5-monopole looks like an octahedron.

2.3 Dodecahedral 7-monopole

When it was found that there is no icosahedrally symmetric 6-monopole, it was asked whether there is an icosahedrally symmetric 7-monopole. Since the discovery of the Jarvis

rational map description it would be possible to show, without recourse to the Nahm equations, that there is such a monopole. How this is done is the subject of Sect. 2.7. However, the question of the existence of the icosahedrally symmetric 7-monopole was first answered using Nahm data [HS2]. In this section the Nahm data for this monopole is constructed. The reward for finding this Nahm data is the picture of the monopole. This picture is at the end of this section. Solving the Nahm equations has this advantage over the rational map descriptions: it allows convenient numerical evaluation of the fields.

7×7 Nahm data transforms as

$$(\underline{15}_u + \underline{13}_m + \underline{11}_u) + (\underline{13}_u + \underline{11}_l + \underline{9}_l) + \dots + (\underline{5}_u + \underline{3}_l + \underline{1}_l). \quad (2.38)$$

In addition to the SO_3 invariant $\underline{1}_l$ there are icosahedral invariant data in $\underline{13}_m$ and $\underline{13}_u$. These are constructed explicitly.

The minimum degree icosahedrally invariant homogeneous polynomial is [K]

$$\zeta_1^{11} \zeta_0 + 11 \zeta_1^6 \zeta_0^6 - \zeta_1 \zeta_0^{11}. \quad (2.39)$$

Polarizing this gives

$$\xi_1^2 \times (110 \zeta_1^9 \zeta_0 + 330 \zeta_1^4 \zeta_0^6) + 2 \xi_1 \xi_0 \times (11 \zeta_1^{10} + 396 \zeta_1^5 \zeta_0^5 - 11 \zeta_0^{10}) + \xi_0^2 \times (330 \zeta_1^6 \zeta_0^4 - 110 \zeta_1 \zeta_0^9). \quad (2.40)$$

This is proportional to

$$\begin{aligned} \xi_1^2 \times \left(\zeta_0 \frac{\partial}{\partial \zeta_1} + \frac{1}{5040} \left(\zeta_0 \frac{\partial}{\partial \zeta_1} \right)^6 \right) \zeta_1^{10} + 2 \xi_1 \xi_0 \times \left(1 + \frac{1}{840} \left(\zeta_0 \frac{\partial}{\partial \zeta_1} \right)^5 - \frac{1}{10!} \left(\zeta_0 \frac{\partial}{\partial \zeta_1} \right)^{10} \right) \zeta_1^{10} \\ + \xi_0^2 \times \left(\frac{1}{168} \left(\zeta_0 \frac{\partial}{\partial \zeta_1} \right)^4 - \frac{1}{9!} \left(\zeta_0 \frac{\partial}{\partial \zeta_1} \right)^9 \right) \zeta_1^{10}, \end{aligned} \quad (2.41)$$

which gives matrices

$$\begin{aligned} X \times (\text{ad}Y + \frac{1}{5040} (\text{ad}Y)^6) X^5 + \text{ad}Y X \times \left(1 + \frac{1}{840} (\text{ad}Y)^5 - \frac{1}{10!} (\text{ad}Y)^{10} \right) X^5 \\ + \frac{1}{2} (\text{ad}Y)^2 X \times \left(\frac{1}{168} (\text{ad}Y)^4 - \frac{1}{9!} (\text{ad}Y)^9 \right) X^5. \end{aligned} \quad (2.42)$$

A basis for $\underline{\mathfrak{g}}$ is given by

$$H = \begin{bmatrix} 6 & 0 & 0 & 0 & 0 & 0 & 0 \\ 0 & 4 & 0 & 0 & 0 & 0 & 0 \\ 0 & 0 & 2 & 0 & 0 & 0 & 0 \\ 0 & 0 & 0 & 0 & 0 & 0 & 0 \\ 0 & 0 & 0 & 0 & -2 & 0 & 0 \\ 0 & 0 & 0 & 0 & 0 & -4 & 0 \\ 0 & 0 & 0 & 0 & 0 & 0 & -6 \end{bmatrix}, \quad (2.43)$$

$$Y = \begin{bmatrix} 0 & 0 & 0 & 0 & 0 & 0 & 0 \\ \sqrt{6} & 0 & 0 & 0 & 0 & 0 & 0 \\ 0 & \sqrt{10} & 0 & 0 & 0 & 0 & 0 \\ 0 & 0 & \sqrt{12} & 0 & 0 & 0 & 0 \\ 0 & 0 & 0 & \sqrt{12} & 0 & 0 & 0 \\ 0 & 0 & 0 & 0 & \sqrt{10} & 0 & 0 \\ 0 & 0 & 0 & 0 & 0 & \sqrt{6} & 0 \end{bmatrix},$$

$$X = \begin{bmatrix} 0 & \sqrt{6} & 0 & 0 & 0 & 0 & 0 \\ 0 & 0 & \sqrt{10} & 0 & 0 & 0 & 0 \\ 0 & 0 & 0 & \sqrt{12} & 0 & 0 & 0 \\ 0 & 0 & 0 & 0 & \sqrt{12} & 0 & 0 \\ 0 & 0 & 0 & 0 & 0 & \sqrt{10} & 0 \\ 0 & 0 & 0 & 0 & 0 & 0 & \sqrt{6} \\ 0 & 0 & 0 & 0 & 0 & 0 & 0 \end{bmatrix}.$$

Using MAPLE, the invariant Nahm triplet is calculated to give the $\underline{13}_u$ invariant

$$\begin{aligned}
Z_1 &= \begin{bmatrix} 0 & 5\sqrt{6} & 0 & 0 & 7\sqrt{60} & 0 & 0 \\ -5\sqrt{6} & 0 & -9\sqrt{10} & 0 & 0 & 0 & 0 \\ 0 & 9\sqrt{10} & 0 & 5\sqrt{12} & 0 & 0 & -7\sqrt{60} \\ 0 & 0 & -5\sqrt{12} & 0 & 5\sqrt{12} & 0 & 0 \\ -7\sqrt{6}\sqrt{10} & 0 & 0 & -5\sqrt{12} & 0 & -9\sqrt{10} & 0 \\ 0 & 0 & 0 & 0 & 9\sqrt{10} & 0 & 5\sqrt{6} \\ 0 & 0 & 7\sqrt{60} & 0 & 0 & -5\sqrt{6} & 0 \end{bmatrix}, \quad (2.44) \\
Z_2 &= i \begin{bmatrix} 0 & 5\sqrt{6} & 0 & 0 & -7\sqrt{60} & 0 & 0 \\ 5\sqrt{6} & 0 & -9\sqrt{10} & 0 & 0 & 0 & 0 \\ 0 & -9\sqrt{10} & 0 & 5\sqrt{12} & 0 & 0 & 7\sqrt{60} \\ 0 & 0 & 5\sqrt{12} & 0 & 5\sqrt{12} & 0 & 0 \\ -7\sqrt{60} & 0 & 0 & 5\sqrt{12} & 0 & -9\sqrt{10} & 0 \\ 0 & 0 & 0 & 0 & -9\sqrt{10} & 0 & 5\sqrt{6} \\ 0 & 0 & 7\sqrt{60} & 0 & 0 & 5\sqrt{6} & 0 \end{bmatrix}, \\
Z_3 &= i \begin{bmatrix} -12 & 0 & 0 & 0 & -14\sqrt{6} & 0 & 0 \\ 0 & 48 & 0 & 0 & 0 & 0 & -14\sqrt{6} \\ 0 & 0 & -60 & 0 & 0 & 0 & 0 \\ 0 & 0 & 0 & 0 & 0 & 0 & 0 \\ 0 & 0 & 0 & 0 & 60 & 0 & 0 \\ -14\sqrt{6} & 0 & 0 & 0 & 0 & -48 & 0 \\ 0 & -14\sqrt{6} & 0 & 0 & 0 & 0 & 12 \end{bmatrix}.
\end{aligned}$$

To calculate the $\underline{13}_m$ invariant (2.42) is put in the form (2.36). It is proportional to

$$[11!(\text{ad}Y \times 1 + 1 \times \text{ad}Y) + 7920(\text{ad}Y \times 1 + 1 \times \text{ad}Y)^6 - (\text{ad}Y \times 1 + 1 \times \text{ad}Y)^{11}]X \times X^5. \quad (2.45)$$

Then, using the isomorphism mentioned earlier, the matrices

$$\begin{aligned}
Y_1 &= \begin{bmatrix} 0 & \sqrt{6} & 0 & 0 & -\sqrt{60} & 0 & 12 \\ \sqrt{6} & 0 & -3\sqrt{10} & 0 & 0 & 12 & 0 \\ 0 & -3\sqrt{10} & 0 & 5\sqrt{12} & 0 & 0 & -\sqrt{60} \\ 0 & 0 & 5\sqrt{12} & 0 & -5\sqrt{12} & 0 & 0 \\ -\sqrt{60} & 0 & 0 & -5\sqrt{12} & 0 & 3\sqrt{10} & 0 \\ 0 & 12 & 0 & 0 & 3\sqrt{10} & 0 & -\sqrt{6} \\ 12 & 0 & -\sqrt{60} & 0 & 0 & -\sqrt{6} & 0 \end{bmatrix}, \quad (2.46) \\
Y_2 &= i \begin{bmatrix} 0 & \sqrt{6} & 0 & 0 & \sqrt{60} & 0 & 12 \\ -\sqrt{6} & 0 & -3\sqrt{10} & 0 & 0 & -12 & 0 \\ 0 & 3\sqrt{10} & 0 & 5\sqrt{12} & 0 & 0 & \sqrt{60} \\ 0 & 0 & -5\sqrt{12} & 0 & -5\sqrt{12} & 0 & 0 \\ -\sqrt{60} & 0 & 0 & 5\sqrt{12} & 0 & 3\sqrt{10} & 0 \\ 0 & 12 & 0 & 0 & -3\sqrt{10} & 0 & -\sqrt{6} \\ -12 & 0 & -\sqrt{60} & 0 & 0 & \sqrt{6} & 0 \end{bmatrix}, \\
Y_3 &= i \begin{bmatrix} 0 & 0 & 0 & 0 & 0 & -10\sqrt{6} & 0 \\ 0 & 0 & 0 & 0 & 0 & 0 & 10\sqrt{6} \\ 0 & 0 & 0 & 0 & 0 & 0 & 0 \\ 0 & 0 & 0 & 0 & 0 & 0 & 0 \\ 0 & 0 & 0 & 0 & 0 & 0 & 0 \\ 10\sqrt{6} & 0 & 0 & 0 & 0 & 0 & 0 \\ 0 & -10\sqrt{6} & 0 & 0 & 0 & 0 & 0 \end{bmatrix}
\end{aligned}$$

are obtained

The reduced Nahm equations are derived from the commutation relations. The required relations involving ρ matrices and Z matrices are

$$\begin{aligned}
[\rho_1, \rho_2] &= 2\rho_3, \\
[Z_1, Z_2] &= -750\rho_3 + 90Z_3, \\
[Z_1, \rho_2] + [\rho_1, Z_2] &= -10Z_3.
\end{aligned} \tag{2.47}$$

Because of the closed form of these relations, it is possible to derive a consistent set of Nahm equations from the icosahedrally invariant Nahm data

$$T_i(t) = x(t)\rho_i + z(t)Z_i. \quad (2.48)$$

The invariant Nahm triplet (Y_1, Y_2, Y_3) can be consistently ignored. Combining (2.47) and (2.48) gives the reduced Nahm equations

$$\begin{aligned} \frac{dx}{dt} &= 2x^2 - 750z^2, \\ \frac{dz}{dt} &= -10xz + 90z^2 \end{aligned} \quad (2.49)$$

with corresponding spectral curve

$$\eta[\eta^6 + a\zeta(\zeta^{10} + 11\zeta^5 + 1)] = 0, \quad (2.50)$$

where

$$a = 552960(14xz - 175z^2)(x + 5z)^4 \quad (2.51)$$

is a constant.

To solve equations (2.49), let $u = x + 5z$ and $v = x - 30z$ so that

$$\begin{aligned} \frac{du}{dt} &= 2uv \\ \frac{dv}{dt} &= 6u^2 - 4v^2, \\ a &= 110592(u^6 - v^2u^4) \equiv 110592\kappa^6. \end{aligned} \quad (2.52)$$

Using the constant to eliminate v , the equation for u becomes

$$\frac{du}{dt} = -2u^2\sqrt{1 - \kappa^6u^{-6}}. \quad (2.53)$$

If $u = -\kappa\sqrt{\wp(s)}$, where $s = 2\kappa(t + 1)$, then $\wp(s)$ is the Weierstrass function satisfying

$$\left(\frac{d\wp}{ds}\right)^2 = 4(\wp^3 - 1). \quad (2.54)$$

Thus the Nahm equations are solved by

$$x(t) = \frac{2\kappa}{7} \left[-3\sqrt{\wp} + \frac{1}{4\wp} \frac{d\wp}{ds} \right], \quad (2.55)$$

$$z(t) = -\frac{\kappa}{35} \left[\sqrt{\wp} + \frac{1}{2\wp} \frac{d\wp}{ds} \right]. \quad (2.56)$$

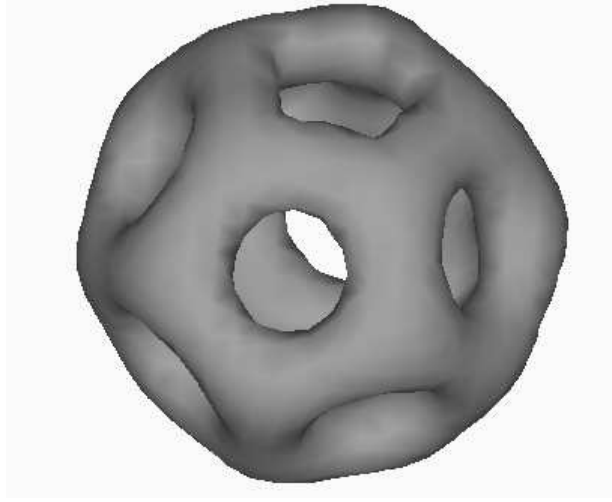


Figure 2.5: Dodecahedral 7-monopole; surface of constant energy density.

These functions are analytic in $t \in (-1, 1)$ and have simple poles at $t = -1$ and $t = 1$ provided $\kappa = \omega_1$, where $2\omega_1$ is the real period of $\wp(s)$. ω_1 is explicitly known for this Weierstrass function;

$$\omega_1 = \frac{\Gamma(1/6)\Gamma(1/3)}{8\sqrt{3}\pi} \quad (2.57)$$

and, so,

$$a = 110592\kappa^6 = \frac{\Gamma(1/6)^6\Gamma(1/3)^6}{64\pi^3}. \quad (2.58)$$

Near $t = -1$

$$\wp(s) \sim \left(\frac{1}{s}\right)^2 \quad (2.59)$$

and, so, the residues of x and z are $-1/2$ and 0 respectively. At $t = 1$ they are, respectively, $-5/14$ and $-1/35$. At both poles, the eigenvalues of the matrix residue of iT_3 are $\{\pm 3, \pm 2, \pm 1, 0\}$. This demonstrates that the matrix residues define the irreducible representation at each end of the interval. Hence, there is a 7-monopole with icosahedral symmetry given by the spectral curve

$$\eta^7 + \frac{\Gamma(1/6)^6\Gamma(1/3)^6}{64\pi^3}\zeta(\zeta^{10} + 11\zeta^5 - 1)\eta = 0. \quad (2.60)$$

The energy density of this monopole is computed using the numerical implementation of the ADHMN construction. Figure 2.5 shows a surface of constant energy density. The

surface resembles a dodecahedron. The energy density takes its maximum value on the twenty vertices of the dodecahedron.

2.4 Octahedral 5-monopole

Towards the end of the last section is found the spectral curve of the dodecahedral 7-monopole (2.60). It is a reducible curve, the two components are the star; $\eta = 0$, and an icosahedrally symmetric degree six algebraic curve. It is simple to envisage a similar octahedrally symmetric degree five algebraic curve derived by multiply an octahedrally symmetric degree four curve by η . In this section it is shown that there is a 5-monopole whose spectral curve has this form. The methods are very similar to those of the last section.

From Fig. 2.1, the lowest degree octahedrally invariant homogeneous polynomial is

$$\zeta_1^8 + 14\zeta_1^4\zeta_0^4 + \zeta_0^8. \quad (2.61)$$

Polarizing this gives

$$\xi_1^2 \times (56\zeta_1^6 + 168\zeta_1^2\zeta_0^4) + 2\xi_1\xi_0 \times (224\zeta_1^3\zeta_0^3) + \xi_0^2 \times (56\zeta_0^6 + 168\zeta_1^4\zeta_0^2) \quad (2.62)$$

which is written in the form

$$\xi_1^2 \times \left(56 + \frac{7}{15} \left(\zeta_0 \frac{\partial}{\partial \zeta_1}\right)^4\right) \zeta_1^6 + 2\xi_1\xi_0 \times \frac{28}{15} \left(\zeta_0 \frac{\partial}{\partial \zeta_1}\right)^3 \zeta_1^6 + \xi_0^2 \times \left(\frac{7}{90} \left(\zeta_0 \frac{\partial}{\partial \zeta_1}\right)^6 + \frac{28}{5} \left(\zeta_0 \frac{\partial}{\partial \zeta_1}\right)^2\right) \zeta_1^6, \quad (2.63)$$

giving matrices

$$X \times \left(56 + \frac{7}{15} \text{ad}Y^4\right) X^3 + \text{ad}Y X \times \frac{28}{15} \text{ad}Y^3 X^3 + \frac{1}{2} \text{ad}Y^2 X \times \left(\frac{7}{90} \text{ad}Y^6 + \frac{28}{5} \text{ad}Y^2\right) X^3. \quad (2.64)$$

The \mathfrak{su}_2 basis (2.25) may be represented by

$$H = \begin{bmatrix} -4 & 0 & 0 & 0 & 0 \\ 0 & -2 & 0 & 0 & 0 \\ 0 & 0 & 0 & 0 & 0 \\ 0 & 0 & 0 & 2 & 0 \\ 0 & 0 & 0 & 0 & 4 \end{bmatrix}, \quad (2.65)$$

$$X = -i \begin{bmatrix} 0 & 0 & 0 & 0 & 0 \\ 2 & 0 & 0 & 0 & 0 \\ 0 & \sqrt{6} & 0 & 0 & 0 \\ 0 & 0 & \sqrt{6} & 0 & 0 \\ 0 & 0 & 0 & 2 & 0 \end{bmatrix},$$

$$Y = i \begin{bmatrix} 0 & 2 & 0 & 0 & 0 \\ 0 & 0 & \sqrt{6} & 0 & 0 \\ 0 & 0 & 0 & \sqrt{6} & 0 \\ 0 & 0 & 0 & 0 & 2 \\ 0 & 0 & 0 & 0 & 0 \end{bmatrix}.$$

This gives the invariant Nahm triplet in \mathfrak{g}_u

$$Y_1 = i \begin{bmatrix} 0 & -6 & 0 & 10 & 0 \\ -6 & 0 & 2\sqrt{6} & 0 & 10 \\ 0 & 2\sqrt{6} & 0 & 2\sqrt{6} & 0 \\ 10 & 0 & 2\sqrt{6} & 0 & -6 \\ 0 & 10 & 0 & -6 & 0 \end{bmatrix}, \quad (2.66)$$

$$Y_2 = \begin{bmatrix} 0 & -6 & 0 & -10 & 0 \\ 6 & 0 & 2\sqrt{6} & 0 & -10 \\ 0 & -2\sqrt{6} & 0 & 2\sqrt{6} & 0 \\ 10 & 0 & -2\sqrt{6} & 0 & -6 \\ 0 & 10 & 0 & 6 & 0 \end{bmatrix},$$

$$Y_3 = i \begin{bmatrix} 8 & 0 & 0 & 0 & 0 \\ 0 & -16 & 0 & 0 & 0 \\ 0 & 0 & 0 & 0 & 0 \\ 0 & 0 & 0 & 16 & 0 \\ 0 & 0 & 0 & 0 & -8 \end{bmatrix}.$$

The $\underline{\mathfrak{g}}_u$ invariant (2.64) is written in the form (2.36) as

$$\left[56 + \frac{7}{15}(\text{ad}Y \times 1 + 1 \times \text{ad}Y)^4 + \frac{1}{720}(\text{ad}Y \times 1 + 1 \times \text{ad}Y)^8 \right] X \times X^3 \quad (2.67)$$

which, when mapped using the isomorphism, produces the invariant Nahm triplet in $\underline{\mathfrak{g}}_m$

$$\begin{aligned} Z_1 &= i \begin{bmatrix} 0 & -1 & 0 & -1 & 0 \\ 1 & 0 & \sqrt{6} & 0 & 1 \\ 0 & -\sqrt{6} & 0 & -\sqrt{6} & 0 \\ 1 & 0 & \sqrt{6} & 0 & I \\ 0 & -1 & 0 & -1 & 0 \end{bmatrix}, \\ Z_2 &= \begin{bmatrix} 0 & -1 & 0 & 1 & 0 \\ -1 & 0 & \sqrt{6} & 0 & -1 \\ 0 & \sqrt{6} & 0 & -\sqrt{6} & 0 \\ 1 & 0 & -\sqrt{6} & 0 & 1 \\ 0 & -1 & 0 & 1 & 0 \end{bmatrix}, \\ Z_3 &= i \begin{bmatrix} 0 & 0 & 0 & 0 & 4 \\ 0 & 0 & 0 & 0 & 0 \\ 0 & 0 & 0 & 0 & 0 \\ 0 & 0 & 0 & 0 & 0 \\ -4 & 0 & 0 & 0 & 0 \end{bmatrix}. \end{aligned} \quad (2.68)$$

In a similar fashion to the icosahedral case, the (Z_1, Z_2, Z_3) can be consistently ignored.

The Nahm equations become

$$\frac{dx}{dt} = 2x^2 - 48y^2, \quad (2.69)$$

$$\frac{dy}{dt} = -6xy - 8y^2 \quad (2.70)$$

and the spectral curve is

$$\eta^5 + 768\kappa^4\eta(\zeta^8 + 14\zeta^4 + 1) = 0 \quad (2.71)$$

where

$$\kappa^4 = 5y(x + 3y)(x - 2y)^2. \quad (2.72)$$

Equations (2.69-2.70) are identical to those for the cubic 4-monopole and are solved by

$$x = 2\kappa(5\wp^2 - 3) \left(5\frac{d\wp}{ds}\right)^{-1}, \quad (2.73)$$

$$y = 2\kappa \left(5\frac{d\wp}{ds}\right)^{-1} \quad (2.74)$$

where $s = 2\kappa(t + 1)$ and $\wp(s)$ is the Weierstrass elliptic function satisfying

$$\left(\frac{d\wp}{ds}\right)^2 = 4(\wp^3 - \wp). \quad (2.75)$$

As in [HMM], the argument of κ is chosen to be $\pi/4$ and s lies on the line from 0 to $\omega_2 = \omega_1 + \omega_3$, where $2\omega_1$ is the real period of the elliptic function (2.75) and $2\omega_3$ is the imaginary period. By examining the eigenvalues of the residue of iT_3 , the boundary conditions at $t = -1$ and $t = 1$ are satisfied provided that

$$\omega_2 = 4\kappa. \quad (2.76)$$

This period may be explicitly calculated, with the result that there exists an octahedral monopole with spectral curve

$$\eta^5 + \frac{3\Gamma(\frac{1}{4})^8}{16\pi^2}(\zeta^8 + 14\zeta^4 + 1)\eta = 0. \quad (2.77)$$

The energy density may be calculated using the numerical scheme. Figure 2.3 shows a surface of constant energy density for this monopole. It resembles an octahedron with the energy density taking its maximum value on the six vertices of the octahedron.

In the geodesic approximation, scattering processes are approximated by geodesics. In this approximation four monopoles moving symmetrically towards a fifth at the origin form the octahedral 5-monopole before separating out again into a stationary axisymmetric 3-monopole and two 1-monopoles moving in opposite directions perpendicular to the plane of scattering. The existence of this surprising process is demonstrated in the next section using rational maps.

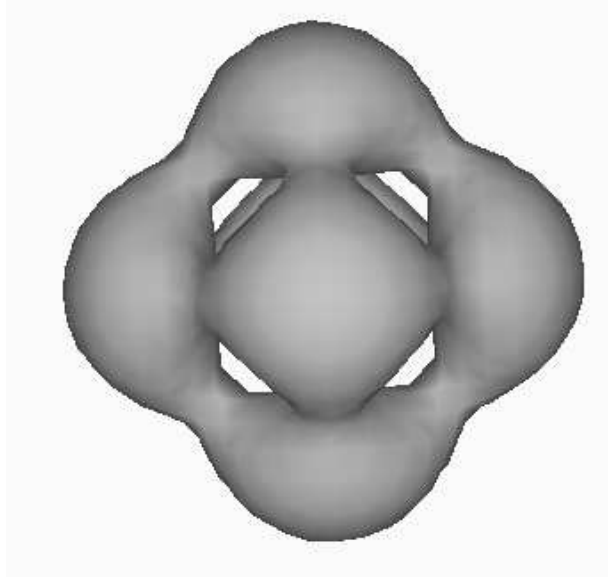


Figure 2.6: Octahedral 5-monopole; surface of constant energy density.

2.5 Monopoles and rational maps

There are two rational map descriptions of monopoles: the Donaldson rational map [Do] and the more recent Jarvis rational map [J]. These give very tractable parameterizations of the moduli space and are useful when studying symmetric monopoles. The existence of a particular monopole may be established before an attempt is made to solve the Nahm equations.

Monopole moduli spaces are equivalent to spaces of rational maps. Like spectral curves, these rational maps describe solutions to the Hitchin equation (1.39). The spectral curve of a monopole is the curve in \mathbf{P}^1 corresponding to lines in space along which the solutions to the Hitchin equation are bounded in both directions. In contrast, the rational map records rational information about solutions to the Hitchin equation along some set of lines. Two different sets of lines give two different rational map descriptions. Lines parallel to a given line give the Donaldson rational map, lines through a given point give the Jarvis rational map.

The remainder of this section is divided into two subsections. In Subsect. 2.5.1 the

Donaldson rational map is described and it is explained how symmetric Donaldson maps are obtained. In Subsect. 2.5.2 the Donaldson rational maps for C_{4h} symmetric 5-monopoles are studied. It is shown, with reference to this example, how qualitative features about a scattering process can be extracted from a one-parameter family of symmetric Donaldson rational maps. These methods are applied in the next section to the twisted line scattering geodesics. The section after that, Sect. 2.7, concerns the construction of symmetric Jarvis maps.

2.5.1 The Donaldson rational map and symmetry

Following Hurtubise [Hu2], to construct the Donaldson rational map, a line and an orthogonal plane in \mathbf{R}^3 are chosen to give the decomposition

$$\mathbf{R}^3 \cong \mathbf{C} \times \mathbf{R}. \quad (2.78)$$

For convenience, the line is chosen to be the x_3 -axis and the complex coordinate on the x_1x_2 -plane is denoted by z . Solutions to the linear differential equation (1.39) are considered along lines parallel to the x_3 -axis. This equation has two independent solutions. A basis (v_0, v_1) for the solutions can be chosen such that

$$\begin{aligned} \lim_{x_3 \rightarrow \infty} v_0(x_3)x_3^{-k/2}e^{x_3} &= e_0, \\ \lim_{x_3 \rightarrow \infty} v_1(x_3)x_3^{k/2}e^{-x_3} &= e_1, \end{aligned} \quad (2.79)$$

where e_0, e_1 are constant in some asymptotically flat gauge. Thus, v_0 is bounded and v_1 is unbounded as $x_3 \rightarrow \infty$. Similarly, there is a basis (v'_0, v'_1) such that v'_0 is bounded and v'_1 is unbounded as $x_3 \rightarrow -\infty$. The lines parallel to the x_3 -axis are parameterized by z and for a general line

$$v'_0 = a(z)v_0 + b(z)v_1, \quad (2.80)$$

$$v_0 = a'(z)v'_0 + b(z)v'_1. \quad (2.81)$$

for some scattering data $a(z)$ and $b(z)$. The ratio of $a(z)$ and $b(z)$ is formed. By cancelling common factors

$$\frac{a(z)}{b(z)} = \frac{p(z)}{q(z)}, \quad (2.82)$$

where $p(z)$ and $q(z)$ are coprime polynomials. $p(z)$ is degree $k - 1$ and $q(z)$ is degree k and monic.

In this way, the rational map is then given by

$$R(z) = \frac{p(z)}{q(z)}. \quad (2.83)$$

Furthermore, since the spectral curve $P(\eta, \zeta) = 0$ of a monopole corresponds to the bounded solutions to (1.39),

$$q(z) = P(z, 0) = 0. \quad (2.84)$$

Finally, it can be shown [AH] that the full scattering data are given by

$$\begin{bmatrix} a & b \\ -b' & -a' \end{bmatrix} \begin{pmatrix} v_0 \\ v_1 \end{pmatrix} = \begin{pmatrix} v'_0 \\ v'_1 \end{pmatrix} \quad (2.85)$$

where

$$aa' = 1 + b'b. \quad (2.86)$$

Since the construction of the rational map requires the choice of a direction in \mathbf{R}^3 , it is not possible to study the full symmetries of a monopole from its rational map. However, some isometries are known [HMM]. These are the isometries which respect the $\mathbf{R}^3 \cong \mathbf{R} \times \mathbf{C}$ decomposition. They are, rotation in the plane: $\lambda \in \mathbf{U}_1$, translation in plane: $\nu \in \mathbf{C}$, translation perpendicular to the plane: $x \in \mathbf{R}$ and constant gauge transformation: $\mu \in \mathbf{U}_1$. Under the composition of these transformations, a rational map $R(z)$ transforms as

$$R(z) \rightarrow \mu^2 e^{2x} \lambda^{-k} R(\lambda^{-1}(z - \nu)). \quad (2.87)$$

Furthermore, under space reflection, $x_3 \rightarrow -x_3$, $R(z) = p(z)/q(z)$ transforms as

$$\frac{p(z)}{q(z)} \rightarrow \frac{\sigma(p)(z)}{q(z)} \quad (2.88)$$

where $\sigma(p)(z)$ is the unique polynomial of degree less than k such that $\sigma(p)(z)p(z) \equiv 1 \pmod{q(z)}$. These formulae are used to construct rational maps invariant under some subgroups of \mathbf{O}_3 . Because of the constant gauge transform μ appearing in (2.87) a rational map is considered invariant under a rotation λ if its effect on the rational map is to change its

$$\prod_i p(\beta_i) = 1. \quad (2.94)$$

2.5.2 C_{4h} 5-monopoles, an example

As an example of the construction of symmetric rational maps, let us consider C_{4h} symmetric 5-monopoles. C_{4h} is the group generated by a $\pi/2$ rotation and a reflection in an orthogonal plane. Using (2.87) and (2.88), the most general rational map of a strongly centred 5-monopole, which is symmetric under both reflection in the x_1x_2 -plane, denoted σ_{xy} , and C_4 rotation around the x_3 -axis, is

$$R_5(z) = \frac{\frac{2}{a}z^4 + 1}{z^5 + az} \quad (2.95)$$

with $a \in (0, \infty)$. It is a one-parameter family of based rational maps.

This one-parameter family is significant because it is a geodesic. Since \mathcal{M}_k^0 is a Riemannian manifold, the fixed point set of the action of a group on it is totally geodesic. A one-dimensional totally geodesic submanifold is a geodesic. In fact, this presents a strategy for finding geodesics without knowledge of the metric. If a symmetry group G can be found, so that there is only a one-parameter family of G symmetric k -monopoles, that one-parameter family corresponds to a geodesic. In the geodesic approximation the monopole dynamics proceed along that geodesic.

To understand the rate at which scattering processes proceed; to calculate, for example the time advance or delay, the metric is needed. Nonetheless, qualitative information about a scattering process may be derived if the geodesic is known but not the metric on it.

Qualitative information may be extracted from the rational map. It was suggested in [HMM] and proved by Bielawski [Bi1] that for a rational map $p(z)/q(z)$ with well-separated poles β_1, \dots, β_k the corresponding monopole is approximately composed of unit charge monopoles located at the points (x_1, x_2, x_3) , where $x_1 + ix_2 = \beta_i$ and $x_3 = \frac{1}{2} \log |p(\beta_i)|$. Thus, for large values of a , $R_5(z)$ corresponds to a monopole located at the origin and a monopole a distance $\pm a$ along each of the diagonals $x_1 = \pm x_2$. This interpretation breaks down for $a \sim 1$ since, for $a \sim 1$, the poles of the denominator are not well-separated.

In [AH], it is argued that for monopoles strung out in well-separated clusters along, or nearly along, the x_3 -axis the first term in a large z expansion of the rational map $R(z)$ is $e^{2x+i\chi}/z^k$ where k is the charge of the topmost cluster and x is its elevation above the plane. In [HS2], this is extended to the next highest cluster. If the next highest cluster has charge m and is y above the plane, then the first two terms in the large z expansion of the rational map are given by

$$R(z) \sim \frac{e^{2x+i\chi}}{z^k} + \frac{e^{2y+i\phi}}{z^{2k+m}} + \dots \quad (2.96)$$

The topmost cluster, (A_1, ϕ_1) , is assumed to be separated from the other monopoles. Let v_0'' be the solution bounded at $x_3 \rightarrow -\infty$. For z large, the scattering is along lines well removed from the spectral lines and so, in the region of (A_1, ϕ_1) , the solution is dominated by the exponentially growing one and is, therefore, close to v_0'' . Thus, the dominant term in the rational map is the effect of scattering off (A_1, ϕ_1) .

Now, the second highest monopole cluster, (A_2, ϕ_2) , is separated from the monopoles below it. The incoming solution is close to v_0'' . The bounded solution leaving the (A_2, ϕ_2) region is called v_0' and the unbounded one v_1' . From (2.90)

$$v_0'' = e^{2y+i\phi} v_0' + z^m v_1'. \quad (2.97)$$

Subsequent scattering off (A_1, ϕ_1) gives

$$\begin{aligned} v_0' &= -e^{-2x-i\chi} v_1, \\ v_1' &= e^{2x+i\chi} v_0 + z^k v_1, \end{aligned} \quad (2.98)$$

where v_0 and v_1 are the unbounded and bounded solutions, respectively, as $x_3 \rightarrow \infty$. Substituting (2.98) into (2.97)

$$v_0'' = z^k e^{2x+i\chi} v_0 + (z^{k+m} - e^{-2(x-y)-i(\chi-\phi)}) v_1, \quad (2.99)$$

and so the rational map is dominated by

$$R(z) \sim \frac{z^m e^{2x+i\chi}}{z^{k+m} - e^{-2(x-y)-i(\chi-\phi)}} \quad (2.100)$$

and, since $x \gg y \gg 1$,

$$R(z) - \frac{e^{2x+i\chi}}{z^k} \sim \frac{e^{2y+i\phi}}{z^{2k+m}}. \quad (2.101)$$

In the example of $R_5(z)$

$$R_5(z) \sim \frac{2}{az} - \frac{1}{z^5} \quad (2.102)$$

for large z and so $k = 1$ and $m = 3$. This means that there is a cluster of three monopoles at the origin and a monopole above the origin on the x_3 -axis.

Thus, $R_5(z)$ describes four monopoles approaching a monopole at the origin along the positive and negative $x_1 = \pm x_2$ diagonals. Since the octahedral 5-monopole has C_{4h} symmetry, it must lie on this geodesic and so the monopoles coalesce at some point to form the octahedral 5-monopole. As $a \rightarrow 0$, from (2.96), one monopole travels up the x_3 -axis and three remain in a cluster at the origin. By reflection, the fifth monopole travels down the x_3 -axis. In the $a = 0$ limit, there are 1-monopoles at $(0, 0, \pm\infty)$ and a toroidal 3-monopole centred on the origin.

2.6 Twisted line scattering

With only the Donaldson rational map description, the only way to use symmetry to find geodesics is to find spatial symmetries which respect the decomposition of \mathbf{R}^3 into $\mathbf{C} \times \mathbf{R}$ and, nonetheless, reduce the relevant moduli space to one parameter. The twisted line scattering geodesics were discovered in this way.

These geodesics are geodesics of k -monopoles symmetric under the rotary-reflection symmetry S_{2l} , where l is an integer satisfying $k - 1 \geq l > k/2$ and $k > 2$. The rotary-reflection S_{2l} is $\sigma_{xy} \circ \text{Rot}_{\pi/l}$. Symmetry under S_{2l} implies C_l symmetry. This is imposed on the Donaldson rational map of a k -monopole. By (2.87) and (2.88) this requires the rational map to have the form

$$R(z) = \frac{c + bz^l}{z^{k-l}(z^l - a)} \quad (2.103)$$

for some complex constants a, b, c . The requirement of S_{2l} symmetry for this rational map gives the constraint

$$(c - bz^l)(c + bz^l) = 1 \pmod{z^{k-l}(z^l - a)}. \quad (2.104)$$

This can only be satisfied if $a = 0$ and $c = \pm 1$. By a phase choice, $c = 1$. The symmetric rational maps are

$$R = \frac{1 + bz^l}{z^k}, \quad (2.105)$$

parameterised by the complex number b . The rational maps in this family are strongly centred. This family defines a surface of two real dimensions in the k -monopole moduli space, denoted by Σ_k^l . It is a totally geodesic submanifold: it is the fixed point set of a symmetry. Σ_k^l is a surface of revolution: the phase of b corresponds to the orientation about the x_3 -axis. A reflection symmetry on the rational map may be imposed so that b is real. This gives a geodesic in Σ_k^l corresponding to the generator of the surface of revolution. Geodesic flow corresponds to b increasing monotonically from $b = -\infty$ to $b = +\infty$. If $b = 0$ then (2.105) is the rational map of the axisymmetric k -monopole, with the x_3 -axis as the axis of symmetry. Writing (2.105) in the form

$$R = \frac{b}{z^{k-l}} + \frac{1}{z^k}, \quad (2.106)$$

the cluster decomposition (2.96) can be used to deduce that, as $b \rightarrow \pm\infty$, the rational map (2.105) describes axisymmetric monopoles of charge $k - l$ at the positions $(0, 0, \pm\frac{1}{2} \log |b|)$ and an axisymmetric charge $2l - k$ monopole at the origin.

The simplest example is when $k = 3$, in this case l must be two. The rational map is

$$R = \frac{1 + bz^2}{z^3}, \quad (2.107)$$

where, $-\infty < b < \infty$. Setting $k = 3$ and $l = 2$ in the cluster decomposition, the geodesic is interpreted as the following scattering event. At large negative times, there are three well-separated monopoles which are all located on the x_3 -axis. One monopole is stationary at the origin, a second monopole is on the positive x_3 -axis and a third monopole is on the negative x_3 -axis. The second and third monopoles are equidistant from the origin and are moving towards the stationary monopole. For large positive times, the situation is similar but now the two monopoles which are on the positive and negative x_3 -axis are moving away from the monopole at the origin. The twisted line scattering geodesic describes motion along the x_3 -axis.

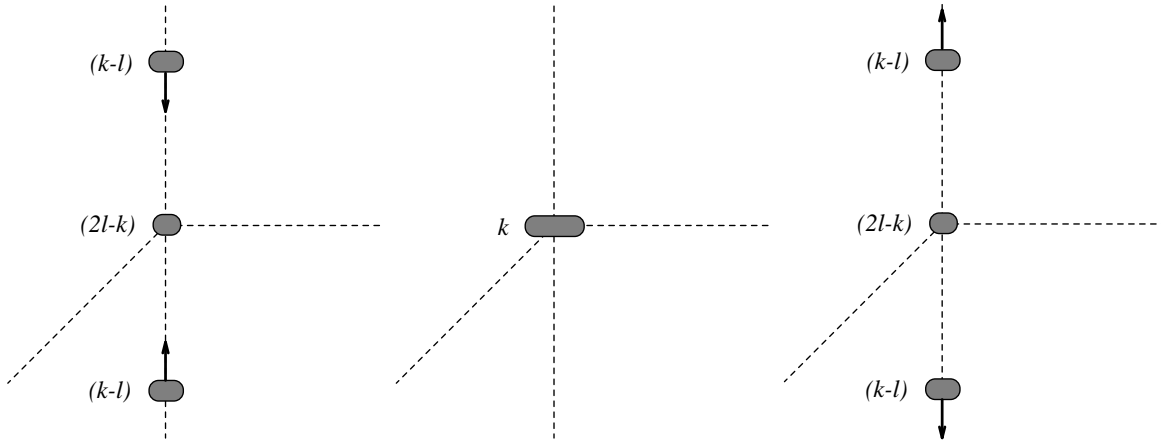


Figure 2.7: The Σ_k^l twisted line scattering as b goes from large and positive to large and negative.

This is true of all the geodesic motions along generators on the surfaces Σ_k^l . They all describe monopole scattering along a line. The initial configuration is of two $(k-l)$ -monopoles approaching a $(2l-k)$ -monopole at the origin along the positive and negative x_3 -axis. The final configuration is of two $(k-l)$ -monopoles receding along the positive and negative x_3 -axis leaving a $(2l-k)$ -monopole at the origin. Figure 2.7 is a schematic representation of this. The one-parameter family of rational maps given by (2.105) is invariant, up to a phase change, under $b \rightarrow -b$ and $z \rightarrow e^{i\pi/l}z$. This means that the outgoing configurations are always like the incoming configurations but twisted by π/l about the x_3 -axis. The scattering angle is zero in each case.

The S_4 symmetry imposed to obtain the surface Σ_3^2 is a combined reflection and $\pi/2$ rotation symmetry. The 3-monopole with tetrahedral symmetry [HMM, HS1] has S_4 symmetry so for some value, $b = b_c$ say, (2.107) is the rational map of the tetrahedral monopole. When $b = -b_c$, the tetrahedral 3-monopole is again formed but this time in the orientation dual to the previous one. So, although the asymptotic in and out monopole states may suggest a simple scattering process, the dynamics must be relatively complicated since a tetrahedral monopole, then an axisymmetric monopole, then another tetrahedral monopole

are all formed during the scattering. The Nahm data are actually known in this case and are discussed in Chapter 3.

The cubic 4-monopole has S_8 symmetry and is on the surface Σ_4^3 . The cubic 4-monopole is formed twice during the twisted line scattering associated with the generator on Σ_4^3 . During the scattering two 1-monopoles approach an axisymmetric 2-monopole at the origin. The axisymmetric 4-monopole is also formed between the formation of the two cubes.

There is a similar scattering through the octahedral 5-monopole. The surface Σ_5^3 describes monopoles with S_6 symmetry. The octahedral 5-monopole has S_6 symmetry. Thus, geodesic motion along the generator of Σ_5^3 describes two 2-monopoles approaching the origin along the positive and negative x_3 -axis. At the origin, there is a single 1-monopole. The monopoles coalesce to form the octahedral 5-monopole. This deforms into the toroidal 5-monopole and then into the octahedral 5-monopole rotated through $\pi/3$. It then separates into two 2-monopoles again. They recede along the x_3 -axis, leaving a single monopole at the origin.

The dodecahedral 7-monopole occurs during the geodesic scattering on the surface Σ_7^5 . The scattering involves two axisymmetric 2-monopoles approaching from the positive and negative x_3 -axis with an axisymmetric 3-monopole at the origin. The dodecahedral monopole is formed, followed by the axisymmetric 7-monopole, then the dodecahedral monopole rotated $\pi/5$ relative to the previous one. Finally, two 2-monopoles separate out again along the x_3 -axis, leaving a 3-monopole behind.

2.7 Symmetry and the Jarvis rational map

Some cunning is required in choosing the symmetry when working with the Donaldson rational map. With the Jarvis rational map, any rotational symmetry can be applied because the construction of the rational map does not nominate a direction along which the Hitchin scattering is performed. The problem of applying symmetry to the monopole moduli space is just a problem of constructing symmetric Jarvis rational maps.

The Jarvis map is constructed in a similar way to the Donaldson map, except that in

the Jarvis map the Hitchin scattering is performed along lines radiating in all directions from a single point. These lines are parameterized by z , the inhomogeneous coordinate on \mathbf{P}^1 . The solutions to the Hitchin equation are two component functions of radial distance. Along a given halfline from the origin the asymptotically decaying solution is projectively unique. The ratio of the two components of this solution at the origin is the Jarvis rational map. The space of Jarvis maps is the $(4k + 2)$ -dimensional space of unbased degree k rational maps. A given k -monopole is identified with the SU_2 orbit of rational maps given by the Möbius action

$$R(z) \mapsto \frac{\alpha R(z) + \beta}{-\bar{\beta} R(z) + \bar{\alpha}}, \quad (2.108)$$

where α and β are complex numbers such that $|\alpha|^2 + |\beta|^2 = 1$. This SU_2 action on the rational map corresponds to a constant SU_2 gauge transformation of the k -monopole. There is no analogous action on the Donaldson rational map since the ratio there is between gauge invariant quantities. The action is a consequence of the need to consider halflines in the Jarvis construction.

To construct symmetric Jarvis rational maps, it is convenient to employ homogeneous projective coordinates x and y on the Riemann sphere, rather than the inhomogeneous $z = x/y$ employed elsewhere. In homogeneous coordinates, a rational map is a map from Riemann sphere to Riemann sphere of the form

$$R(x, y) = (p(x, y), q(x, y)) \quad (2.109)$$

where p and q are homogeneous polynomials. In the (x, y) coordinates, an SO_3 rotation in space by θ about the direction of the unit vector (n_1, n_2, n_3) is realized by the SU_2 transformation $\exp(i\frac{\theta}{2}\mathbf{n} \cdot \boldsymbol{\sigma})$, whose action on the Riemann sphere is

$$\begin{aligned} x \mapsto x' &= (d + ic)x - (b - ia)y \\ y \mapsto y' &= (b + ia)x + (d - ic)y \end{aligned} \quad (2.110)$$

where $a = n_1 \sin \frac{\theta}{2}$, $b = n_2 \sin \frac{\theta}{2}$, $c = n_3 \sin \frac{\theta}{2}$ and $d = \cos \frac{\theta}{2}$. Furthermore, in this context, two rational maps are equivalent if they can be mapped into each other by an SU_2 transformation of the target sphere, that is by a transformation of p and q of the form (2.110).

A rational map is symmetric under some finite group $G \subset \text{SU}_2$ if G transformations of x and y map it into an equivalent map.

A degree k homogeneous polynomial is a polynomial of the form

$$p(x, y) = \sum_{i=0}^k a_i x^i y^{k-i}. \quad (2.111)$$

Under SU_2 transformations (2.110) of x and y , the space of degree k homogeneous polynomials transforms under $\underline{k+1}$. This $\underline{k+1}$ is also a representation of any finite subgroup G of SU_2 . Though irreducible as a representation of SU_2 it is generally reducible as a representation of G . It is easy to calculate the decomposition of $\underline{k+1}$ into irreducible representations because in $\underline{k+1}$ the element $\exp(i\frac{\theta}{2}\mathbf{n} \cdot \boldsymbol{\sigma})$ has character

$$\frac{\sin\left(\frac{k+1}{2}\theta\right)}{\sin\frac{\theta}{2}} \quad (2.112)$$

for any \mathbf{n} . There are tables of these reductions given in, for example, [KDWS].

Suppose two degree k homogeneous polynomials $p(x, y)$ and $q(x, y)$ lie in the same two-dimensional representation of G ; G transformations of x and y will then result in $\text{GL}_2\mathbf{C}$ transformations of $(p(x, y), q(x, y))$. If, further, $p(x, y)$ and $q(x, y)$ are orthonormal as vectors in the $\underline{k+1}$ carrier space, then, projectively, the G action on x and y results only in SU_2 transformations of $(p(x, y), q(x, y))$. Therefore, the rational map $R(x, y) = (p(x, y), q(x, y))$ is G symmetric.

This means that there is a systematic way of deciding whether there are G symmetric maps of some degree k . The representation $\underline{k+1}$ is decomposed into irreducible representations of G . If

$$\underline{k+1}|_G = E + \text{other irreducible representations of } G, \quad (2.113)$$

where E is a two-dimensional irreducible representation of G , and if the basis polynomials for E have no common factor, then there is a G symmetric degree k map. If they have a common factor then the resulting rational map has lower degree. This occurs when the E in $\underline{k+1}$ is in the product of lower degree representations; this is illustrated with an

example below. It might also happen that

$$\underline{k+1}|_G = A_1 + A_2 + \text{other irreducible representations of } G, \quad (2.114)$$

where A_1 and A_2 are one-dimensional representations of G . In this case, there is a one-parameter family of G symmetric rational maps: if $p(x, y)$ is in A_1 and $q(x, y)$ is in A_2 then the family

$$R(x, y) = (ap(x, y), q(x, y)) \quad (2.115)$$

is G symmetric. It is one parameter because a can be made real by Möbius transformation.

An example of this type is the geodesic of tetrahedral 4-monopoles. Degree four polynomials transform as $\underline{5}$ and

$$\underline{5}|_T = A_1^T + A_2^T + F^T \quad (2.116)$$

The face polynomial, q_F , of the tetrahedron is a basis for A_1^T . The vertex polynomial, q_V , is a basis for A_2^T . Thus, in the usual orientation,

$$R(x, y) = (aq_F, q_V), \quad (2.117)$$

$$q_F(x, y) = x^4 - 2\sqrt{3}ix^2y^2 + y^4, \quad (2.118)$$

$$q_V(x, y) = x^4 + 2\sqrt{3}ix^2y^2 + y^4 \quad (2.119)$$

is the one-parameter family of tetrahedrally symmetric Jarvis rational maps. For $a = 1$ the map is octahedrally symmetric: the map

$$(x, y) \rightarrow (e^{-\frac{i\pi}{4}}x, e^{\frac{i\pi}{4}}y) \quad (2.120)$$

sends q_F to $-q_V$ and q_V to $-q_F$ and is a Möbius transformation of $R(x, y)$. This octahedrally symmetric map corresponds to the cubic 4-monopole of Sect. 2.1. Since the tetrahedral symmetry has a one-parameter family of fixed points, there is a geodesic of tetrahedral 4-monopoles. Such a family could not have been discovered using the Donaldson rational map because the group transformations do not respect the $\mathbf{R}^3 = \mathbf{R} \times \mathbf{C}$ decomposition. Historically, however, the geodesic was discovered without using the Jarvis rational map either. In [HS1] it is demonstrated that the Nahm equations only have a one-parameter family of solutions. These solutions to the Nahm equations allow the monopoles to be plotted using the numerical ADHM construction. This is discussed in Chapter 3.

In the degree four example above, the symmetric polynomials are easy to find, they are bases of one-dimensional representations of low degree. Higher charge cases are more difficult. The case of tetrahedrally symmetric degree seven maps is a good example of how symmetric Jarvis rational maps can be calculated in general.

Under restriction to T

$$\underline{\mathfrak{g}}|_T = 2E'^T + G'^T, \quad (2.121)$$

that is, two two-dimensional irreducible representations of T occur in the decomposition of $\underline{\mathfrak{g}}$. Furthermore, there is an arbitrariness in the decomposition

$$2E'^T = E'^T + E'^T, \quad (2.122)$$

and this allows a one-parameter family of tetrahedrally symmetric rational maps to be constructed.

The tetrahedral group is both a subgroup of the octahedral group O and a subgroup of the icosahedral group Y . $\underline{\mathfrak{g}}$ is decomposed as a representation of Y and of O ,

$$\underline{\mathfrak{g}}|_O = E_1'^O + E_2'^O + G'^O, \quad (2.123)$$

$$\underline{\mathfrak{g}}|_Y = E_2'^Y + I'^Y. \quad (2.124)$$

These representations decompose further by restriction to T

$$E_1'^O|_T = E'^T, \quad (2.125)$$

$$E_2'^O|_T = E'^T,$$

$$G'^O|_T = G'^T$$

and

$$E_2'^Y|_T = E'^T, \quad (2.126)$$

$$I'^Y|_T = E'^T + G'^T.$$

In this way, T has two identical two-dimensional irreducible representations in $\underline{\mathfrak{g}}$. O also has two but they are different and Y only has one. The carrier spaces of these representations

are two-dimensional subspaces of the carrier space of $\underline{\mathfrak{g}}$: a space which is realised as degree seven homogeneous polynomials. The symmetric rational maps that are to be calculated can be constructed from the bases of the two-dimensional spaces.

There are simple and venerable methods for calculating such bases explicitly. They are explained in Serre's book [Se]. U , a reducible representation of a group G , is considered,

$$\begin{aligned} G &\rightarrow \text{GL}(U), \\ g &\mapsto \rho(g), \end{aligned} \tag{2.127}$$

which decomposes into irreducible representations V_i ,

$$\begin{aligned} U &= V_1 + \dots + V_1 + V_2 + \dots + V_2 + \dots + V_h + \dots + V_h \\ &= W_1 + \dots + W_h \end{aligned} \tag{2.128}$$

where

$$W_i = V_i + V_i + \dots + V_i. \tag{2.129}$$

If the irreducible representation V_i has character $\chi_i(g)$ for $g \in G$, and $n_i = \dim W_i$, then

$$P_i = \frac{n_i}{|G|} \sum_{g \in G} \chi_i(g)^* \rho(g) \tag{2.130}$$

is the projection operator

$$P_i : U \rightarrow W_i. \tag{2.131}$$

Using MAPLE, these projection operators can be calculated.

Since E'^T appears twice in $\underline{\mathfrak{g}}|_T$, projection onto E'^T gives a four-dimensional space. To work out a basis for this space, the projection operator

$$P : \underline{\mathfrak{g}} \rightarrow 2E'^T \tag{2.132}$$

must be calculated using (2.130). The $T \subset \text{SU}_2$ transformations of (x, y) are first calculated explicitly. In the orientation where each edge of the tetrahedron has its midpoint on a Cartesian axis, the C_2 element about the x_3 -axis has $c = -1$ and $a = b = d = 0$, and

hence,

$$x' = -ix, \quad (2.133)$$

$$y' = iy.$$

The C_3 element about the $x_1 = x_2 = x_3$ axis has $a = b = c = d = 1/2$, and hence,

$$\begin{aligned} x' &= \frac{1+i}{2}x + \frac{1-i}{2}y, \\ y' &= -\frac{1+i}{2}x + \frac{1-i}{2}y. \end{aligned} \quad (2.134)$$

These two transformations generate T and so expressions for the (x, y) transformations can be calculated for all 24 elements of T . Using MAPLE, the effects of these transformations on degree seven polynomials are calculated determining the 8×8 matrices $\rho(g)$ for each element $g \in T$ and, using (2.130), the projection operator P . The polynomials in the image of P are

$$p_1(x, y) = -7x^4y^3 - y^7, \quad (2.135)$$

$$p_2(x, y) = x^7 + 7x^3y^4,$$

$$p_3(x, y) = x^6y - x^2y^5,$$

$$p_4(x, y) = x^5y^2 - xy^6.$$

This particular basis is chosen because it is convenient for what follows.

From (2.125), it follows that two different representations of the octahedral group O lie in this four-dimensional space. In the usual orientation, O is generated by T and the C_4 rotation around the x_3 -axis:

$$\begin{aligned} x' &= \frac{1+i}{\sqrt{2}}x, \\ y' &= \frac{1-i}{\sqrt{2}}y \end{aligned} \quad (2.136)$$

and so the projection operators for E_1^O and E_2^O can be calculated. It is found that $p_1(x, y)$ and $p_2(x, y)$ are a basis for E_1^O and $p_3(x, y)$ and $p_4(x, y)$ are a basis for E_2^O . The rational map

$$R(x, y) = (p_1(x, y), p_2(x, y)) \quad (2.137)$$

is, therefore, octahedrally symmetric. However, $p_3(x, y)$ and $p_4(x, y)$ have a common factor and the corresponding rational map is spurious; it is not of degree seven. This is not surprising. The one-dimensional representation A_2^O in $\underline{7}|_O = A_2^O + F_1^O + F_2^O$ has basis $x^5y - xy^5$, the two-dimensional representation $\underline{2}|_O = E_1^O$ has basis x, y , and $A_2^O \times E_1^O = E_2^O$.

T is also a subgroup of Y . In fact, for our choice of orientation of the tetrahedral group, there are two possible icosahedral groups with it as a subgroup. The group Y is generated by T and a C_5 element. The two choices of Y correspond to adding a C_5 rotation about the radial line passing through $(-1, 0, \tau)$ or about the line passing through $(1, 0, \tau)$, where $\tau = (1 + \sqrt{5})/2$. The two possibilities are related by a rotation by $\pi/2$ about the x_3 -axis. The E_2^Y has basis $p_1(x, y) \pm (7/\sqrt{5})p_3(x, y)$ and $p_2(x, y) \pm (7/\sqrt{5})p_4(x, y)$; the sign depends on the choice of C_5 element.

$2E'^T$ decomposes into $E'^T + E'^T$. Luckily, such decompositions are discussed in [Se] where the following construction is presented. Some general reducible representation U is considered, where, as in (2.128),

$$U = W + \text{other irreducible representations of } G \quad (2.138)$$

and W is the sum of m identical irreducible representations V ,

$$W = mV. \quad (2.139)$$

Let $n = \dim V$. In V each $g \in G$ is represented by an $n \times n$ matrix, say $r(g)$. From these the projection operators

$$P_{\alpha\beta} = \frac{n}{|G|} \sum_{g \in G} r_{\alpha\beta}(g^{-1})\rho(g) \quad (2.140)$$

are calculated. Here α and β are simply the matrix indices of r . Now $P_{\alpha\alpha}$ projects onto an m -dimensional space: Ω_α . W can be expressed as the direct sum

$$W = \Omega_1 + \Omega_2 + \dots + \Omega_n. \quad (2.141)$$

Furthermore, the map $P_{\beta\alpha}$ is an isomorphism from Ω_α to Ω_β and vanishes on all Ω_γ for $\gamma \neq \alpha$. If $(\omega_1, \omega_2, \dots, \omega_m)$ is a basis for Ω_1 then the space spanned by

$$Y_\nu = (\omega_\nu, P_{21}(\omega_\nu), P_{31}(\omega_\nu), \dots, P_{n1}(\omega_\nu)) \quad (2.142)$$

is isomorphic to V and

$$W = Y_1 + Y_2 + \dots + Y_m \quad (2.143)$$

is a decomposition of W of the form (2.139). Choosing a particular decomposition is equivalent to choosing a particular basis $(\omega_1, \omega_2, \dots, \omega_m)$ for the space Ω_1 .

The space $W = 2E'^T$ is spanned by the polynomials (2.135). Using `MAPLE`, the projection operators P_{11} and P_{21} are constructed. It is found that the space $P_{11} : W \rightarrow \Omega_1$ is spanned by p_1 and p_3 . Choosing a vector $p_1 + bp_3$ in this space defines a particular $E'^T \subset 2E'^T$. P_{21} is used to derive the one-parameter family of tetrahedrally symmetric rational maps

$$R(x, y) = (p_1 + bp_3, p_2 + bp_4) \quad (2.144)$$

or, in inhomogenous coordinates,

$$R(z) = \frac{bz^6 - 7z^4 - bz^2 - 1}{z(z^6 + bz^4 + 7z^2 - b)}, \quad (2.145)$$

where b is complex. For $b = 0$, there is octahedral symmetry. For $b = \pm 7/\sqrt{5}$, there is icosahedral symmetry.

2.7.1 The tangent space to a symmetric monopole

The rotational SO_3 action on the moduli space \mathcal{M}_k induces an action on its tangent bundle $\text{T}\mathcal{M}_k$. Under the action of $g \in \text{SO}_3$ a point m in \mathcal{M}_k is mapped to the point gm corresponding to the rotated k -monopole. In the same way, a curve γ through m is mapped to another curve $g\gamma$ through gm . The vector in $\text{T}_m\mathcal{M}_k$ tangent to γ is mapped under the SO_3 action on $\text{T}\mathcal{M}_k$ to the vector in $\text{T}_{gm}\mathcal{M}_k$ tangent to $g\gamma$. However, if m corresponds to a G symmetric k -monopole and $g \in G$ then $gm = m$ and a vector in $\text{T}_m\mathcal{M}_k$ is mapped to another vector in $\text{T}_m\mathcal{M}_k$. Thus, the dodecahedral 7-monopole is a point in the 7-monopole moduli space and this point is fixed by the icosahedral group. As a consequence, the SO_3 action on $\text{T}\mathcal{M}_7$ defines an icosahedral action on the tangent space to the dodecahedral 7-monopole and the tangent vectors transform under a representation of the icosahedral group.

Generally, the tangent space to a G symmetric k -monopole transforms under a representation of G . This subsection describes this representation. It is calculated using the Jarvis rational map description.

A degree k rational map, $R = (p_0, q_0)$, is G symmetric when p_0 and q_0 span a two-dimensional representation of G inside $\underline{k+1}$. This means that acting with $g \in G$ on (x, y) has the effect of transforming (p_0, q_0) by some 2×2 matrix D_g . Put another way, the g transformation of (x, y) followed by the D_g^{-1} transformation of the rational map leaves (p_0, q_0) unchanged. To find the transformation properties of tangent vectors in $\mathbb{T}_{(p_0, q_0)}\mathcal{M}_k$, a general $(p, q) = (p_0 + \delta p, q_0 + \delta q)$ is transformed in this way.

A general homogeneous polynomial transforms under G in the representation $\underline{k+1}|_G$. The D_g representation is the two-dimensional representation in $\underline{k+1}|_G$ corresponding to R . The D_g^{-1} representation E can be calculated from this. Transforming p and q under $\underline{k+1}|_G$ and then under E is a $\underline{k+1}|_G \times E$ transformation of (p, q) , where (p, q) is regarded as a $(2k+2)$ -dimensional vector. Thus, to find the transformation properties of the tangent vectors, $\underline{k+1}|_G \times E$ must be decomposed into irreducible representations of G .

In the case of the dodecahedral 7-monopole

$$\underline{\mathfrak{g}}|_Y = E_2'^Y + I^Y. \quad (2.146)$$

The dodecahedral 7-monopole corresponds to $E_2'^Y$. That is the representation of the D_g 's mentioned above. All elements of Y lie in the same conjugacy class as their inverses, so the D_g^{-1} representation is also $E_2'^Y$. Each character of $\underline{\mathfrak{g}}|_Y \times E_2'^Y$ is obtained by multiplying the corresponding one for $\underline{\mathfrak{g}}|_Y$ with that for $E_2'^Y$. The characters are known and the decomposition is

$$\underline{\mathfrak{g}}|_Y \times E_2'^Y = A^Y + F_1^Y + F_2^Y + G^Y + H^Y. \quad (2.147)$$

There are copies of this decomposition corresponding to real variations and to imaginary variations. This means that the variations around the 7-monopole transform as $2A^Y + 2F_1^Y + 2F_2^Y + 2G^Y + 2H^Y$. The $2A^Y$ are the trivial variations caused by multiplying the icosahedral p_0 and q_0 by the same constant. The Mobius transformations account for an F_2^Y . Thus, the action decomposes in the irreducible components $2F_1^Y + F_2^Y + 2G^Y + 2H^Y$.

The vector representation of the icosahedral group is F_1^Y so translations and rotations account for $2F_1^Y$. The vectors carrying $F_2^Y + 2G^Y + 2H^Y$ are tangent to curves which actually deform the monopole.

Chapter 3

Elliptic solutions to the Nahm equations

In the previous chapter the Nahm equations were solved for the octahedral 5-monopole and dodecahedral 7-monopole. These solutions to the Nahm equations are elliptic. In the first chapter, the 2-monopole case was discussed, it was argued that the Nahm equations have elliptic solutions because the 2-monopole spectral curve is genus one.

Neither the 5-monopole nor the 7-monopole have genus one spectral curves, but the Nahm equations have elliptic solutions. The explanation for this is given in [HMM]. A 3-monopole has a genus four spectral curve. However, the spectral curve, P , of the tetrahedral 3-monopole is acted on by the tetrahedral group, T . The genus of the quotient curve, P/T , can be calculated using the Riemann-Hurwitz relation (1.35). It is genus one. In fact, in each of the cases considered, the quotient curve is genus one and this is why these cases are tractable. The solutions to the Nahm equations are elliptic because the spectral curves are effectively genus one.

In this chapter, some attempt is made to exhaust the list of such monopoles. This leads to two interesting families of monopoles. The first is the one-parameter family of tetrahedrally symmetric 4-monopoles introduced in [HS1]. In the geodesic approximation, the four monopoles approach each other on the vertices of a contracting tetrahedron and scatter through the cubic configuration.

The second family are 3-monopoles with D_2 symmetry. In Sect. 3.3, the space of such monopoles is described using the Jarvis description. The Nahm data are derived, they are parameterized by constants appearing in the spectral curve. Inside the space of D_2 symmetric monopoles are 3-monopoles with still higher symmetry: there are one-parameter families with twisted line symmetry and with inversion symmetry. In the geodesic approximation, these one-parameter families describe scattering processes.

All 3-monopoles with inversion symmetry are D_2 symmetric. In Sect. 3.4, the moduli space of inversion symmetric 3-monopoles is proved to be an Atiyah-Hitchin submanifold of the 3-monopole moduli space. This allows what is known about 2-monopole dynamics to be translated into results about the dynamics of 3-monopoles. Using the numerical ADHMN construction, the monopole energy density is plotted on two geodesics. The first is a geodesic corresponding to right angle scattering. This geodesic has D_2 symmetry about a fixed set of axes. The second is a closed geodesic for three orbiting monopoles.

Twisted line scattering is discussed in Sect. 3.5. In the 3-monopole case, the Nahm data are known since S_4 symmetric 3-monopoles are D_2 symmetric. The numerical ADHMN construction is used to compute the energy density at various times during this motion. The dynamics of the zeros of the Higgs field are rich; there exist 3-monopoles with more than three zeros of the Higgs field. This is discussed in Sect. 3.6. Historically, Higgs anti-zeros were first observed in this example.

3.1 The genus one cases

The D_2 group is the viergruppe of π rotations about orthogonal axes. Choosing the orthogonal axes to be the Cartesian axes, D_2 is generated on $T\mathbf{P}^1$ by

$$C_2^z : (\eta, \zeta) \mapsto (-\eta, -\zeta) \tag{3.1}$$

and

$$C_2^x : (\eta, \zeta) \mapsto \left(-\frac{\eta}{\zeta^2}, \frac{1}{\zeta}\right). \tag{3.2}$$

The spectral curve of a D_2 symmetric 3-monopole, P , must be symmetric under these transformations and, hence, of the form,

$$\eta^3 + [r_1(\zeta^4 + 1) - r_2\zeta^2]\eta + c_1(\zeta^5 - \zeta) = 0, \quad (3.3)$$

where r_1 and r_2 are real and c_1 is imaginary. D_2 acts freely on those points on this curve with nonzero η . There are six points on the curve where $\eta = 0$, they are $\zeta = 0$, $\zeta = \infty$, $\zeta = \pm 1$ and $\zeta = \pm i$; the solutions of

$$\zeta^5 - \zeta = 0. \quad (3.4)$$

Each of these points is fixed by two elements of D_2 and so has branching number one. The whole action has branching number six. The curve has genus four and so the factor $2 - 2g$ on the left hand side of the Riemann-Hurwitz relation (1.35) cancels with the $-B$ on the right hand side and the factored curve P/D_2 has genus one.

This calculation can be done for the spectral curve P of a general D_{k-1} symmetric k -monopole. If k is even, then P/D_{k-1} has genus $\frac{k}{2}$. If k is odd it has genus $\frac{k-1}{2}$. This means that the only cases where P/D_{k-1} has genus one are 2-monopoles and 3-monopoles. The same applies to D_k ; the factored curve only has genus one for 2-monopoles and 3-monopoles.

To reduce the charge four curve to genus one, a larger symmetry group is required. A T symmetric 4-monopole has spectral curve, P , of the form

$$\eta^4 + c_1(\zeta^5 - \zeta)\eta + r_1(\zeta^8 + 14\zeta^4 + 1) = 0. \quad (3.5)$$

The only points on this curve fixed by the T action have $\eta = 0$. As a consequence ζ solves

$$\zeta^8 + 14\zeta^4 + 1 = 0. \quad (3.6)$$

These are the vertex and face points of a tetrahedron. Each has branching number two and so the total branching number is sixteen. The Riemann-Hurwitz relation implies the genus of P/T is one.

The octahedral 5-monopole and icosahedral 7-monopoles of Chapter 2 are more subtle. In both of these cases, the symmetric spectral curves are reducible. A octahedrally symmetric 5-monopole curve, P , has the form

$$\eta[\eta^4 + c_1(\zeta^5 - \zeta)\eta + r_1(\zeta^8 + 14\zeta^4 + 1)] = 0. \quad (3.7)$$

The $\eta^4 + c_1(\zeta^5 - \zeta)\eta + r_1(\zeta^8 + 14\zeta^4 + 1) = 0$ factor is genus one when it is divided by the octahedral group. The $\eta = 0$ factor is a sphere. The two factors touch at the faces point of the octahedron. The octahedral group acts transitively on these points and so in P/O they touch at just one point. Thus, P/O is a reducible curve in which a sphere touches a torus at a single point and so the Nahm equations have elliptic solutions. The icosahedral 7-monopole case is similar.

From the Jarvis rational map the only tetrahedrally symmetric 5-monopole is the octahedral 5-monopole. Furthermore, there is no tetrahedral 6-monopole. The most general T and O symmetric 7-monopole curves are not genus one curves after division. The next icosahedral monopole after the dodecahedral 7-monopole is charge eleven. The most general icosahedral 11-monopole curve is not genus one after division. The reducible curve of the form

$$\eta^5[\eta^6 + r\zeta(\zeta^{10} + 11\zeta^5 - 1)] = 0 \quad (3.8)$$

is genus one after division. However, this is only one of a family of possible icosahedral degree eleven algebraic curves. Since it is not known which curve the 11-monopole corresponds to, the fact (3.8) is genus one after division does not demonstrate the Nahm equations will have elliptic solutions.

The arguments above apply only to the most general algebraic curves of the correct form with given symmetry. Because of this, there may be cases beyond those listed where the Nahm equations have elliptic solutions. There is an example of this known; although D_2 monopoles of charge higher than three do not, in general, have spectral curves such that P/D_2 is genus one, the curves corresponding to the subfamily of 2-monopole-like k -monopoles discovered by Bielawski do [Bi2].

3.2 Tetrahedral 4-monopoles

The existence of a tetrahedral 4-monopole geodesic is proved in Sect. 2.7. It is noted in the previous section that the Nahm equations have elliptic equations in this case. Here, the Nahm data are constructed using the same methods as in Chapter 2.

The lowest degree T invariant polynomial is of degree six. It is

$$\zeta_1^5 \zeta_0 - \zeta_1 \zeta_0^5. \quad (3.9)$$

There is a degree eight T -invariant polynomial

$$\zeta_1^8 + 14\zeta_1^4 \zeta_0^4 + \zeta_0^8, \quad (3.10)$$

which is also invariant under the octahedral group. Therefore, there are T invariant Nahm triplets lying in the $\underline{9}_u$ representation and in both the $\underline{7}$ representations.

A basis for $\underline{7}$ is;

$$X = \begin{bmatrix} 0 & \sqrt{3} & 0 & 0 \\ 0 & 0 & 2 & 0 \\ 0 & 0 & 0 & \sqrt{3} \\ 0 & 0 & 0 & 0 \end{bmatrix}, Y = \begin{bmatrix} 0 & 0 & 0 & 0 \\ \sqrt{3} & 0 & 0 & 0 \\ 0 & 2 & 0 & 0 \\ 0 & 0 & \sqrt{3} & 0 \end{bmatrix}, H = \begin{bmatrix} 3 & 0 & 0 & 0 \\ 0 & 1 & 0 & 0 \\ 0 & 0 & -1 & 0 \\ 0 & 0 & 0 & -3 \end{bmatrix}. \quad (3.11)$$

Polarizing (3.9) yields

$$\xi_1^2 \otimes (20\zeta_1^3 \zeta_0) + 2\xi_1 \xi_0 \otimes (5\zeta_1^4 - 5\zeta_0^4) - \xi_0^2 \otimes (20\zeta_1 \zeta_0^3), \quad (3.12)$$

which is rewritten as

$$\begin{aligned} \xi_1^2 \otimes 5\left(\zeta_0 \frac{\partial}{\partial \zeta_1}\right) \zeta_1^4 + \left(\xi_0 \frac{\partial}{\partial \xi_1}\right) \xi_1^2 \otimes \left[5 - \frac{5}{24}\left(\zeta_0 \frac{\partial}{\partial \zeta_1}\right)^4\right] \zeta_1^4 \\ + \frac{1}{2}\left(\xi_0 \frac{\partial}{\partial \xi_1}\right)^2 \xi_1^2 \otimes \left[-\frac{5}{6}\left(\zeta_0 \frac{\partial}{\partial \zeta_1}\right)^3 \zeta_1^4\right] \end{aligned} \quad (3.13)$$

and converted to 4×4 matrices

$$X \otimes 5\text{ad}Y X^2 + \text{ad}Y X \otimes \left[5 - \frac{5}{24}(\text{ad}Y)^4\right] X^2 + \frac{1}{2}(\text{ad}Y)^2 X \otimes \left[-\frac{5}{6}(\text{ad}Y)^3\right] X^2. \quad (3.14)$$

These matrices are calculated explicitly using MAPLE and are proportional to

$$\begin{aligned}
Z_1 &= \begin{bmatrix} 0 & 2\sqrt{3} & 0 & 0 \\ 0 & 0 & 0 & 0 \\ 0 & 0 & 0 & -2\sqrt{3} \\ 0 & 0 & 0 & 0 \end{bmatrix}, \quad Z_2 = \begin{bmatrix} 0 & 0 & \sqrt{3} & 0 \\ 0 & 0 & 0 & \sqrt{3} \\ -\sqrt{3} & 0 & 0 & 0 \\ 0 & -\sqrt{3} & 0 & 0 \end{bmatrix}, \\
Z_3 &= \begin{bmatrix} 0 & 0 & 0 & 0 \\ \sqrt{3} & 0 & 0 & 0 \\ 0 & 0 & 0 & 0 \\ 0 & 0 & -\sqrt{3} & 0 \end{bmatrix}. \tag{3.15}
\end{aligned}$$

Polarizing the O invariant (3.10) yields

$$\xi_1^2 \otimes (56\zeta_1^6 + 168\zeta_1^2\zeta_0^4) + 2\xi_1\xi_0 \otimes (224\zeta_1^3\zeta_0^3) + \xi_0^2 \otimes (168\zeta_1^4\zeta_0^2 + 56\zeta_0^6), \tag{3.16}$$

which becomes

$$\begin{aligned}
\xi_1^2 \otimes [56 + \frac{7}{15}(\zeta_0 \frac{\partial}{\partial \zeta_1})^4] \zeta_1^6 + (\xi_0 \frac{\partial}{\partial \xi_1}) \xi_1^2 \otimes \frac{28}{15} (\zeta_0 \frac{\partial}{\partial \zeta_1})^3 \zeta_1^6 \\
+ \frac{1}{2} (\xi_0 \frac{\partial}{\partial \xi_1})^2 \xi_1^2 \otimes [\frac{28}{5} (\zeta_0 \frac{\partial}{\partial \zeta_1})^2 + \frac{7}{90} (\zeta_0 \frac{\partial}{\partial \zeta_1})^6] \zeta_1^6 \tag{3.17}
\end{aligned}$$

and, thus, the invariant Nahm triplet

$$\begin{aligned}
Y_1 &= \begin{bmatrix} 0 & 0 & 0 & -20 \\ 4\sqrt{3} & 0 & 0 & 0 \\ 0 & -12 & 0 & 0 \\ 0 & 0 & 4\sqrt{3} & 0 \end{bmatrix}, \quad Y_2 = \begin{bmatrix} -4 & 0 & 0 & 0 \\ 0 & 12 & 0 & 0 \\ 0 & 0 & -12 & 0 \\ 0 & 0 & 0 & 4 \end{bmatrix}, \\
Y_3 &= \begin{bmatrix} 0 & -2\sqrt{3} & 0 & 0 \\ 0 & 0 & 6 & 0 \\ 0 & 0 & 0 & -2\sqrt{3} \\ 10 & 0 & 0 & 0 \end{bmatrix}. \tag{3.18}
\end{aligned}$$

The T invariant in $\underline{7}_m$ is calculated by constructing an isomorphism between $\underline{7}_m$ and $\underline{7}_u$. It is

$$\begin{aligned}
& [5(\text{ad}Y \otimes 1 + 1 \otimes \text{ad}Y) - \frac{1}{24}(\text{ad}Y \otimes 1 + 1 \otimes \text{ad}Y)^5](\text{ad}Y X \otimes X^3 - \frac{1}{3}X \otimes \text{ad}Y X^3) \\
&= X \otimes (-\frac{5}{3}(\text{ad}Y)^2 + \frac{1}{72}(\text{ad}Y)^6)X^3 + \text{ad}Y X \otimes (\frac{10}{3}\text{ad}Y + \frac{1}{36}(\text{ad}Y)^5)X^3 \\
&\quad + (\text{ad}Y)^2 X \otimes (5 - \frac{5}{72}(\text{ad}Y)^4)X^3 \tag{3.19}
\end{aligned}$$

with corresponding matrices

$$\begin{aligned}
W_1 &= \begin{bmatrix} 0 & -2\sqrt{3} & 0 & 0 \\ 0 & 0 & 6 & 0 \\ 0 & 0 & 0 & -2\sqrt{3} \\ -6 & 0 & 0 & 0 \end{bmatrix}, \quad W_2 = \begin{bmatrix} 0 & 0 & 2\sqrt{3} & 0 \\ 0 & 0 & 0 & -2\sqrt{3} \\ 2\sqrt{3} & 0 & 0 & 0 \\ 0 & -2\sqrt{3} & 0 & 0 \end{bmatrix}, \\
W_3 &= \begin{bmatrix} 0 & 0 & 0 & 3 \\ \sqrt{3} & 0 & 0 & 0 \\ 0 & -3 & 0 & 0 \\ 0 & 0 & \sqrt{3} & 0 \end{bmatrix}. \tag{3.20}
\end{aligned}$$

The basis change (2.33) is made:

$$(Y_1, Y_2, Y_3) \rightarrow (Y'_1, Y'_2, Y'_3) = (\frac{1}{2}Y_1 + Y_3, -\frac{i}{2}Y_1 + iY_3, -iY_2) \tag{3.21}$$

and similarly for (Z_1, Z_2, Z_3) and (W_1, W_2, W_3) . The primes are dropped on the transformed quantities.

The commutation relations satisfied by the invariant Nahm vectors are calculated using

MAPLE;

$$\begin{aligned}
[Y_1, Y_2] &= -48\rho_3 - 8Y_3, & [Z_1, Z_2] &= \frac{6}{5}\rho_3 + \frac{3}{5}Y_3, \\
[W_1, W_2] &= \frac{12}{5}\rho_3 + \frac{6}{5}Y_3, & [\rho_1, Y_2] + [Y_1, \rho_2] &= -6Y_3, \\
[\rho_1, Z_2] + [Z_1, \rho_2] &= -4Z_3, & [\rho_1, W_2] + [W_1, \rho_2] &= 2W_3, \\
[Y_1, Z_2] + [Z_1, Y_2] &= -32Z_3, & [Z_1, W_2] + [W_1, Z_2] &= 0, \\
[Y_1, W_2] + [W_1, Y_2] &= 16W_3.
\end{aligned} \tag{3.22}$$

Writing

$$T_i(t) = x(t)\rho_i + y(t)Y_i + z(t)Z_i + w(t)W_i \tag{3.23}$$

the reduced Nahm equations are

$$\frac{dx}{dt} = 2x^2 - 48y^2 + \frac{6}{5}z^2 + \frac{12}{5}w^2, \tag{3.24}$$

$$\frac{dy}{dt} = -8y^2 + \frac{3}{5}z^2 + \frac{6}{5}w^2 - 6xy, \tag{3.25}$$

$$\frac{dz}{dt} = -4xz - 32yz, \tag{3.26}$$

$$\frac{dw}{dt} = 2xw + 16wy. \tag{3.27}$$

The spectral curve is

$$\eta^4 + c_1\eta\zeta(\zeta^4 - 1) + c_1c_2(\zeta^8 + 14\zeta^4 + 1) = 0, \tag{3.28}$$

where

$$c_1 = 288z(x^2 + 4y^2 + 3w^2 - 4xy) \equiv 288ic'_1 \tag{3.29}$$

and

$$c_2 = -\frac{48}{288z}(60y^2 + 3z^2 - 3w^2 + 20xy) \equiv \frac{48}{288}ic'_2 \tag{3.30}$$

are constants.

The equations are simplified by setting w to zero and letting $u = x - 2y$ and $v = x + 8y$ to get

$$\frac{du}{dt} = 2uv, \quad (3.31)$$

$$z = i \frac{c'_1}{u^2} \quad (3.32)$$

and

$$c'_2 = \frac{u^2}{c'_1} \left[v^2 - u^2 - \frac{3c_1'^2}{u^4} \right]. \quad (3.33)$$

Define $\kappa^4 \equiv -16c'_1c'_2$ and $a \equiv 8c'_1/\kappa^3$ to obtain

$$4 \frac{du}{ds} = -\sqrt{64u^4 - 4\kappa^4 + 3a^2\kappa^6u^{-2}}. \quad (3.34)$$

Let $s = \kappa(t + 1)$ and $u(t) = -\kappa\sqrt{\wp(s)}/2$ giving

$$\left(\frac{\kappa^2}{\sqrt{\wp}} \frac{d\wp}{ds} \right)^2 = 4\kappa^4 \left(\wp^2 - 1 + \frac{3a^2}{\wp} \right), \quad (3.35)$$

so that $\wp(s)$ is the Weierstrass function satisfying

$$\left(\frac{d\wp}{ds} \right)^2 = 4\wp^3 - 4\wp + 12a^2. \quad (3.36)$$

Hence (3.24)-(3.27) are solved by

$$x = \frac{\kappa}{5} \left(-2\sqrt{\wp} + \frac{1}{4} \frac{1}{\wp} \frac{d\wp}{ds} \right), \quad (3.37)$$

$$y = \frac{\kappa}{20} \left(\sqrt{\wp(\kappa s)} + \frac{1}{2} \frac{1}{\wp(\kappa s)} \frac{d\wp}{ds} \right), \quad (3.38)$$

$$z = \frac{ia\kappa}{2\wp}, \quad (3.39)$$

$$w = 0. \quad (3.40)$$

In order to determine that these Nahm data correspond to a monopole, the boundary conditions must be examined. As $t \rightarrow -1$,

$$x \sim -\frac{1}{2(t+1)}, \quad (3.41)$$

$$y \sim 0,$$

$$z \sim 0.$$

Therefore, at $t = -1$ the residues of T_i are $-\frac{1}{2}\rho_i$ and, so, form an irreducible representation of \mathfrak{su}_2 . If $\kappa = \omega_1$ there is a second pole at $t = 1$. The residues here also form an irreducible representation of \mathfrak{su}_2 demonstrating the existence of a one parameter family of monopoles with spectral curves

$$\eta^4 + i36a\kappa^3\eta\zeta(\zeta^4 - 1) + 3\kappa^4(\zeta^8 + 14\zeta^4 + 1) = 0. \quad (3.42)$$

The spectral curve of a 1-monopole with position (x_1, x_2, x_3) , (1.45), is

$$\eta - (x_1 + ix_2) + 2x_3\zeta + (x_1 - ix_2)\zeta^2 = 0.$$

The product of four spectral curves corresponding to four monopoles positioned at the vertices

$$\{(+b, +b, +b), (+b, -b, -b), (-b, -b, +b), (-b, +b, -b)\} \quad (3.43)$$

of a regular tetrahedron (where $b > 0$) is

$$\eta^4 - 16ib^3\eta(\zeta^5 - \zeta) + 4b^4(\zeta^8 + 14\zeta^4 + 1) = 0. \quad (3.44)$$

The spectral curve (3.42) has this form when

$$a = -3^{-5/4}\sqrt{2}. \quad (3.45)$$

Examination of the integral expression for κ

$$\kappa = \int_0^X \frac{dx}{\sqrt{1 - x^4 + 3a^2x^6}}, \quad (3.46)$$

where X is the first positive real root of $0 = 1 - x^4 + 3a^2x^6$, shows that $\kappa \rightarrow \infty$ as $a \rightarrow \pm 3^{-5/4}\sqrt{2}$ but it is finite for $a \in (-3^{-5/4}\sqrt{2}, 3^{-5/4}\sqrt{2})$. Thus, as a approaches $-3^{-5/4}\sqrt{2}$, (3.42) describes the superposition of four well-separated monopoles on the the vertices of a tetrahedron (3.43), with the distance between monopoles equal to $3^{1/4}\kappa$. The tetrahedron dual to the one above, has vertices

$$\{(-b, -b, -b), (-b, +b, +b), (+b, +b, -b), (+b, -b, +b)\} \quad (3.47)$$

with a corresponding product of spectral curves given by

$$\eta^4 + 16ib^3\eta(\zeta^5 - \zeta) + 4b^4(\zeta^8 + 14\zeta^4 + 1) = 0. \quad (3.48)$$

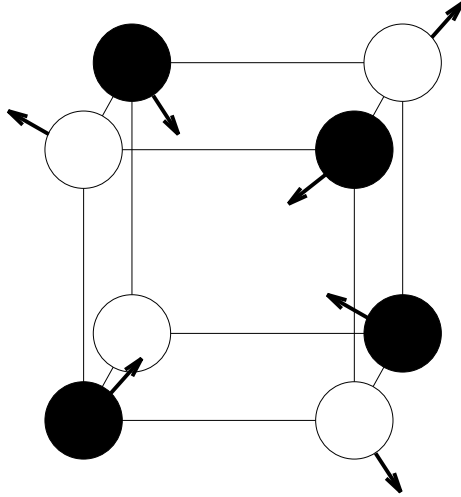


Figure 3.1: Schematic representation of 4-monopole scattering.

Clearly this is the form of the spectral curve (3.42) when $a = 3^{-5/4}\sqrt{2}$.

If $a = 0$ then $z = 0$ and κ is given by

$$\kappa = \int_0^1 \frac{dx}{\sqrt{1-x^4}} = \frac{\Gamma(1/4)^2}{4\sqrt{2\pi}}, \quad (3.49)$$

so that the spectral curve becomes that of the cubic 4-monopole given by (2.17).

This 1-parameter family is a geodesic in the 4-monopole moduli space. It corresponds to a tetrahedral scattering process. Figure 3.1 is a schematic representation of this process. The cube has centre at the origin and edges parallel to the coordinate axes; it is to be associated with the cubic 4-monopole. The incoming monopoles are represented by black spheres and the outgoing monopoles by white spheres, with an arrow indicating the direction of motion for each.

To obtain a true picture of the scattering process, energy density plots are needed. This can be done using the numerical scheme. Figure 3.2 shows a surface of constant energy density for the five values $a = -0.25, -0.18, 0.00, 0.18, +0.25$. The energy density is initially localized in four regions, roughly centred on the vertices of a tetrahedron. These vertices are opposite corners of a cube as in Fig. 3.1. On any one face of the cube, the incoming energy density is concentrated on two opposite corners of the face, the black spheres in Fig. 3.1. It flows around the edges of the face until it is localized on the other

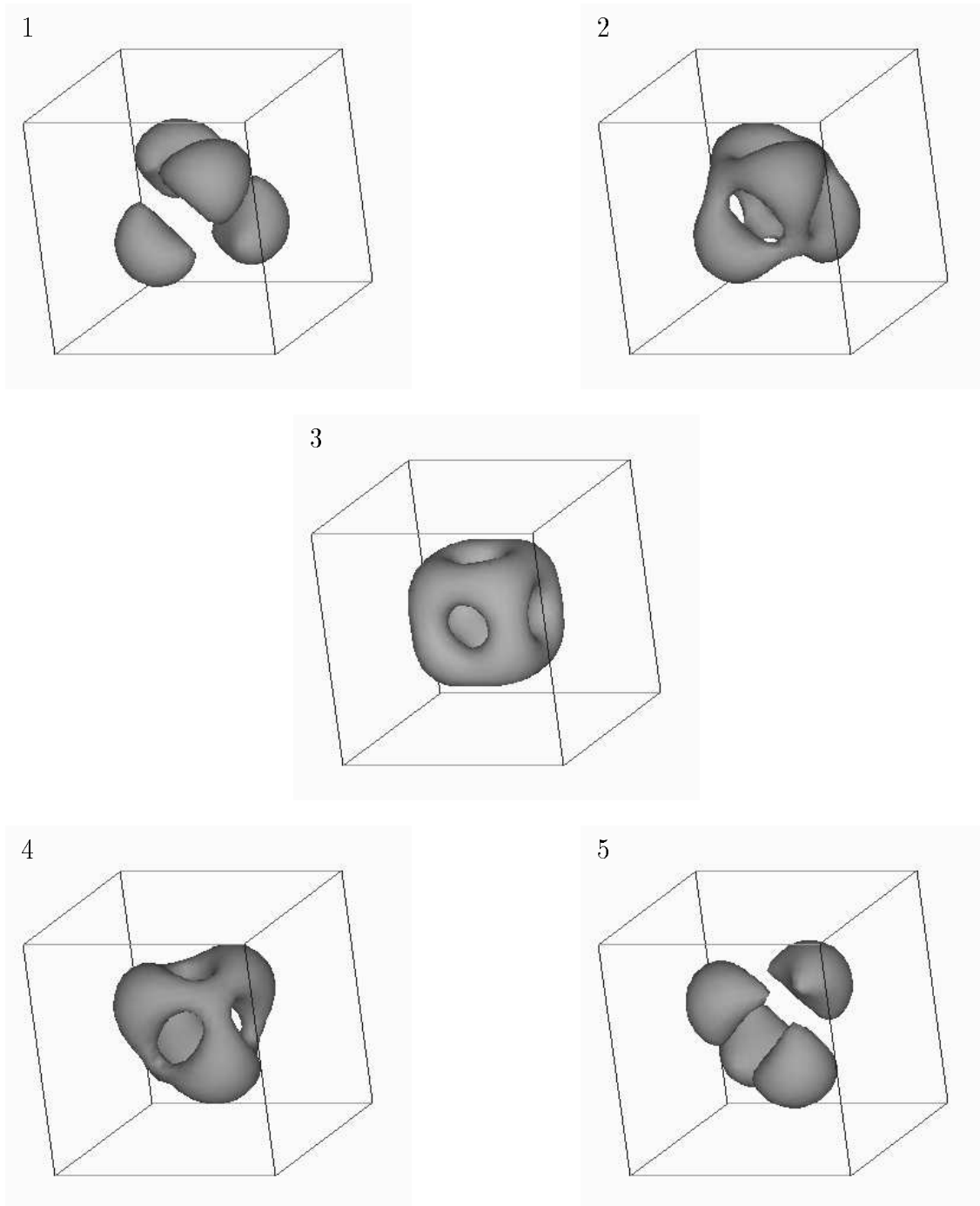


Figure 3.2: Tetrahedral 4-monopole scattering; surface of constant energy density for values (1) $a = -0.25$, (2) $a = -0.18$, (3) $a = 0.00$, (4) $a = 0.18$, (5) $a = 0.25$.

two corners, the white spheres in Fig. 3.1, as the monopoles separate.

Historically, this was the first higher charge monopole geodesic for which the Nahm data was explicitly known. Sutcliffe has subsequently calculated the metric numerically along the geodesic [Su]. An analytic expression for this metric was then provided by Braden and Sutcliffe [BrS]. Geodesics in the two-dimensional space of tetrahedral $(4,[3],[2],[1])$ -monopoles have even been calculated numerically [HS5].

3.3 D_2 3-monopoles

The space of D_2 symmetric 3-monopoles is two dimensional. This follows from the Jarvis rational maps description. D_2 is generated by

$$C_2^z : z \mapsto -z \tag{3.50}$$

and

$$C_2^x : z \mapsto \frac{1}{z}. \tag{3.51}$$

The Jarvis rational map that is symmetric under these transformations is

$$R(z) = \frac{\alpha z^2 - 1}{z(z^2 - \alpha)}, \tag{3.52}$$

where α is complex. This rational map degenerates when $\alpha = \infty$ or $\alpha = \pm 1$. At these points, one monopole is infinitely far along each direction of a Cartesian axis and the third is at the origin.

There are exceptional values of α where the symmetry is larger than D_2 . The obvious example is $\alpha = 0$ where

$$R(z) = -\frac{1}{z^3} \tag{3.53}$$

and has axial symmetry about the x_3 -axis. There is axial symmetry about the x_1 -axis if $\alpha = -3$ and about the x_2 -axis if $\alpha = 3$.

If α is real, the rational map is symmetric under inversion. In this case, the 3-monopoles have the same symmetries as 2-monopoles. Since this one-parameter family is obtained by applying symmetry, it is geodesic in the moduli space. The point $\alpha = \infty$ is the same as

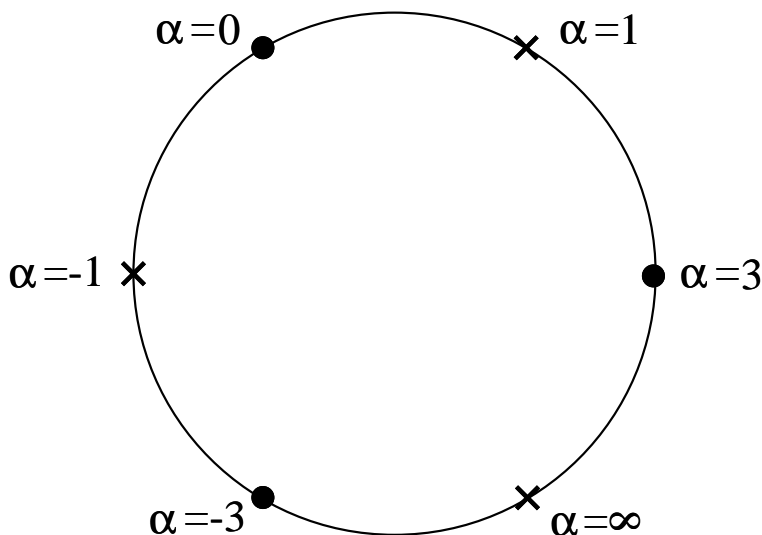


Figure 3.3: Head-on scattering geodesics. The crosses are degenerate maps and the dots are axially symmetric maps.

$\alpha = -\infty$ and the one-parameter family is represented by a circle in Fig. 3.3. Around the circle are three points with axial symmetry and three degenerate points. Geodesics run from one degenerate point, through a point with axial symmetry and then on to another degenerate point. The geodesics correspond to $\pi/2$ scattering of two monopoles incident on a third. They mimic the classic 2-monopole head-on scattering geodesics, except there is an extra monopole at the origin.

If α is imaginary, the rational map is symmetric under the S_4 rotary-reflection in the x_3 -axis. This transformation is a rotation of $\pi/2$ about the x_3 -axis followed by a reflection in the x_1x_2 -plane and is

$$z \mapsto \frac{i}{\bar{z}}. \quad (3.54)$$

It intersects the α real geodesic at the torus $\alpha = 0$. If $\alpha = \pm\sqrt{3}i$, then there is an additional C_3 symmetry

$$z \mapsto \frac{iz + 1}{-iz + 1} \quad (3.55)$$

about $x_1 = x_2 = x_3$. Along with the D_2 symmetry, this generates the tetrahedral group and so these points are the tetrahedral 3-monopole. A C_4 rotation about any Cartesian

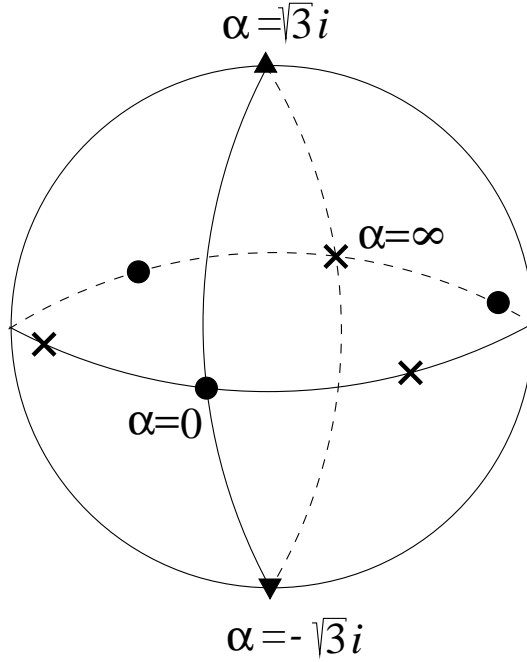


Figure 3.4: The α -sphere of D_2 symmetric rational maps. Crosses denote degenerate maps, dots denote axially symmetric maps and triangles denote the tetrahedral maps.

axis swops $\alpha = \sqrt{3}i$ and $\alpha = -\sqrt{3}i$ and each possibility is just the dual of the other. This geodesic is one of the twisted line scattering geodesics discussed in Sect. 2.6. Monopoles approach along the x_3 -axis, coalesce to form a tetrahedron, then a torus and finally the dual tetrahedron, before separating again along the same axis. These are also twisted line scattering geodesics in the x_1 -axis with $|\alpha|^2 + 2\mathcal{R}e(\alpha) = 3$ and in the x_2 -axes with $|\alpha|^2 - 2\mathcal{R}e(\alpha) = 3$.

In Fig. 3.4, α is represented by a sphere and the various exceptional values are marked. The α real circle of Fig. 3.5 is the horizontal equator. The other great circle is the geodesic of twisted line scattering in the x_3 -axis. The northern hemisphere of this sphere is drawn as a disc in Fig. 3.5. The diameters are the northern halves of each of the twisted line scattering lines. Each wedge of the disk is mapped to each of the others by tetrahedral and S_4 transformations. The southern hemisphere of Fig. 3.4 is related to the northern hemisphere by inversion. In this sense, the shaded wedge is typical of all twelve wedges.

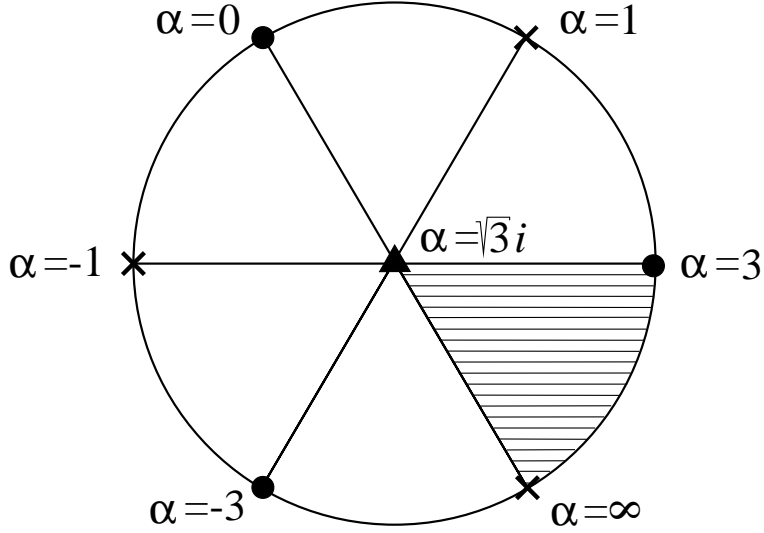


Figure 3.5: The northern hemisphere of the α -sphere.

The Nahm data for D_2 symmetric 3-monopoles are calculated using the usual methods and are

$$\begin{aligned}
 T_1 &= \frac{f_1}{2} \begin{pmatrix} 0 & i\sqrt{2}e^{-i\theta_1} & 0 \\ i\sqrt{2}e^{i\theta_1} & 0 & i\sqrt{2}e^{i\theta_1} \\ 0 & i\sqrt{2}e^{-i\theta_1} & 0 \end{pmatrix}, \\
 T_2 &= \frac{f_2}{2} \begin{pmatrix} 0 & \sqrt{2}e^{i\theta_2} & 0 \\ -\sqrt{2}e^{-i\theta_2} & 0 & \sqrt{2}e^{-i\theta_2} \\ 0 & -\sqrt{2}e^{i\theta_2} & 0 \end{pmatrix}, \\
 T_3 &= \frac{f_3}{2} \begin{pmatrix} -2i \cos \theta_3 & 0 & -2 \sin \theta_3 \\ 0 & 0 & 0 \\ 2 \sin \theta_3 & 0 & 2i \cos \theta_3 \end{pmatrix},
 \end{aligned} \tag{3.56}$$

where the f_i 's and the θ_i 's are functions of t . Substituting these data into the Nahm equations gives

$$\frac{dF_1}{dt} = \bar{F}_2 \bar{F}_3 \tag{3.57}$$

and two others by cyclic permutation, where $F_i = e^{i\theta_i} f_i$. These equations are similar to the Euler-Poinsot equations.

It was solved some time ago in a paper about the propagation of light in a nonlinear dielectric [ABDP]. Equation (3.57) is rewritten as

$$\frac{df_3}{dt} + i\frac{d\theta_3}{dt} = f_1 f_2 e^{-(\theta_1 + \theta_2 + \theta_3)} \quad (3.58)$$

and two others by cyclic permutation. Writing $\theta = \theta_1 + \theta_2 + \theta_3$ the real and imaginary equations are given by cyclic permutations of

$$\frac{df_3}{dt} = f_1 f_2 \cos \theta, \quad (3.59)$$

$$\frac{d\theta_3}{dt} = -f_1 f_2 \sin \theta, \quad (3.60)$$

The Lax curve calculated from the Nahm data are

$$\eta^3 - 2[A\zeta^4 + 2B\zeta^2 + A]\eta + 4i\Gamma(\zeta^5 - \zeta) = 0, \quad (3.61)$$

where

$$A = \frac{1}{2}(f_1^2 - f_2^2), \quad (3.62)$$

$$B = -\frac{1}{2}(f_1^2 + f_2^2 - 2f_3^2),$$

$$\Gamma = \mathcal{I}m(F_1 F_2 F_3) = f_1 f_2 f_3 \sin \theta$$

are constants.

The Nahm equations are solved explicitly by drawing the θ triangle. Hence,

$$f_1 f_2 f_3 \cos \theta = \sqrt{(f_1 f_2 f_3)^2 - \Gamma^2} \quad (3.63)$$

and so from (3.59)

$$\frac{df_i^2}{dt} = 2\sqrt{(f_1 f_2 f_3)^2 - \Gamma^2} \quad (3.64)$$

for $i = 1, 2$ or 3 . Substituting $q_3 = f_3^2 - \frac{2B}{3}$ into the $i = 3$ equation puts it into Weierstrass elliptic form

$$\left(\frac{d}{ds}q_3\right)^2 = 4q_3^3 - g_2q_3 - g_3. \quad (3.65)$$

where $g_2 = 4(A^2 + \frac{B^2}{3})$, $g_3 = 4(\frac{2}{3}A^2B - \frac{2}{27}B^3 + \Gamma^2)$ and $s = t + 1$.

This form is preserved under the scaling transformation $q_3(s) = Cq'_3$ and $s = s'/\sqrt{C}$. Under this transformation, (3.65) becomes

$$\left(\frac{d}{ds'}q'_3\right)^2 = 4q'^3_3 - g'_2q'_3 - g'_3, \quad (3.66)$$

where $g'_2 = C^2g_2$ and $g'_3 = C^3g_3$. In the case where $f_1^2 \leq f_2^2 < f_3^2$, $C = 1/B > 0$ is used to obtain

$$\begin{aligned} g'_2 &= 4\left(x^2 + \frac{1}{3}\right), \\ g'_3 &= -4\left(\frac{2}{3}x^2 - \frac{2}{27} - y^2\right), \end{aligned} \quad (3.67)$$

where $x = A/B$ and $y = \Gamma/\sqrt{B^3}$.

The scale, B , is set by the requirement that the second pole lies at $t = 1$ and, so, x and y parameterize the solutions to the Nahm equations in the $f_1^2 \leq f_2^2 < f_3^2$ sector. The function f_3 is now known, it is

$$f_3^2 = B\left(\wp(s') + \frac{2}{3}\right), \quad (3.68)$$

where $\wp(s')$ is the Weierstrass function satisfying

$$\left(\frac{d\wp(s')}{ds'}\right)^2 = 4\wp(s') - g'_2\wp(s') - g'_3, \quad (3.69)$$

g'_2 and g'_3 are given in (3.67) and $s' = \sqrt{B}s$. The other two f_i 's are related to this one by (3.62). The angles are given by integrating (3.60). Substituting for $\sin\theta$, these equations are

$$\frac{d\theta_i}{ds} = \frac{-\Gamma}{f_i}. \quad (3.70)$$

The poles of $\wp(s')$ are order two and at such poles $\sin\theta = 0$. The matrix residues are an irreducible representation of \mathfrak{su}_2 . Thus the Nahm boundary conditions are satisfied if the poles are at $s = 0$ and $s = 2$. This is the case if $B = \omega_1^2$, where $2\omega_1$ is the real period of the Weierstrass function.

In terms of $x > 0$ and $y > 0$, the spectral curve is

$$\eta^3 - 2\omega_1^2(x\zeta^4 + 2\zeta^2 + x)\eta + 4i\omega_1^3y(\zeta^5 - \zeta) = 0. \quad (3.71)$$

This curve has D_2 symmetry. For certain values of x and y the spectral curve has further symmetries. By observing which values correspond to which symmetries it is possible to locate this sector of Nahm data on the whole sphere of D_2 3-monopoles.

If $x = 0$, this curve has S_4 symmetry in the x_3 -axis:

$$(\eta, \zeta) \mapsto \left(\frac{-i\bar{\eta}}{\bar{\zeta}^2}, \frac{i}{\bar{\zeta}} \right). \quad (3.72)$$

If $x = 1$, the curve has S_4 symmetry in the x_2 -axis:

$$(\eta, \zeta) \mapsto \left(\frac{2\bar{\eta}}{(1 - \bar{\zeta})^2}, \frac{\bar{\zeta} + 1}{1 - \bar{\zeta}} \right). \quad (3.73)$$

If $y = 0$, the curve is symmetric under reflections in the Cartesian planes.

At the point $x = 0$ and $y = 0$, the Weierstrass function has infinite real period. This point corresponds to infinite separation along the x_3 -axis. The spectral curve factorizes into three stars at this point;

$$\eta(\eta + 2\omega_1\zeta)(\eta - 2\omega_1\zeta) = 0 \quad (3.74)$$

and since $2\omega_1$ is the real period it is infinite. Finally, at $x = 1$ and $y = 0$ the spectral curve is axially symmetric about the x_2 -axis. Treating the $B = 0$ case separately shows that $y = \infty$ corresponds to the tetrahedron.

Thus, the region $0 \leq x \leq 1$, $y \geq 0$ is the shaded wedge in Fig. 3.5. Figure 3.6 is a picture of the (x, y) region. The curve of zero discriminant is also drawn. The discriminant is

$$\Delta = g_2^3 - 27g_3^2 \quad (3.75)$$

and when $\Delta = 0$ one of the periods is infinite; in the case of the line in Fig. 3.6 the imaginary period is infinite. The Weierstrass function with infinite imaginary period is

$$\wp(s') = -\frac{Y}{3} + \frac{Y}{\sin^2 \sqrt{Y} s'}, \quad (3.76)$$

and $g_2 = \frac{4}{3}Y^2$ and $g_3 = \frac{8}{27}Y^3$. These equations can be solved for x and y and the spectral curve for these monopoles can be written down exactly, it is

$$\eta^3 - \frac{\pi^2}{2Y} \left[\frac{Y^2 - 1}{3}(\zeta^4 + 1) + 2\zeta^2 \right] + \frac{i\pi^3}{27Y^{\frac{3}{2}}} [Y^2(Y - 3) + 4](\zeta^5 - \zeta) = 0 \quad (3.77)$$

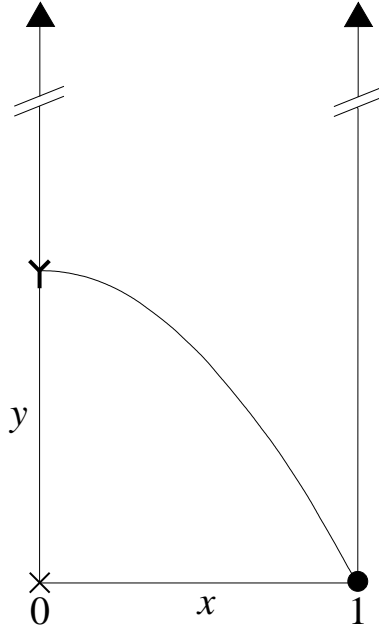


Figure 3.6: The (x, y) region corresponding to the shaded wedge in Fig. 3.5.

where $1 \leq Y \leq 2$. The significance of this exceptional class of monopoles is unclear. It is suggested at the end of this chapter that such monopoles divide the moduli space into regions where there are extra zeros of the Higgs field and regions where there are not.

3.4 Inversion symmetric 3-monopoles

In this section, 3-monopoles with inversion symmetry are considered. All 3-monopoles symmetric under inversion are D_2 symmetric about some set of orthogonal axes. From the previous section, the Nahm data are known if the D_2 symmetry is about the Cartesian axes. By considering how the Nahm data transform under rotation, the whole space of inversion symmetric 3-monopoles is demonstrated to be the Atiyah-Hitchin manifold.

The spectral curve of an inversion symmetric 3-monopole must be of the general form

$$\eta^3 + [c_1 + c_2\zeta + r\zeta^2 - \bar{c}_2\zeta^3 + \bar{c}_1\zeta^4]\eta = 0, \quad (3.78)$$

where $c_i \in \mathbf{C}$ and $r \in \mathbf{R}$. In the Cartesian orientation of the previous section, the spectral curve is (3.61) with $\Gamma = 0$; the angles θ_i may all be set to zero in this case. Thus, the

Nahm data simplify to

$$\begin{aligned}
T_1(t) &= \frac{f_1(t)}{2} \begin{pmatrix} 0 & \sqrt{2}i & 0 \\ \sqrt{2}i & 0 & \sqrt{2}i \\ 0 & \sqrt{2}i & 0 \end{pmatrix}, \\
T_2(t) &= \frac{f_2(t)}{2} \begin{pmatrix} 0 & \sqrt{2} & 0 \\ -\sqrt{2} & 0 & \sqrt{2} \\ 0 & -\sqrt{2} & 0 \end{pmatrix}, \\
T_3(t) &= \frac{f_3(t)}{2} \begin{pmatrix} -2i & 0 & 0 \\ 0 & 0 & 0 \\ 0 & 0 & 2i \end{pmatrix}.
\end{aligned} \tag{3.79}$$

These invariant Nahm data correspond to the SO_3 invariant $\underline{1}$ and the SO_2 and D_4 invariant vectors in $\underline{5}$. The Nahm equations also simplify: since $f_i(s) = F_i(s)$ and is real, the reduced Nahm equations are the Euler-Poinsot equations and the spectral curve is

$$\eta^3 - (1 - k^2)K(k)^2(\zeta^4 - 2\frac{1 + k^2}{1 - k^2}\zeta^2 + 1)\eta = 0. \tag{3.80}$$

This spectral curve is very similar to the 2-monopole spectral curve. The 2-monopole Nahm data transforms under SO_3 as $\underline{5} \oplus \underline{3} \oplus \underline{1}$. As with the 3-monopole Nahm data the D_2 -symmetric Nahm data correspond to the SO_3 invariant $\underline{1}$ and the SO_2 and D_4 invariant vectors in $\underline{5}$.

The whole manifold of inversion symmetric rational maps is four dimensional. This is easily demonstrated using the Donaldson rational map description. Inversion is $I = \sigma_{xy} \circ \text{Rot}_\pi$. The action of the reflection does not affect the numerator $q(z)$. This means that it must be invariant under Rot_π . Since Rot_π acts on $q(z)$ by changing the sign of z and the overall sign $q(z) = z(z^2 - \beta^2)$ for some $\beta \in \mathbf{C}$. The candidate inversion symmetric rational map is

$$R(z) = \frac{az^2 + bz + c}{(z - \beta)z(z + \beta)} \tag{3.81}$$

for complex a, b and c . This is inversion invariant if, and only if,

$$p(-z)p(z) \equiv 1 \pmod{z^3 - \beta^2 z} \tag{3.82}$$

or equivalently,

$$p(\beta)p(-\beta) = 1, \quad (3.83)$$

$$p(0)^2 = 1. \quad (3.84)$$

The first strong-centring condition (2.93) is automatically satisfied by $q(z)$. The second strong-centring condition (2.94) is

$$p(\beta)p(0)p(-\beta) = 1. \quad (3.85)$$

When combined with (3.83) and (3.84) this gives $p(0) = 1$ and thus $c = 1$. Explicitly substituting $p(z)$ into (3.83) gives the condition

$$b^2 - a^2\beta^2 = 2a. \quad (3.86)$$

This defines a surface in \mathbf{C}^3 of two complex dimensions, corresponding to inversion symmetric strongly centred 3-monopoles. The argument above assumes that the roots are distinct. That is, $\beta \neq 0$. In fact, (3.86) applies in the $\beta = 0$ case as well.

This four-dimensional submanifold of the 3-monopole moduli space is the fixed set of the inversion action on the entire 3-monopole moduli space. The fixed point set of a finite group action on a Riemannian manifold is totally geodesic and so this submanifold is a totally geodesic submanifold of \mathcal{M}_3^0 . This metric is the Atiyah-Hitchin metric.

This is because the space of 2-monopoles and the space of inversion symmetric 3-monopoles have the same Nahm data. Along the Cartesian orientated D_2 geodesic, the latter is mapped to the former by replacing the matrix basis of $\underline{2}$ by that of $\underline{3}$. The Nahm data transform under SO_3 like a vector in $\underline{5}$ in each case. This means that the space of 2-monopole Nahm data are identical to the space of 3-monopole Nahm data except that the matrices appearing in the 2-monopole case are the basis of $\underline{2}$ and in the 3-monopole case they are the basis of $\underline{3}$. Since the metric on the space of Nahm data are given by

$$\|Y_0, Y_1, Y_2, Y_3\|^2 = - \int_{-1}^1 \sum_{i=0 \dots 3} \text{tr}(Y_i^2) dt, \quad (3.87)$$

the two metrics are identical apart from an overall factor. This factor is easy to calculate. It is given by the ratio between the traces of the squares of the matrices in the two cases.

This factor is four and the metric for 3-monopoles is four times that for 2-monopoles. It is noted that there is a difference in topology between the two spaces [Bi2].

It is instructive to construct the Gibbons-Manton point particle metric for 3-monopoles with inversion symmetry. In the case of three monopoles that are symmetric under inversion symmetry $\mathbf{r}_1 = \boldsymbol{\rho}$, $\mathbf{r}_2 = 0$ and $\mathbf{r}_3 = -\boldsymbol{\rho}$. Furthermore $d\chi_1 = d\theta$, $d\chi_2 = 0$ and $d\chi_3 = -d\theta$ is required. Denoting $\mathbf{w}_{12} = \mathbf{w}_{23}$ by \mathbf{w} so that $\mathbf{w}_{13} = \frac{1}{2}\mathbf{w}$;

$$g_{ij} = \frac{1}{\rho} \begin{pmatrix} \rho - \frac{3}{2} & 1 & \frac{1}{2} \\ 1 & \rho - 2 & 1 \\ \frac{1}{2} & 1 & \rho - \frac{3}{2} \end{pmatrix} \quad (3.88)$$

$$\mathbf{W}_{ij} = \frac{1}{2} \begin{pmatrix} -3\mathbf{w} & 2\mathbf{w} & \mathbf{w} \\ 2\mathbf{w} & -4\mathbf{w} & 2\mathbf{w} \\ \mathbf{w} & 2\mathbf{w} & -3\mathbf{w} \end{pmatrix},$$

so

$$ds^2 = 4 \left[\frac{1}{2} \left(1 - \frac{2}{\rho} \right) d\boldsymbol{\rho} \cdot d\boldsymbol{\rho} + \frac{1}{2} \left(1 - \frac{2}{\rho} \right)^{-1} (-d\theta + 2\mathbf{w} \cdot d\boldsymbol{\rho})^2 \right]. \quad (3.89)$$

Up to the overall factor of four this is the asymptotic metric for two strongly centred monopoles separated by a distance ρ . Note that in the 2-monopole case, ρ is the separation of the two monopoles, whereas in the 3-monopole case it is the distance from the monopole at the origin to either of the other two monopoles.

It is possible to apply inversion symmetry to k -monopoles for $k > 3$. However, the resulting geodesic submanifold has more than four dimensions and so cannot be an Atiyah-Hitchin submanifold. However, Bielawski [Bi2] has succeeded in finding geodesic Atiyah-Hitchin submanifolds of the k -monopole moduli space for each k . These submanifolds correspond to k -monopoles with inversion symmetry and the individual monopoles are equally spaced along an axis. Bielawski derives his result by considering the moment map construction.

One interesting property of these equally spaced monopoles is clear from the asymptotic metric. Inversion symmetry requires that $\boldsymbol{\rho}_1 = \boldsymbol{\rho}$, $\boldsymbol{\rho}_2 = 0$ and $\boldsymbol{\rho}_3 = -\boldsymbol{\rho}$. It is then necessary

to fix $d\theta_1 = d\theta$, $d\theta_2 = 0$ and $d\theta_3 = -d\theta$ in order to derive the asymptotic 2-monopole metric. Similarly, for the asymptotic metric for k equally spaced monopoles to be the same, up to a factor, as that for two monopoles the monopoles must be have $d\theta$'s proportional to their distance from the origin. This means, Bielawski's equally spaced monopoles have electric charge proportional to their distance from the centre of mass.

Since the Nahm data for these monopoles are known, the monopole fields can be constructed. Figure 3.7 shows a surface of constant energy density for various times along the head-on scattering geodesic of Fig. 3.3. In Fig. 3.7(a) are three separated monopoles. As they approach, they deform and merge to form a pretzel shape, Fig. 3.7(b). Moving along the geodesic, the monopole becomes more ring-like, Fig. 3.7(c). It instantaneously forms the torus, Fig. 3.7(d), before separating out again, through the same configurations, rotated through $\pi/2$, Fig. 3.7(e-g).

There is a closed 2-monopole geodesic [BM] corresponding to two orbiting monopoles. It can immediately be concluded that a closed 3-monopole geodesic exists. Following [BM], the value of the elliptic modulus k for the rotating 3-monopole configuration is determined as the root of the equation

$$\int_0^{\frac{1}{2}\pi} \frac{2k^2 \sin^2 \phi - 1}{\sqrt{1 - k^2 \sin^2 \phi}} d\phi = 0 \quad (3.90)$$

giving $k \approx 0.906$.

Figure 3.8 shows a surface of constant energy density for this monopole. The monopole has been rotated so that the axis of rotation is in the plane of the page. The monopole motion is a periodic orbit, rotating at constant angular velocity about the axis, which is at an angle of approximately $\pi/9$ to the vertical [BM].

3.5 Twisted line scattering of 3-monopoles

The numerical ADHMN construction may also be used to plot surfaces of constant energy density for 3-monopoles along the twisted line scattering geodesic. Figure 3.9

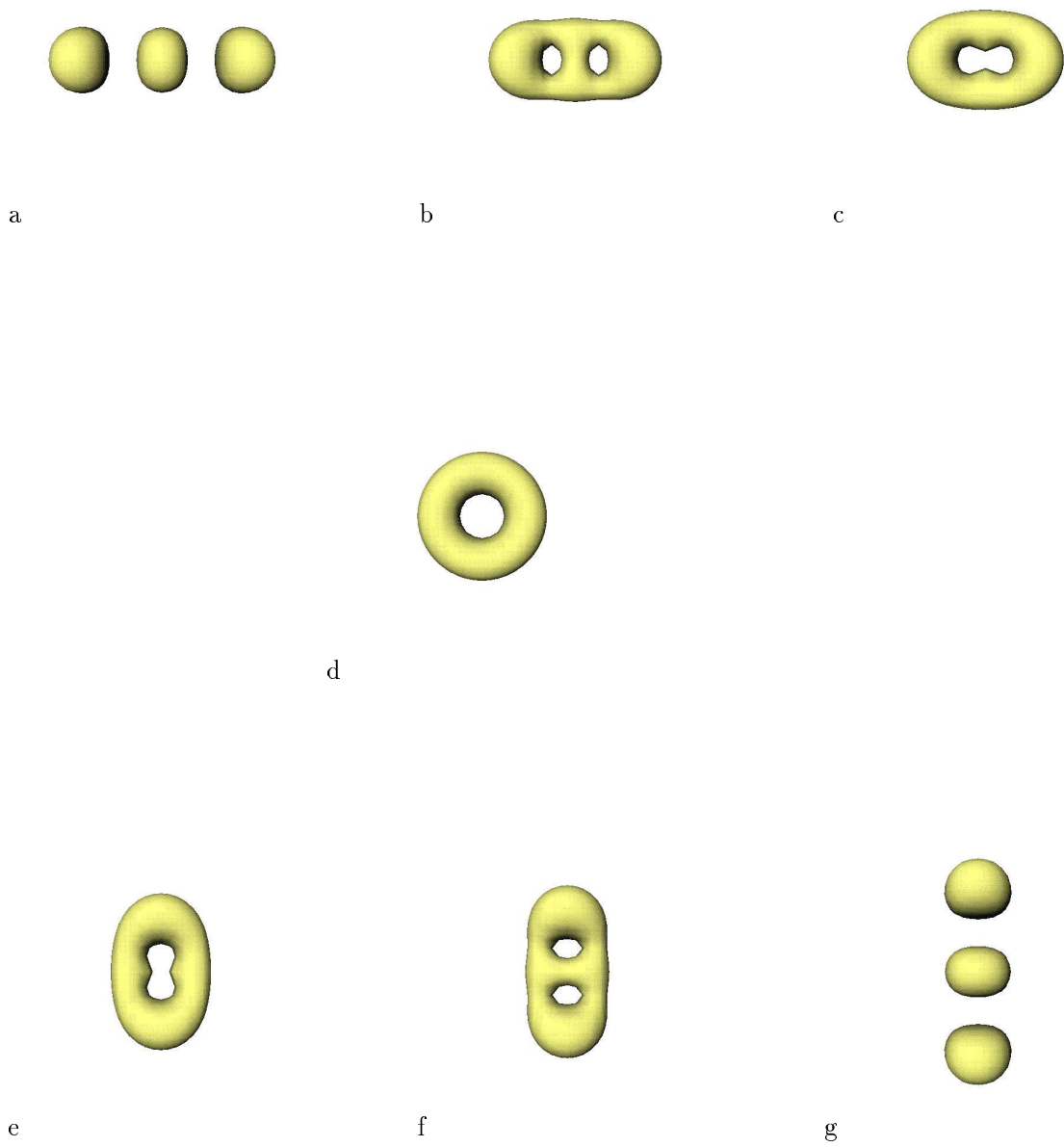


Figure 3.7: A surface of constant energy density at increasing times.

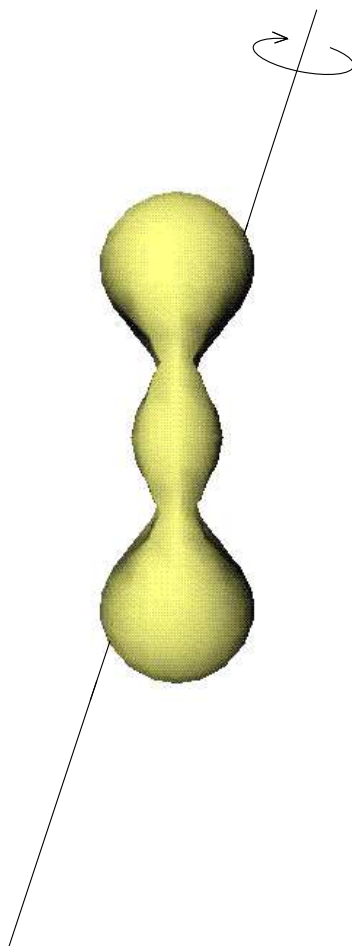


Figure 3.8: A surface of constant energy density for the rotating 3-monopole, together with the axis of rotation.

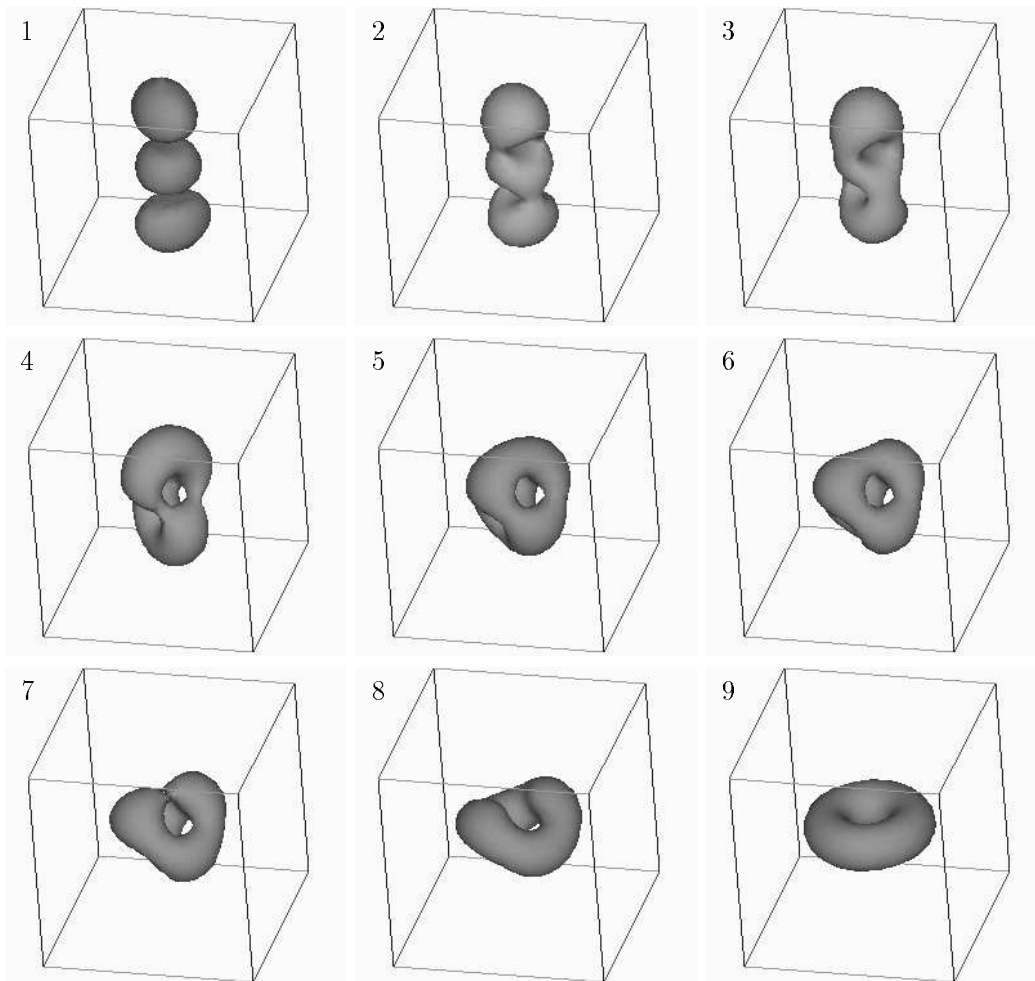


Figure 3.9: Twisted line scattering of 3-monopoles; surface of the constant energy density at increasing times.

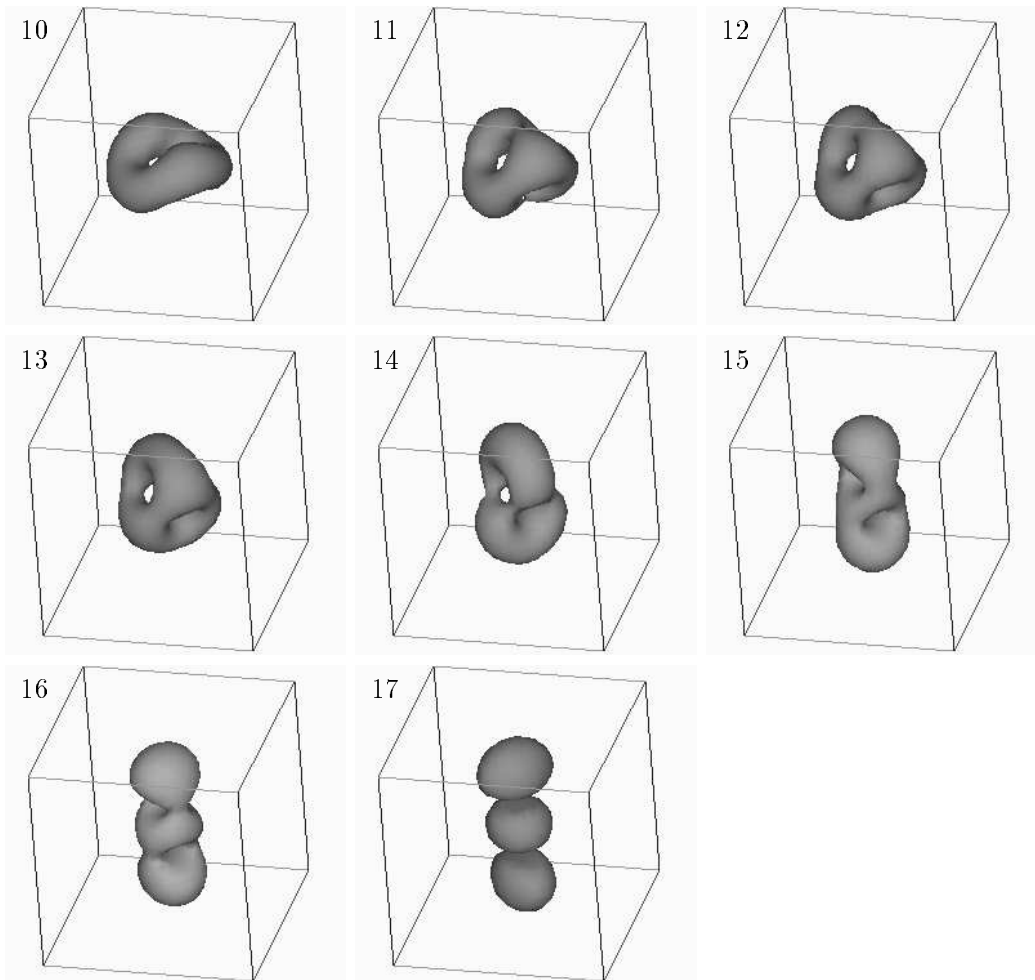


Figure 3.9: continued.

displays a surface of constant energy density for seventeen different members of the family of monopoles. At large negative times (1) there are three well-separated monopoles. One monopole is stationary at the origin, a second monopole is approaching along the positive x_3 -axis and a third is approaching along the negative x_3 -axis. As the monopoles merge, (2), the one in the centre twists as it attempts to align with both the top and bottom monopoles. The energy tries to flow towards the centre but gets squeezed out sideways to form the twisted figure-of-eight shape (4). In picturing these 3-monopoles, this twisted figure-of-eight shape is instructive. It resembles a twisted figure-of-eight, with the bottom loop at right angles to the top loop. It is similar to a tetrahedron in which two opposite edges have been bent into half circles. The energy continues to flow towards the x_1x_2 -plane, but now it has more of a sideways motion. This leads to the formation of the tetrahedral monopole (6). The diagonal movement of the energy density pulls the tetrahedron apart (7) into a buckled torus (8). This then straightens out to form the axisymmetric 3-monopole (9) at time zero. The energy continues to flow in the same direction so that the torus buckles in the opposite sense (10). The motion at positive times goes backwards through the configurations just described, except that the monopoles are inverted so, for example, the tetrahedral monopole (12) formed at positive time is dual to the one (6) formed at negative time.

3.6 The zeros of the Higgs field

In this section, an aspect of the charge three twisted line scattering process is discussed. During this scattering process, the number of zeros of the Higgs field is not conserved. The total number of zeros of the Higgs field, counted with their multiplicity, is k for a k -monopole and these zeros are not always isolated, but may coalesce to form zeros of higher multiplicity. For example, in the case of the toroidal 3-monopole there is a single zero but it has multiplicity three. What is surprising about the charge three twisted line scattering geodesic, is that there are intervals when the total number of zeros exceeds three.

The scattering process passes from three well-separated monopoles through the tetra-

hedral configuration to the toroidal configuration. When there are three well-separated monopoles the Higgs field has exactly three zeros. The axisymmetric monopole has all three Higgs zeros at the origin and it is clear that the only way to arrange three points with tetrahedral symmetry is to put all three points at the origin. Thus, if the tetrahedral monopole has three zeros of the Higgs field, then they must all be at the origin; as in the case of the axisymmetric monopole. Moreover, throughout twisted line scattering the imposed symmetry means that if there are three zeros of the Higgs field, then one must be at the origin with the other two on the x_3 -axis and equidistant from the origin. However, numerical investigations reveal that there are no zeros of the Higgs field on the x_3 -axis, except at the origin, for all the monopole solutions between the tetrahedral monopole, Fig. 3.9(5) and the axisymmetric monopole, Fig. 3.9(9). So, if the number of Higgs zeros remains three, then the surprising conclusion is that the zeros of the Higgs field must stick at the origin for a period of time.

The above argument fails because it assumes that the number of zeros of the Higgs field is always three for a 3-monopole solution of the Bogomolny equation. In the case of Abelian Higgs vortices at critical coupling, the vortex number not only gives the total number of zeros counted with their multiplicity but also bounds the total number of zeros [JT]. However, some of the monopoles in the one-parameter family have more than three zeros. In fact, at different points along the twisted line scattering geodesic the number of zeros is one, three, five or seven.

The first approach is to compute the winding number, $Q(r_0)$, of the normalized Higgs field on a two-sphere of radius r_0 , centred at the origin. This integer winding number counts the number of zeros of the Higgs field counted with multiplicity inside this two-sphere. Necessarily, $Q(\infty) = k$ for a k -monopole. A numerical scheme is used to compute the winding number and is described in [HS3].

First, the tetrahedral monopole is considered and it is computed that $Q(1.0) = +3$. The winding number is equal to three when r_0 is sufficiently large. If all three Higgs zeros were at the origin then the winding number would equal three for all positive values of r_0 . However $Q(0.2) = -1$. Therefore, between the sphere of radius $r_0 = 0.2$ and the sphere

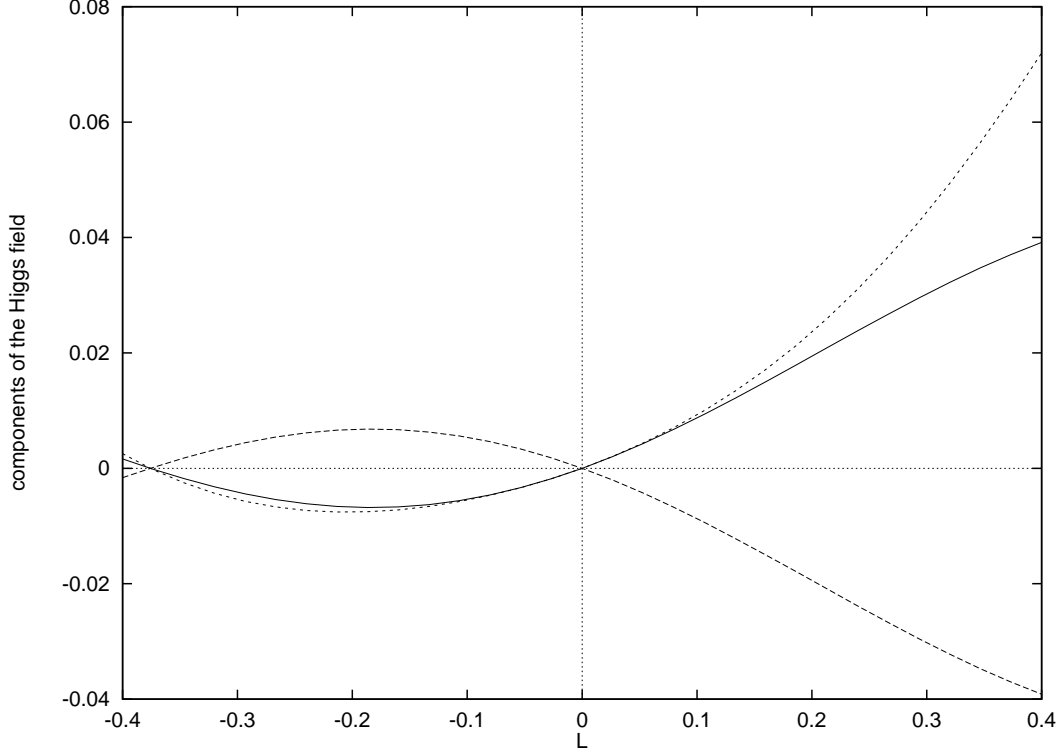


Figure 3.10: Components of the Higgs field of the tetrahedral 3-monopole along the line $x_1 = x_2 = x_3 = L$, for $-0.4 \leq L \leq 0.4$.

of radius $r_0 = 1.0$ there must be four zeros, each of which has have an associated local winding number of $+1$. These extra zeros are located by plotting the components of the Higgs field. The Higgs field is written in terms of Pauli matrices as

$$\Phi = i\sigma_1\varphi_1 + i\sigma_2\varphi_2 + i\sigma_3\varphi_3 \quad (3.91)$$

and the individual components $\varphi_1, \varphi_2, \varphi_3$ are plotted. It is easier to locate a zero of the Higgs field by searching for where all three components are zero rather than simply looking at $|\Phi|$. The task is simple because of the tetrahedral symmetry. Fig. 3.10 shows the components of the Higgs field along the line $x_1 = x_2 = x_3 = L$, for $-0.4 \leq L \leq 0.4$. It is clear that all three curves have a zero at $L = 0$ and $L \approx -0.38$. By tetrahedral symmetry, similar curves are obtained along each of the other three diagonals. Hence, the numerical evidence suggests that there are four positive zeros on the vertices of a regular

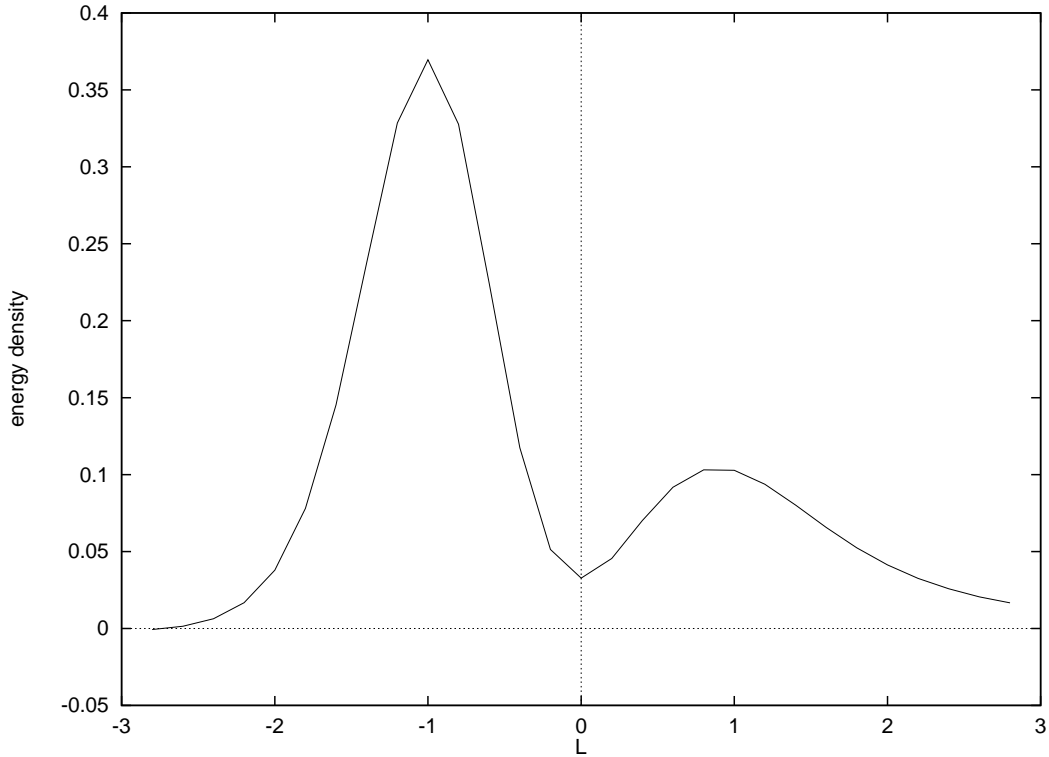


Figure 3.11: Energy density of the tetrahedral 3-monopole along the line $x_1 = x_2 = x_3 = L$, for $-3 \leq L \leq 3$.

tetrahedron and an anti-zero at the origin. Therefore, the tetrahedral 3-monopole is a solution in which the Higgs field has both positive multiplicity and negative multiplicity zeros but nonetheless saturates the Bogomolny energy bound.

An obvious question is whether the positive zeros lie along the directions of the vertices of the tetrahedron, where the energy density is maximal, or along the directions of the faces of the tetrahedron, where a surface of constant energy density has holes. Figure 2(b) shows a plot of the energy density along the line $x_1 = x_2 = x_3 = L$, for $-3 \leq L \leq 3$. The zeros lie along the lines joining the origin to the vertices of the tetrahedron. However, the zeros are not as far from the origin as the points of maximal energy density. The zeros

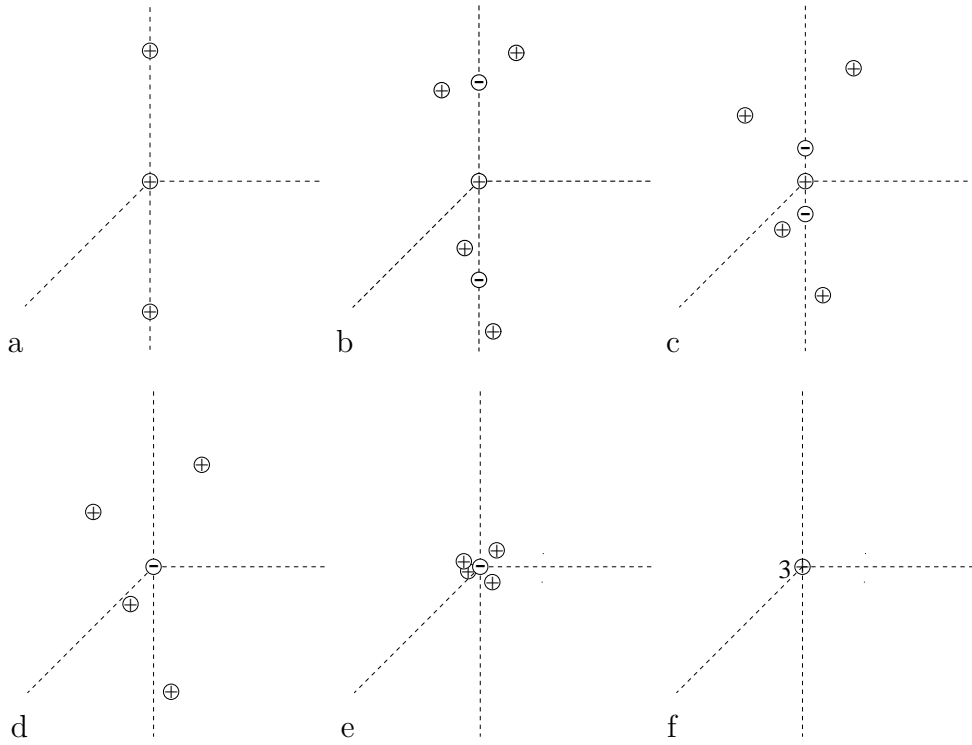


Figure 3.12: Motion of zeros of the Higgs field during twisted line scattering.

occur at $L \approx -0.38$ whereas the energy density takes its maximum value at $L \approx -1$. It is interesting to note that the location of the anti-zero appears to coincide with a local minimum of the energy density.

The motion of the zeros of the Higgs field can be described. This motion is sketched in Fig. 3.12. When the monopoles are well-separated, there are three zeros of the Higgs field, Fig. 3.12(a). One is at the origin and the other two are equidistant above and below the origin along the x_3 -axis. Obviously, in the asymptotic limit of infinite separation each of these zeros lies at the centre of a 1-monopole. At some critical point, as the zeros approach, there is a bifurcation. Each of the zeros above and below the origin split into three zeros: two with positive multiplicity and one with negative multiplicity. In this way, the number of zeros counted with their multiplicity is conserved locally. Unfortunately, neither the precise details of this bifurcation nor the precise point at which it occurs is discernable

numerically. However, it is certain that as the matter begins to coalesce there are seven zeros of the Higgs field, Fig. 3.12(b): one at the origin of positive unit multiplicity, two above and below the origin on the x_3 -axis of negative unit multiplicity and four further positive multiplicity zeros away from the x_3 -axis. These four zeros move consistently with the twisted line symmetry, the two above the x_1x_2 -plane are separated along a line parallel to the line $x_1 = -x_2$ and $x_3 = 0$ and the two below, parallel to the line $x_1 = x_2$ and $x_3 = 0$.

As the monopoles continue to coalesce, the anti-zeros approach the origin, Fig. 3.12(c). They leave behind the four zeros which are off the x_3 -axis. They reach the origin at the tetrahedral configuration, Fig. 3.12(d). At the tetrahedral configuration there are five zeros, a single zero of negative unit multiplicity at the origin and four with positive multiplicity arranged in a tetrahedron. The four positive multiplicity zeros then move towards the origin, Fig. 3.12(e), and finally reach the origin to give a single multiplicity three zero, Fig. 3.12(f).

Numerical evidence to support this description of the configuration of Higgs zeros at the tetrahedral configuration is given above. There are similar numerical results to support the description of the configuration of Higgs zeros prior to the formation of the tetrahedral monopole, but after the splitting of the Higgs zeros.

At one such 3-monopole, the winding numbers are computed to be

$$\begin{aligned} Q(0.2) &= +1, \\ Q(0.5) &= -1, \\ Q(0.7) &= +3. \end{aligned} \tag{3.92}$$

This is consistent with a positive zero at the origin, two negative zeros on the x_3 -axis and four positive zeros which are further from the origin than the negative zeros. The positions of the zeros can be located, in the same manner as in the tetrahedral case, by plotting the components of the Higgs field. By the imposed symmetries, each of the zeros must lie on a line where $x_1 = \pm x_2$. Therefore, the components of the Higgs field are plotted along the line $x_1 = x_2 = L$, with x_3 fixed. Fig. 3.13 shows such a plot, with $x_3 = -0.425$. This clearly shows a zero on the x_3 -axis. Fig. 3.14 shows a similar plot for $x_3 = -0.605$. It can

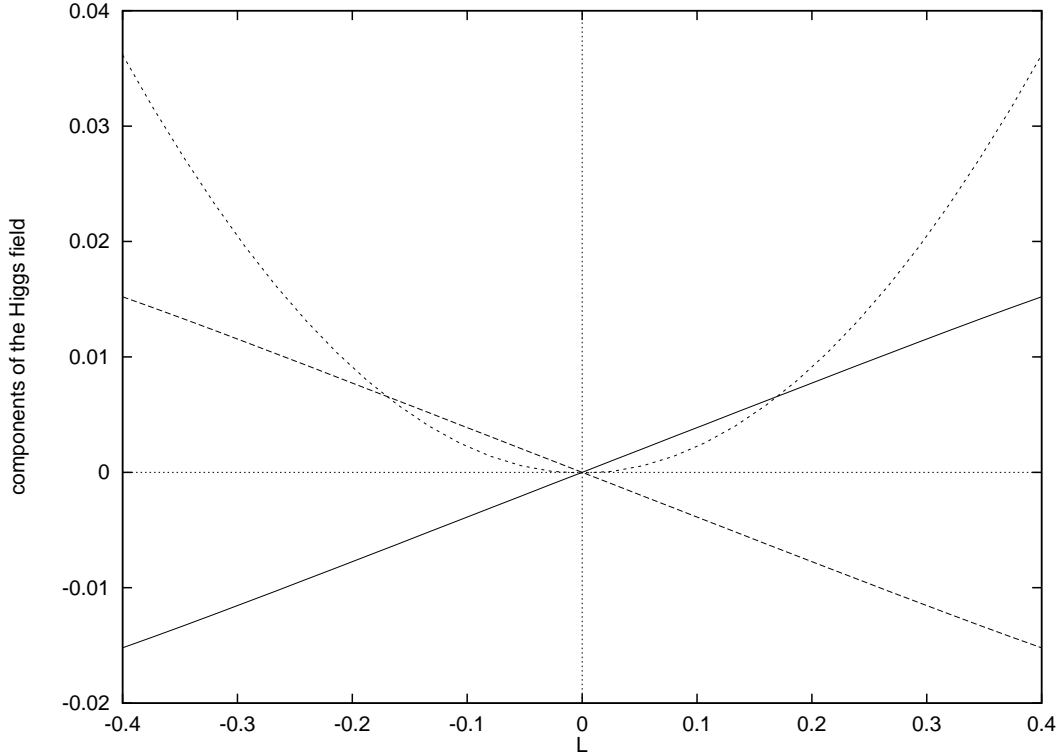


Figure 3.13: Components of the Higgs field of the monopole with parameter $a = 2.05$, along the line $x_3 = -0.425$, $x_1 = x_2 = L$, for $-0.4 \leq L \leq 0.4$.

be seen that there are at two zeros, which are a distance $L \approx 0.17$ from the x_3 -axis. These results are in agreement with the winding number calculations, which placed bounds on the distances of each of the zeros from the origin.

The existence of anti-zeros raises a number of questions. For example, can the presence of an anti-zero be seen from the spectral curve or rational map of a monopole? It seems likely that the appearance and disappearance of anti-zeros has a signature in the space of rational maps or in the space of spectral curves. Unfortunately, the numerical results do not locate the exact 3-monopole at which anti-zeros appear or disappear in the twisted line scattering. One possibility is that such an event is associated with the elliptic curve discriminant of the elliptic curve vanishing. The point at which this happens is marked with a Y in Fig. 3.6. The numerical results are consistent with the bifurcation of zeros

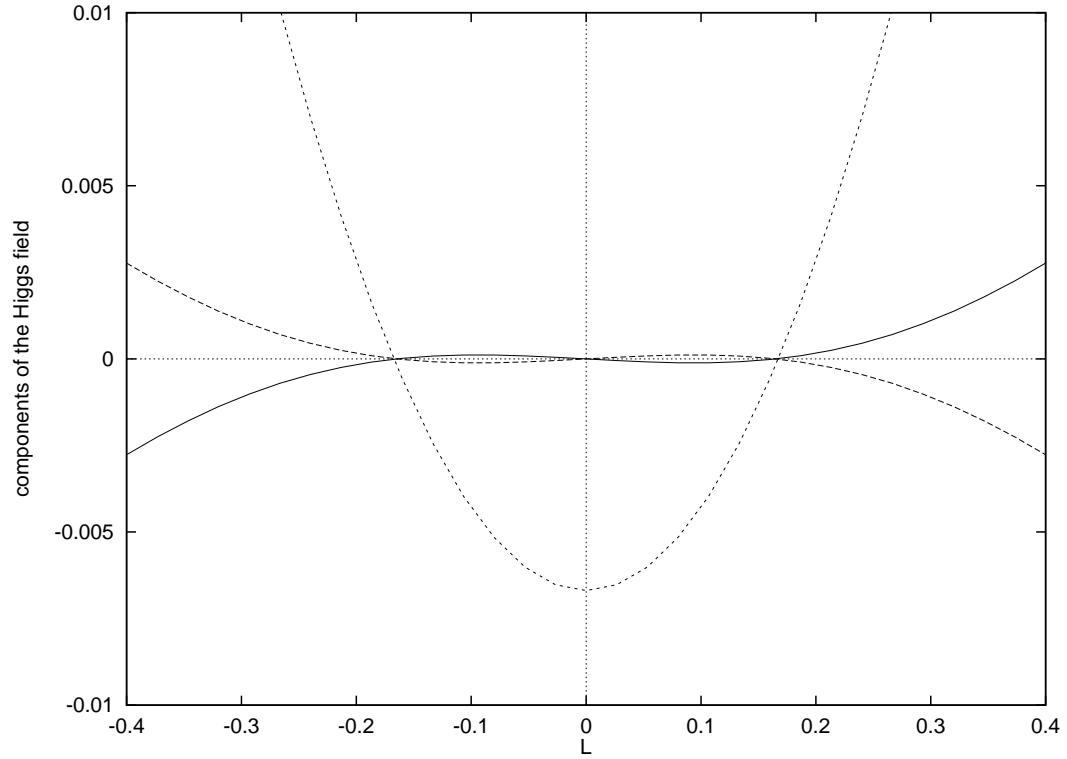


Figure 3.14: Components of the Higgs field of the monopole with parameter $a = 2.05$, along the $x_3 = -0.605$, $x_1 = x_2 = L$, for $-0.4 \leq L \leq 0.4$.

occurring at this 3-monopole. It is possible that the $\Delta = 0$ line divides the space of D_2 symmetric 3-monopoles between a region with anti-zeros and a region without.

Chapter 4

Conclusions

4.1 Symmetric multimonopoles

For the most part, this thesis is about how finite symmetry groups are used to study multimonopoles. In Chapter 1 BPS monopoles are described. BPS monopoles are solutions to the Bogomolny equation, an integrable, first-order equation for algebra-valued fields. Its moduli space is isometrically diffeomorphic to the moduli space of solutions to the Nahm equations, a set of ordinary nonlinear differential equations whose solutions are called Nahm data. Nahm equations are spinning top equations and their integrability has a Lax formulation. This is reviewed in Chapter 1. It is described how, because there is a genus one spectral curve, the Nahm equations for 2-monopoles are tractable.

The Nahm equations for 7-monopoles are generally intractable. However, the Nahm equations for an icosahedrally invariant 7-monopoles are tractable and in Chapter 2 these equations are calculated and solved. From a solution of the Nahm equations the monopole fields are numerically attainable and the icosahedrally symmetric 7-monopole is pictured. The Nahm equations for an octahedrally symmetric 5-monopole are also tractable and this monopole is also pictured. The symmetries of these monopoles make their Nahm equations tractable.

There are only a few special cases where the symmetries of a multimonopole make its Nahm equations tractable. In Chapter 3 it is explained how a monopole's Nahm equations

have elliptic solutions if the curve obtained by dividing the monopole's spectral curve by its symmetries is a genus one curve. The Nahm data give very complete information about a monopole but are not generally available. To study symmetric multimono- poles generally, that is, to study them in cases where the Nahm equations are not tractable, the rational map descriptions are used.

The rational map descriptions are reviewed in Chapter 2. They describe monopole moduli spaces and are used here to study symmetric multimono- poles. Geodesics of symmetric monopoles are found using the Donaldson rational maps. As an example, the geodesic of C_{4h} 5-monopoles is presented. This geodesic passes through the octahedral 5-monopole. With this exception, Nahm data are not known for C_{4h} 5-monopoles. Nonetheless, qualitative information about the 5-monopoles along this geodesic can be deduced from the rational map.

The twisted line scattering geodesics are an interesting family of geodesics which are studied using the Donaldson rational maps. They are geodesics of monopoles with rotary-reflection symmetries. During twisted line scattering three clusters of monopoles collide along a line, an axially symmetric monopole forms and three clusters separate again along the same line. The simplest example is the twisted line scattering of 3-monopoles. Monopoles on the positive and negative x_3 -axis approach a monopole at the origin. They coalesce to form the tetrahedral 3-monopole, then the axially symmetric 3-monopole and then another tetrahedral 3-monopole before separating again along the x_3 -axis.

Using the Jarvis rational map it is possible to tell precisely which symmetric monopoles there are. A rotation of a monopole corresponds to a Möbius transformation of the source sphere of the corresponding Jarvis map. A symmetric monopole corresponds to a symmetric rational map. In this way, the question of which symmetric monopoles exist is reduced to the question of which symmetric rational maps there are, a question answered using elementary group representation theory. This is discussed at the end of Chapter 2. It is found, for example, that there is a geodesic of tetrahedral 4-monopoles.

From Chapter 2 it is known that some symmetric monopoles have tractable Nahm data. It is also known, in principle, which symmetric monopoles exist. Chapter 3 opens with

an explanation of which symmetric monopoles have tractable Nahm equations. This discussion indicates that tetrahedral 4-monopoles and D_2 3-monopoles have tractable Nahm equations. The Nahm equations are calculated in these cases. The tetrahedral 4-monopole Nahm equations are similar to the other symmetric Nahm equations. They are easily solved and the 4-monopoles along the tetrahedral geodesic are pictured.

There is a two-dimensional space of D_2 3-monopoles. The D_2 3-monopole Nahm equations are complex Euler-Poinsot equations and their solutions are known. Some features of this space are deduced from the spectral curve. There are geodesics in this space that are identical to the 2-monopole right-angle scattering geodesics. The 3-monopole twisted line scattering geodesics also lie in this space. Knowing the Nahm data for these monopoles allows the fields to be computed numerically. It is discovered that there are monopoles along the geodesics with anti-zeros of the Higgs field.

The space of D_2 symmetric 3-monopoles illustrates some of those properties of multimonomoles not common to 2-monopoles. It contains monopoles with anti-zeros and monopoles without. It also contains right-angle and zero-angle scattering geodesics. A numerical study of the D_2 symmetric 3-monopole space would show what region of it contains anti-zeros and whether zero-angle scattering is typical or exceptional. It is also probable that the metric on this space could be calculated explicitly.

4.2 Nahm data and new hyperKähler manifolds

Many different hyperKähler manifolds are monopole moduli spaces. These hyperKähler manifolds always have an isometric SO_3 action. In Chapter 1 new hyperKähler manifolds are derived from monopole moduli spaces by fixing monopoles. These fixed monopole spaces do not have an SO_3 action. Dancer's one-parameter family of four-dimensional hyperKähler manifolds are shown to be fixed monopole spaces; Dancer originally constructed the family using the hyperKähler quotient. A three-parameter family of fixed monopole spaces is exhibited. This family is also constructed as a hyperKähler quotient.

Fixed monopole spaces are of interest because of the Hanany-Witten correspondence.

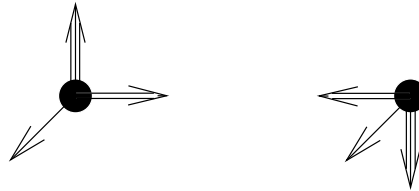


Figure 4.1: Two Skyrmions attracting. The different arrow types correspond to different dipoles.

This correspondence relates monopole moduli spaces and three-dimensional supersymmetric quantum field theories. The fixed monopole spaces correspond to supersymmetric theories with massive hypermultiplets.

In [Da3] the rational map formulation for SU_n monopoles is used to elucidate the structure of Dancer’s manifolds. It will be possible to generalize this to other fixed monopole spaces, allowing the structural predictions for such manifolds which follow from the Hanany-Witten correspondence to be verified. More generally, the fixed monopole construction demonstrates how, in addition to their application to BPS monopoles, the Nahm equations are useful in the study of hyperKähler manifolds and branes.

4.3 Multimonoles and Skyrmions

In [HMS] is an ansatz for minimum energy Skyrmions. This ansatz replaces the hedgehog field of the 1-Skyrmion with a field whose angular distribution is described by a rational map. The ansatz is demonstrated to give good approximation to the known Skyrmions: those of baryon numbers one to nine [BTC, BaS2]. Thus, for example, the tetrahedral degree three rational map yields a good approximation to the minimum energy 3-Skyrmion. In the Jarvis description this tetrahedral rational map is equivalent to the tetrahedral 3-monopole and the 3-Skyrmion resembles this monopole. At the cost of ending this thesis with a speculative aside, it is interesting to note how similar are the behaviours of D_2 3-monopoles and D_2 configurations of three Skyrmions.

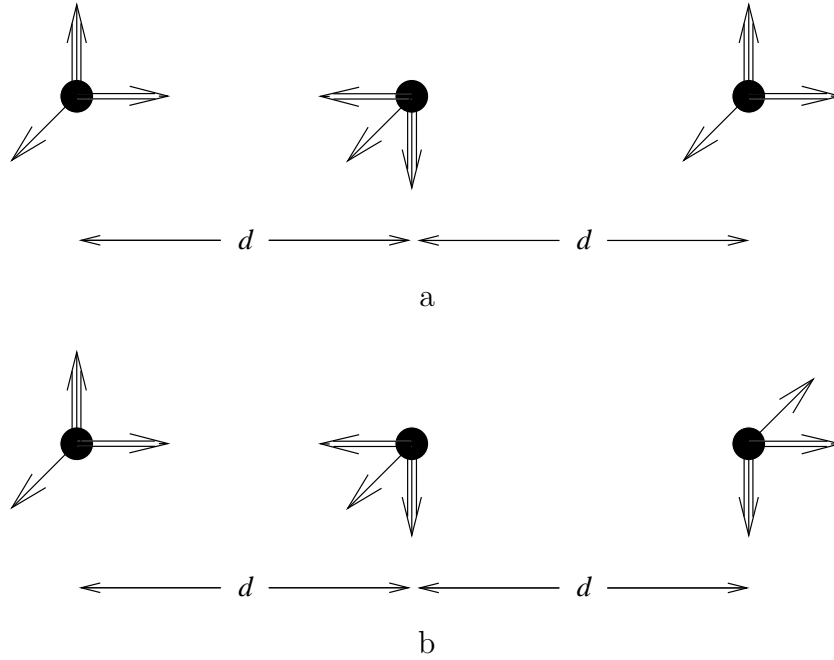


Figure 4.2: Three equally spaced collinear Skyrmions. Configuration (a) evolves into the pretzel, configuration (b) evolves into the tetrahedron.

The product ansatz allows the superposition of well-separated Skyrmions. A Skyrmion has three distinct orthogonal dipoles. Two well-separated Skyrmions attract or repel depending upon the mutual orientation of these dipoles. Two Skyrmions maximally attract if the difference of orientation of their dipoles is a rotation of π about an axis orthogonal to the line of separation. The product ansatz and the attractive orientation are reviewed in [Ma4, Sc]. An attractive orientation is pictured in Fig. 4.1.

Three Skyrmions, superimposed so that they are equally spaced along a line, move towards each other if the two outlying Skyrmions maximally attract the middle one. The relative orientation of the outlying Skyrmions does not affect the fact of overall dipole attraction. However, the orientation is significant in the interaction region where the product ansatz is not valid. If the outlying Skyrmions are in the same orientation, Fig. 4.2a, they form a pretzel configuration reminiscent of Fig. 3.7b, [BaS3]. If there is a relative rotation of π about the separation axis, Fig. 4.2b, they form a tetrahedral configuration,

reminiscent of Fig. 3.9(6), [BaS1].

The similarities of this behaviour to that of D_2 symmetric 3-monopoles is apparent. It is imagined that the unstable manifold of three well-separated D_2 Skyrmions is two dimensional. When the three Skyrmions are well-separated these two dimensions correspond to separation and a relative dipole orientation. In the monopole analogue, the two dimensions are also imagined to correspond to separation and relative phase orientation. The important feature of the analogy is that attraction partially fixes the relative dipole orientation of the individual Skyrmions.

Bibliography

- [AvanM1] M. Adler and P. van Moerbeke, *Adv. Math.* **38** (1980) 267.
- [AvanM2] M. Adler and P. van Moerbeke, *Adv. Math.* **38** (1980) 318.
- [ABDP] J.A. Armstrong, N. Bloemberger, J. Ducuing and P.S. Pershan, *Phys. Rev.* **127** (1962) 1918.
- [AH] M.F. Atiyah and N.J. Hitchin, *The geometry and dynamics of magnetic monopoles* (Princeton University Press, Princeton, 1988).
- [ADHM] M.F. Atiyah, V.G. Drinfeld, N.J. Hitchin and Yu.I. Manin, *Phys. Lett.* **65A** (1978) 185.
- [A] M. Audin, *Spinning tops* (Cambridge University Press, Cambridge, 1996).
- [BBT1] C. Barnes, K. Baskerville and N. Turok, *Phys. Rev. Lett.* **79** (1997) 367.
- [BBT2] C. Barnes, K. Baskerville and N. Turok, *Phys. Lett.* **411B** (1997) 180.
- [BM] L. Bates and R. Montgomery, *Commun. Math. Phys.* **118** (1988) 635.
- [BaS1] R.A. Battye and P.M. Sutcliffe, *Phys. Lett.* **391B** (1997) 150.
- [BaS2] R.A. Battye and P.M. Sutcliffe, *Phys. Rev. Lett.* **79** (1997) 363.
- [BaS3] R.A. Battye and P.M. Sutcliffe (private communication, 1997).
- [Bi1] R. Bielawski, *Ann. Glob. Anal. Geom.* **14** (1996) 123.

- [Bi2] R. Bielawski, *Nonlinearity* **9** (1996) 1463.
- [BTC] E. Braaten, S. Townsend and L. Carson, *Phys. Lett.* **235B** (1990) 147.
- [Bo] E.B. Bogomolny, *Sov. J. Nucl. Phys.* **24** (1976) 449.
- [BrS] H.W. Braden and P.M. Sutcliffe, *Phys. Lett.* **391B** (1997) 366.
- [BPP] S.A. Brown, H. Panagopoulos and M.K. Prasad, *Phys. Rev. D* **26** (1982) 854.
- [BF] P.F. Byrd and M.D. Friedman, *Handbook of elliptic integrals for engineers and scientists* (Springer-Verlag, Berlin, 1971).
- [C] S.A. Connell, *The dynamics of the $SU(3)$ charge (1,1) magnetic monopoles* <ftp://maths.adelaide.edu.au/pure/mmurray/oneone.tex> (unpublished, 1994).
- [CG] E. Corrigan and P. Goddard, *Ann. of Phys.* **154** (1984) 253.
- [Da1] A.S. Dancer, *Nonlinearity* **5** (1992) 1355.
- [Da2] A.S. Dancer, *Commun. Math. Phys.* **158** (1993) 545.
- [Da3] A.S. Dancer, *Q. J. Math.* **45** (1994) 463.
- [DL] A.S. Dancer and R.A. Leese, *Proc. R. Soc. London Ser. A* **440** (1993) 421.
- [Dia] D.-E. Diaconescu, *Nucl. Phys.* **B503** (1997) 220.
- [Dir] P.A.M. Dirac, *Proc. R. Soc. London Ser. A* **133** (1931) 60.
- [Do] S.K. Donaldson, *Commun. Math. Phys.* **96** (1984) 387.
- [FHP] P. Forgács, Z. Horváth and L. Palla, *Phys. Lett.* **99B** (1981) 232.
- [GL] J.P. Gauntlett and D.A. Lowe, *Nucl. Phys.* **B472** (1996) 194.
- [GM1] G.W. Gibbons and N.S. Manton, *Nucl. Phys.* **B274** (1986) 183.
- [GM2] G.W. Gibbons and N.S. Manton, *Phys. Lett.* **356B** (1995) 32.

- [GP] G.W. Gibbons and C. Pope, Commun. Math. Phys. **66** (1979) 267.
- [GRG] G.W. Gibbons, P. Rychenkova and R. Goto, Commun. Math. Phys. **186** (1997) 581.
- [HW] A. Hanany and E. Witten, Nucl. Phys. **B492** (1997) 152.
- [Ha] S.W. Hawking, Phys. Lett. **60A** (1977) 81.
- [Hi1] N.J. Hitchin, Commun. Math. Phys. **83** (1982) 579.
- [Hi2] N.J. Hitchin, Commun. Math. Phys. **89** (1983) 145.
- [Hi3] N.J. Hitchin, *Monopoles, minimal surfaces and algebraic curves* (Les Presses de l'Université de Montréal, Montréal, 1987).
- [HKLR] N.J. Hitchin, A. Karlhede, U. Lindstrom and M. Roček, Commun. Math. Phys. **108** (1987) 535.
- [HMM] N.J. Hitchin, N.S. Manton and M.K. Murray, Nonlinearity **8** (1995) 661.
- [Ho] C.J. Houghton, Phys. Rev. D **56** (1997) 1120.
- [HMS] C.J. Houghton, N.S. Manton and P.M. Sutcliffe, *Rational maps, monopoles and Skyrmions*, hep-th/9705151, to appear Nucl. Phys. **B**.
- [HS1] C.J. Houghton and P.M. Sutcliffe, Commun. Math. Phys. **180** (1996) 342.
- [HS2] C.J. Houghton and P.M. Sutcliffe, Nonlinearity **9** (1996) 385.
- [HS3] C.J. Houghton and P.M. Sutcliffe, Nucl. Phys. **B464** (1996) 59.
- [HS4] C.J. Houghton and P.M. Sutcliffe, Nonlinearity **9** (1996) 1609.
- [HS5] C.J. Houghton and P.M. Sutcliffe, J. Maths. Phys. **38** (1997) 5576.
- [Hu1] J. Hurtubise, Commun. Math. Phys. **92** (1983) 195.

- [Hu2] J. Hurtubise, *Commun. Math. Phys.* **100** (1985) 463.
- [HM] J. Hurtubise and M.K. Murray, *Commun. Math. Phys.* **122** (1989) 35.
- [I] P. Irwin, *Phys. Rev. D* **56** (1997) 5200.
- [JT] A. Jaffe and C. Taubes, *Vortices and monopoles* (Birkhäuser, Boston, 1980).
- [J] S. Jarvis, *A rational map for Euclidean monopoles via radial scattering* (Oxford preprint, 1996).
- [K] F. Klein, *Lectures on the icosahedron* (Kegan Paul, London, 1913).
- [KDWS] G.F. Koster, J.O. Dimmock, R.G. Wheeler, H. Statz, *Properties of the thirty-two point groups* (M.I.T. Press, Cambridge, 1963).
- [LL] K. Lee and C. Lu, *Two massive and One Massless $Sp(4)$ monopoles*, hep-th/9709080.
- [LWY1] K. Lee, E.J. Weinberg and P. Yi, *Phys. Lett.* **376B** (1996) 97.
- [LWY2] K. Lee, E.J. Weinberg and P. Yi, *Phys. Rev. D* **45** (1996) 1633.
- [Ma1] N.S. Manton, *Nucl. Phys.* **B106** (1977) 525.
- [Ma2] N.S. Manton, *Phys. Lett.* **110B** (1982) 54.
- [Ma3] N.S. Manton, *Phys. Lett.* **154B** (1985) 397, (E) *Phys. Lett.* **157B** (1985) 475.
- [Ma4] N.S. Manton, *Acta Phys. Polon.* **B25** (1994) 1757.
- [MS] N.S. Manton and T.M. Samols, *Phys. Lett.* **215B** (1988) 559.
- [Mu] M.K. Murray, *J. Geom. Phys.* **23** (1997) 31.
- [Nah] W. Nahm, *The construction of all self-dual multimonopoles by the ADHM method in Monopoles in quantum field theory* edited by N.S. Craigie, P. Goddard and W. Nahm (World Scientific, Singapore, 1982).

- [Nak] H. Nakajima, *Monopoles and Nahm's equations in Einstein metrics and Yang-Mills connections* edited by T. Mabuchi and S. Mukai (Marcel Dekker, New York, 1993).
- [Pa] H. Panagopoulos, Phys. Rev. D **28** (1983) 380.
- [Pr] M.K. Prasad, Commun. Math. Phys. **80** (1981) 137.
- [PR] M.K. Prasad and P. Rossi, Phys. Rev. Lett. **46** (1981) 806.
- [PS] M.K. Prasad and C.M. Sommerfield, Phys. Rev. Lett. **35** (1975) 760.
- [Sa] T.M. Samols, Ph.D. thesis, Cambridge University, 1990.
- [Sc] B.J. Schroers, Z. Phys. **C61** (1994) 479.
- [Se] J.-P. Serre, *Linear representations of finite groups* (Springer-Verlag, New York, 1993).
- [SW] N. Seiberg and E. Witten, *Gauge dynamics and compactification to three-dimensions*, hep-th/9607163.
- [Sk] T.H.R. Skyrme, Proc. R. Soc. London Ser. A **260** (1961) 127.
- [St] D. Stuart, Commun. Math. Phys. **166** (1994) 149.
- [Su] P.M. Sutcliffe, Phys. Lett. **357B** (1995) 335.
- [Wa1] R.S. Ward, Commun. Math. Phys. **79** (1981) 317.
- [Wa2] R.S. Ward, Phil. Trans. R. Soc. London Ser. A **315** (1985) 451.
- [We1] E.J. Weinberg, Phys. Rev. D **20** (1979) 936.
- [We2] E.J. Weinberg, Nucl. Phys. **B167** (1980) 500.
- [WW] E.T. Whittaker and G.N. Watson, *A course of modern analysis* (Cambridge University Press, Cambridge, 1902).